CHALMERS
UNIVERSITY OF TECHNOLOGY

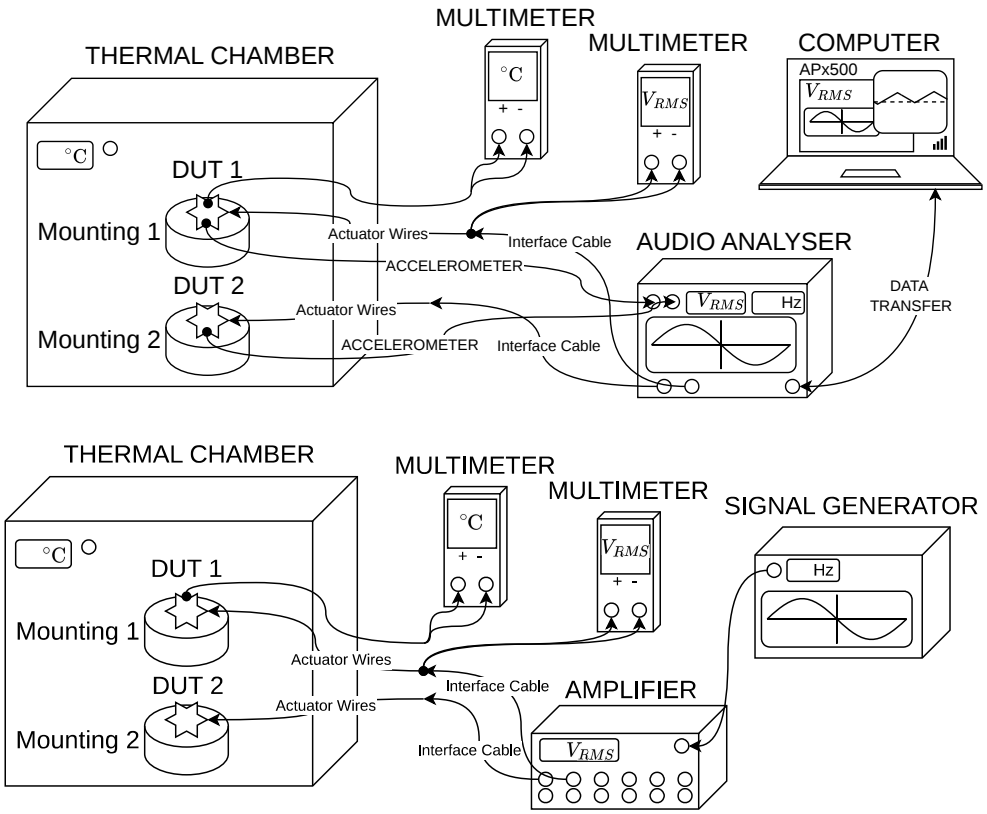

Development of Accelerated Life Testing Method for Bone Conduction Devices

In cooperation with Cochlear Bone Anchored Solutions AB

Master's thesis in Product Development

SAM AZADI, VIKTOR LARSSON ROSÉN

DEPARTMENT OF ELECTRICAL ENGINEERING

CHALMERS UNIVERSITY OF TECHNOLOGY
Gothenburg, Sweden 2026
www.chalmers.se

Master's thesis 2026

Development of Accelerated Life Testing Method for Bone Conduction Devices

SAM AZADI, VIKTOR LARSSON ROSÉN

CHALMERS
UNIVERSITY OF TECHNOLOGY

Department of Electrical Engineering
Division of Signal Processing and Biomedical Engineering
Chalmers University of Technology
Gothenburg, Sweden 2026

Development of Accelerated Life Testing Method for Bone Conduction Devices
In cooperation with Cochlear Bone Anchored Solutions AB
SAM AZADI, VIKTOR LARSSON ROSÉN

Supervisor: Luke Poggi, Cochlear Bone Anchored Solutions AB
Examiner: Sabine Reinfeldt, Electrical Engineering, Chalmers University of Technology

Master's Thesis 2026
Department of Electrical Engineering
Division of Signal Processing and Biomedical Engineering
Chalmers University of Technology
SE-412 96 Gothenburg
Telephone +46 31 772 1000

Cover: Accelerated life testing (ALT) method block diagram

Typeset in LaTeX
Printed by Chalmers Reproservice
Gothenburg, Sweden 2026

Development of Accelerated Life Testing Method for Bone Conduction Devices
In cooperation with Cochlear Bone Anchored Solutions AB
SAM AZADI, VIKTOR LARSSON ROSÉN
Department of Electrical Engineering
Chalmers University of Technology

Abstract

This thesis investigates the development of an accelerated lifetime testing (ALT) methodology for Cochlear's bone conduction hearing devices (BCDs). An ALT is a testing method in which a product is exposed to higher-than-normal stress conditions to accelerate ageing and failure mechanisms. The purpose is to evaluate long-term reliability and predict product lifetime within a significantly shorter testing period. The work was motivated by Cochlear's need for a robust, data-driven ALT methodology. The implementation of this framework provides significant engineering and business value by reducing testing costs, accelerating time-to-market for future products, and supporting verification of regulatory compliance standards. Several theoretical ALT methods and models were evaluated. The aim was to develop theoretical acceleration models together with practical experimental methods capable of identifying long-term performance degradation caused by age-related failure modes in adhesives, nylon thread-locking materials, and piezoelectric components. An ALT concept based on thermal and electrical overstressing was selected. Individual overstress limits for each component were then determined through tailored practical experiments designed around the specific failure mechanisms of each component. A total of 16 experiments were conducted, with a total sample count exceeding 80. The experiments identified safe accelerated operating ranges of 2-5 V_{RMS} and 40-70 °C. Due to time constraints, obtaining long-term ALT degradation results was outside the scope of this thesis. However, validation tests was initiated using conservative inputs of 4.3 V_{RMS} at 70 °C to verify the functionality and stability of the developed test setup. The developed ALT framework contributes to more reliable predictions of long-term actuator performance and supports earlier validation of future design changes. Lastly, the methodology is highly scalable, allowing multiple actuator variants or models to be tested simultaneously.

Keywords: Bone conduction device (BCD), Accelerated life test (ALT), Adhesive failure, Thread loosening, Nylon thread-locker, Piezoelectric behavioural change, APx.

Acknowledgements

This master's thesis was conducted for the Department of Electrical Engineering, Division of Signal Processing and Biomedical Engineering, at Chalmers University of Technology, together with Cochlear Bone Anchored Solutions AB during the Spring term of 2026. This work was carried out by master's students enrolled in the Product Development program (MPPDE). We want to express our gratitude to our examiner, Associate Professor Dr. Sabine Reinfeldt, for her guidance and support throughout the project. We are also grateful to Cochlear's staff for their valuable help and expertise, particularly our supervisor, Senior Mechanical Engineer Luke Poggi, as well as Senior Electroacoustic Development Engineer Armin Azhirnian, Senior Project Engineer Dan Nyström, Principal Mechanical Engineer Tommy Bergs, Senior Acoustics Engineer Felicitas Bederna, Principal CAE Engineer Patrik Kennes, Principal Verification & Validation Engineer Fredrik Ringqvist, and Senior Mechanical Engineer Simon Aleryd.

Sam Azadi, Viktor Larsson Rosén, Gothenburg, June 2026

List of Acronyms

Below is the list of acronyms that have been used throughout this thesis listed in alphabetical order:

atBCD	Active Transcutaneous Bone Conduction Device
AC	Alternating Current
ACT	Actuator Characterisation Tool
AF	Acceleration Factor
ALT	Accelerated Life Test(ing)
BC	Bone Conduction / Bone Conducted
BCD	Bone Conduction Device
CAD	Computer Aided Design
CHL	Conductive Hearing Loss
dB	Decibel
DC	Direct Current
FM	Failure Mode
FEA	Finite Element Analysis
NDA	Non-Disclosure Agreement
OFL	Output Force Level
RMS	Root Mean Square
RQ	Research Question

Nomenclature

Below is the nomenclature of indices, sets, constants, parameters, and variables used throughout this thesis.

Indices

i, j, k	Index for actuators

Sets

$\mathcal{A}$	Set of actuators	
$M(f)$	Set of repeated measurements at frequency f	–

Constants

R	Molar gas constant	J/(mol × K)

Parameters

E_a	Material activation energy	J/mol
f_n	Natural frequency	Hz
f_{test}	Test frequency range	Hz
f_{use}	Use frequency range	Hz
k_{total}	Total required stiffness	N/m
m	Active mass	kg
n_M	Material mechanical fatigue exponent	–

n_V	Material voltage stress exponent	–
T_g	Glass transition temperature	°C
T_C	Curie temperature	°C
T_{test}	Test temperature	K
T_{use}	Use temperature	K
V_{test}	Test voltage	V_{RMS}
V_{use}	Use voltage	V_{RMS}
h_{test}	Weekly testing usage	hours/week
h_{use}	Daily operational usage	hours/day

Variables

AF_M	Mechanical stress acceleration factor	–
AF_T	Thermal acceleration factor	–
AF_{Total}	Total acceleration factor	–
AF_V	Voltage acceleration factor	–
Y_{sim}	Simulated years	years
t_{test}	Required ALT duration	weeks
C	Capacitance	μF
C_{avg}	Average capacitance	μF
$C_{\Delta_{avg}}$	Average percentage change in capacitance	$\Delta\%$
$C_{RT_{avg}}$	Average capacitance in room temperature	μF
f	Frequency	Hz
$\tilde{m}(f)$	Median measurement	–
$m_{\text{extreme}}(f)$	Furthest measurement from median	–
N	Number of cycles to failure	–
$\text{OFL}_{\text{baseline}}(f)$	Pre-test OFL	dB
$\text{OFL}_{\text{24 recovery}}(f)$	Recovery OFL	dB
$\Delta\text{OFL}(f)$	Absolute difference in OFL	dB
$\Delta\text{OFL}_{\text{noise}}(f)$	Baseline measurement noise	dB
Q_ϕ	Quality factor (Q-factor)	–
R	Resistance	Ω
$\tan(\delta)$	Tangent loss	–
X	Reactance	Ω

Z	Impedance	Ω
Z_{avg}	Average impedance	Ω
$Z_{\Delta_{avg}}$	Average percentage change in impedance	$\Delta\%$
$Z_{RT_{avg}}$	Average impedance in room temperature	Ω
μ	Mean	–
σ	Standard deviation	–

Contents

List of Figures

List of Tables

1

Introduction

This chapter presents the background of the thesis, including an introduction to Cochlear and the work conducted by the company. Furthermore, the scope and aims of the thesis are introduced, together with the research questions intended to guide the project and be answered by the end of the work. Finally, the chapter outlines the limitations associated with the thesis.

1.1 Background

Founded in 1981 to commercialise Dr. Graeme Clark's 1978 breakthrough in multichannel cochlear implants, Cochlear Limited initially focused exclusively on sensorineural deafness (Cochlear, 2026b). The company significantly expanded its clinical scope into bone conduction devices (BCDs) in 2005 through the acquisition of Entific Medical Systems, the Swedish firm that pioneered the Baha system. This move integrated technology that had been clinically utilised since 1977 for patients with conductive hearing loss (CHL) or single-sided deafness (Martinez, 2021).

Modern bone conduction devices contain many mechanical and electronic components that must function reliably for long periods of time. The expected lifetime of Cochlear's BCDs is at least 10 years. A failure in any critical component can make the device unusable and require repair or replacement. For this reason, manufacturers perform lifetime testing to evaluate product durability. Currently, Cochlear relies on conventional lifetime testing carried out under normal operating conditions. This testing method requires very long test periods, with the existing setup running continuously, 24 hours a day, for approximately seven years to meet regulatory requirements. The process also involves regular maintenance, calibration, and complex measurements, while the final outcome remains uncertain for much of the testing period (Poggi, 2026).

Accelerated life testing (ALT) offers a more efficient alternative to conventional durability testing. By exposing the product to conditions more severe than normal operating environments, such as increased stress levels, higher usage cycles, intensified vibrations, or elevated electrical loads, failures can be replicated within a much shorter time frame (Nelson, 1980).

1.2 Aim

The primary aim of this thesis was to find accurate input data and develop an ALT method for Cochlear's active transcutaneous bone conduction device (atBCD) to detect long-term failure modes (FM):

- **Adhesive failure caused by ageing (FM2).**
- **Nylon thread-locker loosening caused by ageing (FM3).**
- **Piezoelectric behavioural change caused by ageing (FM4).**

This is performed in order to reduce the time needed compared to the current testing setup, as mentioned earlier. Cochlear BAS intends to use this method to support the development of future product generations.

Accelerated testing will be valuable for both engineering and business purposes. From an engineering perspective, it will enable more reliable predictions of long-term performance, support the validation of design changes, and help identify potential weaknesses early in the development process. From a business perspective, shorter testing times will reduce costs, improve return on investment, and allow new products to reach the market more quickly. In addition, ALT could also contribute to stronger regulatory compliance and help raise overall industry quality standards.

1.3 Research Questions

To help guide the thesis in the right direction, several research questions (RQs) were proposed together with company supervisor (Poggi, 2026):

1. **Which stressors most effectively accelerate these failure modes?**
2. **Can multiple stressors be combined in a single system without compromising validity?**
3. **How accurately does accelerated degradation correlate with the failure mode?**
4. **What inputs are required for the ALT?**
5. **How efficient can the ALT be scaled?**

1.4 Limitations

The first limitation was time. The project was carried out by two students over a relatively short period, from February to June, see Appendix A for the entire schedule. Because of the restricted time frame, the data from the completed ALT test will not be available. As a result, the project aims to provide comprehensive input data for the proposed ALT method and, time permitting, to commence testing. This solution is intended solely for internal use by Cochlear BAS and will not represent a finalised commercial solution.

In addition, the thesis was limited exclusively to the ALT of Cochlear BAS' atBCD. The work focused only on the specific long-term failure modes identified in

Section 1.2 as well as the overall performance of the actuator and will not address other aspects of the device.

Another important limitation was that the project was restricted to the resources and expertise available within Cochlear BAS and Chalmers. This includes access to technical knowledge, materials, and equipment. While both organisations provided substantial competence and infrastructure, the project lacked access to broader industry resources or alternative suppliers. As a result, the range of possible solutions and methods may be constrained by these capabilities.

Confidentiality and non-disclosure agreements (NDAs) represented another limitation of the project. Many of the tested components are subject to confidentiality restrictions and can therefore only be disclosed internally within Cochlear BAS. As a result, some detailed technical information has been omitted from this report.

For example, one failure mode was investigated during the majority of the project was excluded at a late stage due to these confidentiality constraints, although the associated data will be shared with Cochlear. This failure mode was originally designated as FM1 (Failure Mode 1), which explains why some calculations, figures and tables in this report skips FM1.

Lastly, financial resources represented a further limitation. Although the project did not operate under a fixed budget, the available financial resources were very limited.

2

Theory

A substantial amount of theory was required for this project due to its broad scope and multidisciplinary nature. The following chapter presents the theoretical background considered necessary for understanding the project, as well as for developing relevant methodologies and experimental approaches.

2.1 Product Development Framework

The development of a test concept relies on a structured, goal-oriented product development process. A foundational element of this framework is the requirement specification (Almefelt, 2024), which categorises product parameters into two distinct groups:

- **Requirements:** Essential conditions that a product must fulfil to function or to satisfy specific technical constraints.
- **Desires:** Non-essential features intended to enhance the user experience or overall product appeal.

During the early idea generation phases, these specifications act as a dynamic repository for structuring acquired knowledge, establishing the criteria for initial screening, and serving as the benchmark for prototype verification.

2.1.1 Concept Evaluation

Evaluating generated concepts requires a multi-staged approach to filter and refine ideas effectively:

1. **Qualitative Screening (Elimination Matrix):** A preliminary filter to exclude concepts that fail to meet fundamental requirements based on a set of pass/fail criteria.
2. **Comparative Screening (Pugh Matrix):** A systematic method for comparing concepts against a reference concept baseline. It evaluates relative performance across specific criteria to identify consistently strong designs and highlight explicit trade-offs.
3. **Quantitative Evaluation (Kesselring Matrix):** A weighted scoring system applied to finalist concepts. Each criterion is assigned a weight based on its relative importance to project objectives—often determined through pairwise comparison—allowing for a nuanced, mathematical selection of the optimal solution.

2.2 Hearing Loss

Normal hearing is divided into two sound transmission types, air conduction (AC) and bone conduction (BC). When a sound is heard through AC, the sound wave is transmitted to the inner ear's cochlea via the ear-canal, the Tympanic membrane, and the ossicles in the middle ear. Sounds perceived through BC consist of vibrations transmitted through the skull bone to the cochleae. The most common sound heard through BC is one's own voice, but BC can also pick up the surrounding sound field, or from a BC transducer (Reinfeldt, 2009).

Hearing loss can be categorised into three types: sensorineural, conductive, or a mixture of both (Mixed hearing loss). There is also single-sided hearing loss (SSHL), which means only one ear is affected by the hearing loss.

Sensorineural hearing loss (SNHL) occurs when the inner ear (cochlea) cochlear hair cells are damaged or do not work properly. Sounds are softer, but also difficult to understand, especially when it is noisy. The most common forms of SNHL are age-related hearing loss and noise-induced hearing loss. For these types of hearing loss, both AC and BC hearing are affected. Most SNHL can be treated with conventional AC Hearing aids, more severe SNHL cases may require cochlear implants.

Conductive hearing loss (CHL) occurs when damage to the outer ear or middle ear blocks sound vibrations from reaching your inner ear (cochlea). Ears may feel plugged and speech may sound muffled. Mixed hearing loss refers to a combination of CHL and SNHL. This means there may be damage in both the outer or middle and the inner ear (cochlea). Examples of conductive hearing losses are chronic infections in the middle ear.

Conductive and mixed hearing loss can be treated with medication, surgery, and AC hearing aids, however BC hearing aids can work better than AC or be the only alternative, such as a bone conduction implant (Reinfeldt, 2009).

2.3 Bone Conduction Hearing Solutions

Bone conduction devices (BCDs) have undergone significant development over the past 15–20 years. These devices provide an important rehabilitation alternative for patients with conductive or mixed hearing loss, as well as for individuals with single-sided deafness. A BCD operates by converting airborne sound into mechanical vibrations, which are transmitted through the skull bone to stimulate the cochleae of the inner ear. This transmission can be achieved through several different technical solutions, depending on the manufacturer and device design. BCDs can generally be divided into two main categories: direct drive and skin drive systems (Reinfeldt et al., 2022), see Figure 2.1.

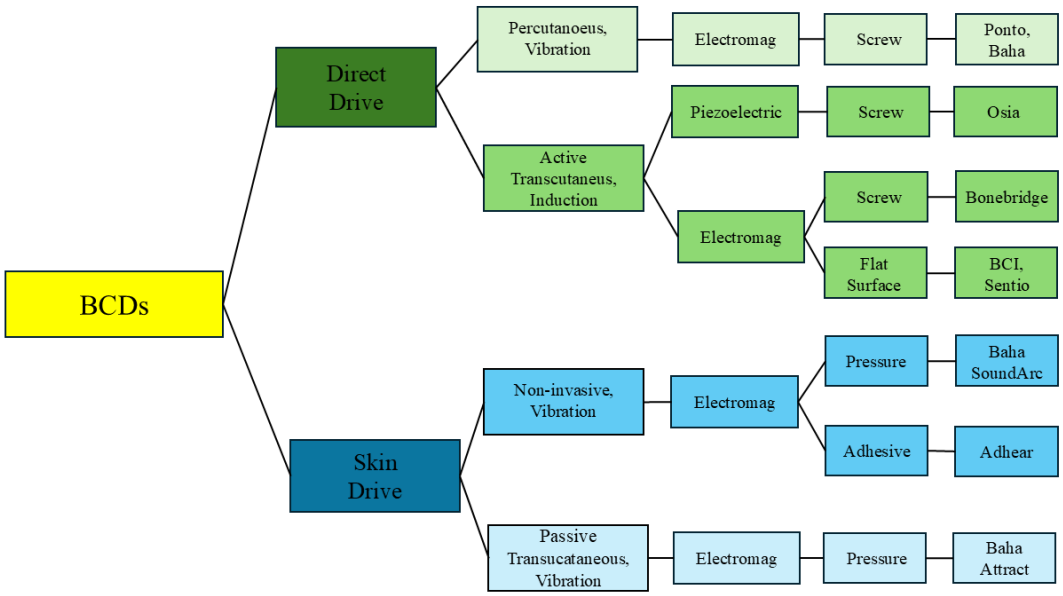

Figure 2.1: Types of BCDs. Inspired by Reinfeldt et al. (2022).

In direct drive systems, vibrations are transmitted directly to the skull bone through physical contact with an implanted component. In contrast, skin drive systems transmit vibrations through intact skin and soft tissue before reaching the bone. All non-invasive BCDs belong to the skin drive category, as the transducer is positioned externally and vibrations must pass through the skin rather than being delivered directly to the skull (Stenfelt and Goode, 2005).

In BC hearing aids, sounds are transmitted directly through the skull bone to the cochlea, more or less bypassing the outer and middle ear. BC hearing aid was first used as aid to defective hearing in the 17^{th} century using bone conduction rod devices (Berger, 1976). In the early 20^{th} century, electric BC transducers were first invented. However, these were pressed against the skin without contact to the bone, which often led to discomfort and pain. Moreover, they would also lose sound quality and sound transmission over time.

Early generations of non-invasive BCDs were associated with several practical drawbacks. Common issues included discomfort due to pressure on the skin, circulation problems, acoustic feedback, and reduced sound quality caused by attenuation in the soft tissue. Although modern devices have addressed many of these challenges, such limitations still exist to some extent.

To overcome these disadvantages, direct drive percutaneous solutions were introduced in the late 1970s (Håkansson et al., 1985). This development led to the creation of the BAHA (Bone Anchored Hearing Aid) system, which has since become the established standard within bone conduction hearing technology. Today, more than 300 000 patients worldwide use BAHA systems. In this design, the sound processor is attached to a titanium implant that penetrates the skin and is

anchored directly in the skull bone, enabling efficient vibration transmission (Reinfeldt et al., 2022). These systems are commercially available from manufacturers such as Cochlear, which manufactures it under the Baha product naming system (Cochlear Limited, 2026b), and Oticon Medical's Ponto system (Oticon Medical, 2026a). Despite the success in better sound quality and transmission, it still had some major drawbacks. Due to penetrating the skin, the penetration site requires lifelong daily care, with some patients developing skin problems, such as infections, which can require surgical revisions or reimplantation (Peñaranda et al., 2018; Reinfeldt et al., 2022). To address this, a new variant of a bone conduction implant was developed in 2003, featuring a transducer type called the Balanced Electromagnetic Separation Transducer (BEST) (Håkansson, 2003), together with a method for transmitting signals from an external audio processor to the implanted transducer. With this approach, the transducer does not penetrate the skin, instead, it is implanted under the skin and soft tissues (Reinfeldt et al., 2022; Håkansson et al., 2019). The BEST transducer technology is currently used in several commercial devices, such as Cochlear's Baha 6 (Reinfeldt, 2026).

Lastly, active transcutaneous BCD systems - where the skin remains intact and vibrations are transmitted directly to the bone - have gained increasing market share in recent years. Examples are the Osia system from Cochlear (Cochlear Limited, 2026a), Bonebrige by MED-EL (MED-EL, 2026), and Sentio from Oticon Medical (Oticon Medical, 2026b). These devices use an induction link to transmit signals across the skin to an implanted transducer, which is directly connected to the skull bone. Unlike most other BCDs, the Osia employs a piezoelectric transducer actuator, offering advantages such as improved magnetic resonance imaging (MRI) compatibility (Reinfeldt et al., 2022). When an electrical current is applied, the piezoelectric material physically bends and contracts. This makes the actuator generate mechanical vibrations, providing conducting output force in the human hearing frequency range.

2.4 Accelerated Life Testing

Accelerated life testing (ALT) provides a framework for quantifying the relationship between applied stress and time-to-failure, enabling extrapolation from accelerated test conditions to normal use conditions. These models are typically derived from physical, chemical, or empirical laws and are selected based on the dominant degradation mechanisms governing product failure (Nelson, 1990a).

In practice, ALT involves subjecting test units to elevated stress levels to induce failures more rapidly than under nominal operating conditions. The resulting data are used to establish a stress–life relationship, which forms the basis for predicting lifetime under use conditions. Figure 2.2 illustrates this principle. The time-to-failure t_f is modelled as a function of stress S, here represented by a generic relation $t_f = A \cdot G(S)$. Two stress levels are considered: a low (use) stress S_L and a higher (accelerated) stress S_H, with corresponding failure times t_{fL} and t_{fH}. Since failures occur more quickly at higher stress, $t_{fH} < t_{fL}$. The ratio between these lifetimes

defines the acceleration factor AF_{LH}, such that $t_{fL} = AF_{LH} \cdot t_{fH}$. This relationship enables extrapolation from accelerated test results at S_H to predict lifetime at S_L (Nelson, 1990b).

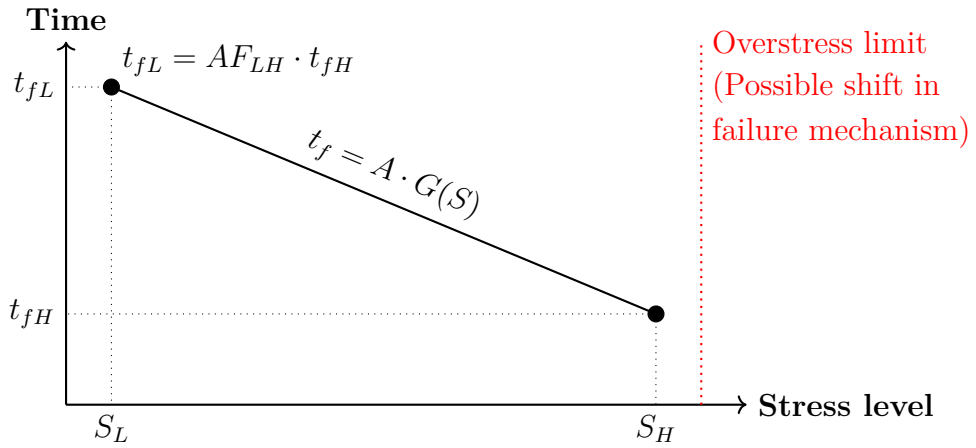

Figure 2.2: Schematic stress–life relationship in ALT.

The figure also highlights an overstress limit beyond which the assumed failure mechanism may change. Operation in this regime violates the model assumptions and can lead to invalid lifetime predictions. Therefore, accelerated stress levels must be chosen to ensure that the same underlying degradation mechanism governs both test and use conditions.

2.4.1 ALT Methods

According to Nelson (1990a), ALT methods are typically classified based on how stress is applied over time, with each approach offering different trade-offs in terms of statistical efficiency, experimental complexity, and modelling requirements. The selection of an appropriate method depends on factors such as the underlying failure mechanisms, available test duration, and resource constraints. Among the various ALT methods, the following three are the most commonly employed.

Constant-stress accelerated life testing applies fixed stress levels to different groups of test units, where each group is exposed to a single elevated stress level throughout the experiment. Failures are observed over time and used to model the relationship between stress and life via appropriate life–stress models, see Figure 2.3. This method provides straightforward statistical analysis and is considered the standard framework for accelerated testing due to its direct correspondence with classical life distribution models (Nelson, 1990a).

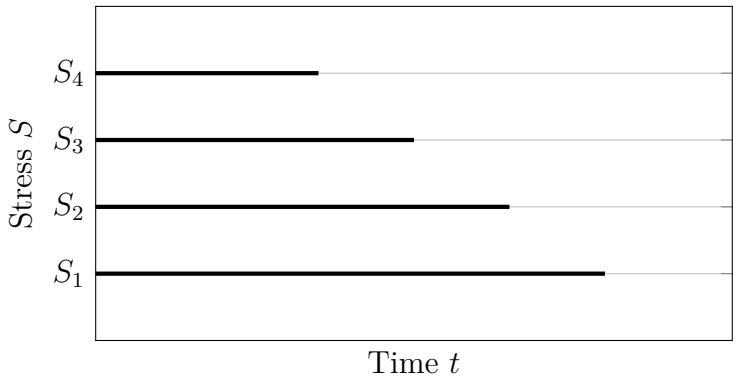

Figure 2.3: Constant stress ALT. Inspired by Zhao (2024).

Step-stress accelerated life testing subjects each test unit to a sequence of increasing stress levels over time. The stress is raised at predetermined time points if failure has not yet occurred, see Figure 2.4. This approach improves experimental efficiency by reducing the number of required specimens, but requires more advanced statistical treatment since the lifetime distribution depends on the cumulative exposure to multiple stress levels (Nelson, 1990a).

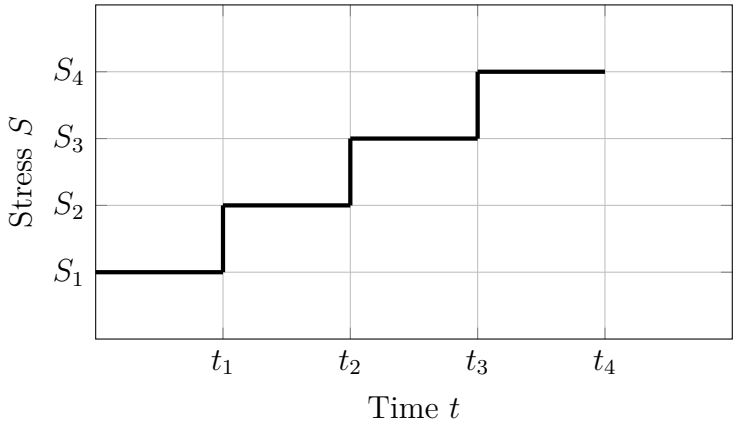

Figure 2.4: Step-stress ALT. Inspired by Zhao (2024).

Decreasing step-stress accelerated life testing begins with a high initial stress level and subsequently reduces the stress in a stepwise manner during the test, see Figure 2.5. Although less commonly applied, this method can be useful for studying early-life failures and screening effects, where high initial stress accelerates failure initiation while later lower stresses provide information closer to normal operating conditions (Nelson, 1990a).

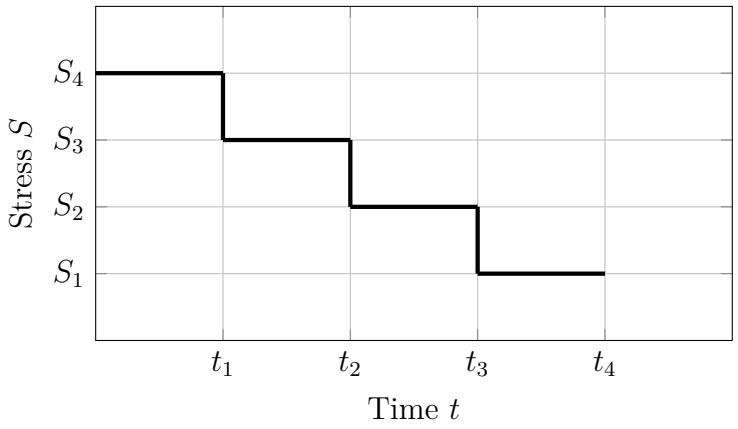

Figure 2.5: Decreasing step-stress ALT. Inspired by Zhao (2024).

2.4.2 ALT Models

ALT models provide the mathematical framework required to relate applied stress conditions to time-to-failure. These models enable extrapolation from accelerated test conditions to normal use conditions by describing how stress influences the dominant failure mechanisms (Nelson, 1990a). Acceleration is often quantified using acceleration factors (AF), which express how much faster degradation occurs under test conditions compared to use conditions.

Temperature acceleration is governed by thermally activated processes such as diffusion and chemical degradation. Based on the Arrhenius relationship (NIST, 2026a), the acceleration factor is shown in Equation 2.1.

$$AF_T = \exp\left[\frac{E_a}{R}\left(\frac{1}{T_{use}} - \frac{1}{T_{test}}\right)\right] \tag{2.1}$$

Where:

- E_a = Activation energy [J/mol]
- R = Molar gas constant [J/mol × K]
- T_{use} = Use temperature [K]
- T_{test} = Test temperature [K]

Electrical stress acceleration follows the inverse power law model, commonly used for dielectric and electromigration-related failures, (Hottinger Bruel & Kjaer , 2025), see Equation 2.2.

$$AF_V = \left(\frac{V_{test}}{V_{use}}\right)^{n_V} \tag{2.2}$$

Where:

- n_V = Voltage stress exponent [-]
- V_{test} = Test voltage [V]
- V_{use} = Use voltage [V]

Mechanical acceleration describes fatigue processes driven by stress, strain, or vibration amplitude. For piezoelectric systems, mechanical loading is directly related

to applied voltage (Hottinger Bruel & Kjaer , 2025), see Equation 2.3.

$$AF_M = \left(\frac{G_{test}}{G_{use}}\right)^{n_G} = \left(\frac{\sigma_{test}}{\sigma_{use}}\right)^{n_M} = \left(\frac{V_{test}}{V_{use}}\right)^{n_V} \tag{2.3}$$

Where:

- n_G = Vibration acceleration exponent [-]
- n_M = Mechanical stress exponent [-]
- n_V = Voltage stress exponent [-]
- G_{test} = Test vibration acceleration $[m/s^2]$
- G_{use} = Use vibration acceleration $[m/s^2]$
- σ_{test} = Test stress [Pa]
- σ_{use} = Use stress [Pa]

This formulation captures the acceleration of crack growth and structural degradation due to increased mechanical loading.

The Peck model is commonly used for humidity-related failures, such as corrosion and insulation degradation (Schenkelberg, 2026), see Equation 2.4.

$$AF_{RH} = \left(\frac{RH_{test}}{RH_{use}}\right)^{n_{RH}} \tag{2.4}$$

Where:

- n_{RH} = Humidity stress exponent [-]
- RH_{test} = Test relative humidity [%]
- RH_{use} = Use relative humidity [%]

In practice, multiple stress factors may act simultaneously. The total acceleration factor represents the combined effect of all applied stresses. Assuming independence between stressors, the overall acceleration can be expressed as the product of individual factors as shown in Equation 2.5, inspired by Lakhloufi (2026).

$$AF_{Total} = AF_T \times AF_V \times AF_M \times AF_{RH} \tag{2.5}$$

2.5 TU-1000 Skull Simulator

Introduced in 1989 by Prof. Bo Håkansson, the TU-1000 skull simulator shown in Figure 2.6 is designed to mimic the inertial properties of a human skull, specifically approximating a mass of 2.5 kg (Håkansson and Carlsson, 1989). Functioning as a standardized attachment platform for bone-anchored hearing devices, the system acts as an accelerometer that converts mechanical force output into measurable electrical signals.

Figure 2.6: TU-1000 skull simulator.

However, when applied to this project, this conventional simulator may underestimate the true mechanical stresses experienced by an atBCD actuator in situ (Cochlear, 2026a), since it only approximates a skull mass of 2.5 kg. Lastly, Cochlear requested that the skull simulator should not be exposed to temperatures above room temperature during testing.

2.6 Adhesive Element (FM2)

An adhesive is a material used to join two or more surfaces together by creating a bond that resists separation. Most modern adhesives are synthetic and primarily based on polymers. The polymer structure provides mechanical strength, flexibility, and the ability to interact effectively with bonded surfaces (Kinloch, 1987; Pike, 2026). Adhesives mainly bond materials through two mechanisms: mechanical interlocking and chemical adhesion. Mechanical interlocking occurs when the adhesive flows into surface irregularities of the substrate and creates a physical connection after curing (Kinloch, 1987). Chemical adhesion is instead governed by intermolecular interactions between the adhesive and the bonded surface. These interactions can include strong primary chemical bonds as well as weaker secondary interactions (Bal-Ozturk et al., 2021).

2.6.1 Ageing and Failure Mechanisms

Several adhesive-related failure modes can occur due to ageing, including debonding, delamination, creep, and fatigue-related degradation. Of particular relevance to this project is how elevated temperatures and the mechanical stresses generated by the voltage-driven actuator can reduce adhesive strength and eventually lead to debonding. Particular interest is also placed on how the adhesive behaves when exposed to temperatures above its glass transition temperature, T_g, since the ALT methodologies often aim to use temperatures as high as possible while avoiding excessive degradation.

Debonding occurs when the adhesive no longer adheres to the bonded surface. This can occur when the physical, chemical, or mechanical forces maintaining the bond are weakened or broken due to mechanical loading or environmental exposure (Kinloch, 1987).

2.6.2 Temperature Effects on Adhesives

Temperature strongly influences both the curing and long-term ageing behaviour of adhesives. Increased temperature generally increases molecular mobility, allowing the adhesive to spread more effectively and accelerating curing or polymerization reactions. However, excessively high temperatures can instead cause thermal degradation, reducing the mechanical integrity, structural stability, and long-term reliability of the adhesive (Frascio et al., 2025).

According to a study conducted by Park et al. (2025), repeated exposure to elevated temperatures can cause thermal degradation in adhesives, resulting in chain scission, volatilization of decomposition products, and reduced mechanical integrity. Thermogravimetric analysis performed during repeated thermal cycling between room temperature and 180 °C demonstrated cumulative mass loss in the adhesive material. An initial rapid decrease in mass was observed during the first thermal cycle, likely caused by evaporation of residual moisture or impurities. Subsequent cycles showed a slower and more stable degradation behaviour. After ten thermal cycles, the adhesive specimen had lost approximately 2.7% of its original mass, indicating progressive thermal degradation caused by repeated exposure to elevated temperatures.

Furthermore, repeated exposure to excessively high temperatures can decrease performance accelerate degradation (Mravljak and Sernek, 2011). At elevated temperatures, additional cross-linking can occur within the polymer structure, restricting molecular motion. As a result, the adhesive gradually changes from a softer and more ductile material into a harder and more brittle one. Although the material may become stiffer and stronger, it also becomes more susceptible to cracking and mechanical failure. The elongation at break can decrease significantly, reducing the material's ability to deform before fracturing. In addition, thermal degradation can alter the internal structure of the adhesive, reducing long-term mechanical integrity and reliability (Ishii et al., 2021).

Lastly, thermal cycling is another important ageing mechanism that can contribute to adhesive failure due to differences in thermal expansion between the adhesive and the bonded materials. During heating and cooling, the materials expand and contract at different rates, creating stresses at the adhesive-substrate interface. These stresses are often highest near the edges of the bond, where the adhesive can deform more freely. Repeated thermal cycling can therefore gradually accumulate interfacial damage and contribute to long-term debonding and failure (InCure Lab, 2026).

2.7 Nylon Thread-locker Element (FM3)

Nylon thread locking elements are frequently applied as patches or coatings on male fastener threads. These act as highly versatile prevailing torque mechanisms, particularly in assemblies that do not use nuts. This is particularly relevant when clamping a flat component directly down onto a more solid, internally threaded base. During installation, the male threads and the female tapped threads compress the polyamide material. Because the polymer conforms to the mating threads, it fills the axial play and creates a jamming action that significantly increases the prevailing torque, providing robust resistance against vibration-induced self-loosening (Woo, 2019).

This resistance is critical for configurations subjected to continuous dynamic forces. In Cochlear's assembly, a 6-screw circular pattern is used to securely clamp the flat component. Since the flat component experiences vibrations from the piezoelectric element, these vibrations significantly increase the likelihood of causing screw loosening (Junker, 1969). Despite their reliability under static conditions, nylon thread lockers in harsher vibrational environments are susceptible to ageing and mechanical degradation much faster. This degradation typically manifests as polymer ageing, yielding, or a severe drop in the push-back force required to maintain contact pressure (Bhattacharya et al., 2010).

The two primary failure mechanisms investigated in this report for nylon thread-locking elements are thermal degradation and mechanical relaxation (Poggi, 2026). High operating temperatures accelerate polymer ageing, thereby reducing the material's elastic recovery. Meanwhile, mechanical relaxation dictates that compressive loading and cyclical stress from vibrations accelerate creep, leading to loss of prevailing torque.

2.7.1 Loosening of Screws due to Ageing (Creep)

Creep is defined as the progressive, time-dependent plastic deformation of a solid material under mechanical stress.

When subjected to compressive forces from the mated threads and vibrations from the flat component, the polyamide material slowly undergoes creep, permanently losing its original geometry. This time-dependent deformation alters the prevailing

torque (T_p), which is a critical component of the total tightening torque (T) required to maintain joint integrity. The relationship governing the total torque in a prevailing-torque fastener system is shown in Equation 2.6 (Bickford, 1995).

$$T = K \cdot D \cdot F + T_p \tag{2.6}$$

Where:

- T = Total required tightening torque [Nm]
- K = Friction/Nut factor [-]
- D = Nominal fastener diameter [m]
- F = Preload to be used in the assembly [N]
- T_p = Prevailing torque [Nm]

As the nylon insert slowly deforms over time, the contact pressure decreases, causing T_p to gradually reduce (Bickford, 1995). In bolted joints exposed to vibrations, this reduction in preload leads to repeated small movements and cyclic strain in the joint (Stephen et al., 2017). Once the nylon has permanently deformed, it can no longer maintain sufficient pressure against the threads to compensate for small gaps and clearances. Together with thermal expansion effects and repeated movement of the clamped flat plate, the reduced bolt tension eventually causes the screws to self-loosen, significantly reducing the structural stability of the joint.

2.8 Piezoelectric Element (FM4)

Piezoelectric ceramics, commonly referred to as piezos or PZT materials, are dielectric materials capable of converting electrical energy into mechanical deformation and vice versa. When subjected to an electric field, the material changes shape, while mechanical stress generates an electrical response. Due to their structure, consisting of two conductive electrodes separated by a dielectric ceramic material, piezoelectric elements electrically behave similarly to capacitors. As a result, they can store electrical charge and exhibit measurable capacitance (Hong et al., 2016).

Piezos are generally categorized into soft and hard materials, which differ in their electrical and mechanical behaviour. As shown in Table 2.1, soft PZT materials exhibit higher permittivity, larger piezoelectric constants, and stronger electromechanical coupling. However, they also exhibited higher dielectric losses and lower mechanical stability. In contrast, hard PZT materials provided better stability, lower losses, and higher mechanical quality factors, but at the cost of reduced sensitivity.

Table 2.1: Comparison between soft and hard PZT ceramics. Inspired by APC International (2026).

Characteristic	Soft Ceramic	Hard Ceramic
Curie Temperature Sensitivity	More	Less
Permittivity	Higher	Lower
Dielectric Constants	Larger	Smaller
Dielectric Losses	Higher	Lower
Electrical Resistance	Higher	Lower
Polarisation Behaviour	Easier	Harder
Electromechanical Coupling Factors	Larger	Smaller

2.8.1 Frequency-Dependent Electrical Properties

The key electrical properties that will be of particular interest in this study are capacitance, resistance, impedance, phase angle, and quality factor.

According to Electronics Tutorials (2026c), in an alternating current (AC) circuit, the complex impedance (Z) represents the total opposition to current flow and is frequency dependent. It combines the resistive component (R) and the reactive component (X) into a single complex quantity.

For an ideal resistor, the effects of capacitance are negligible, meaning its behaviour is independent of frequency. Consequently, the impedance of a pure resistor is equal to its resistance ($Z_C = R_C$), and there is no phase difference between voltage and current, resulting in a phase angle of 0°.

In contrast, reactive components introduce a phase shift between voltage and current. For capacitive elements, which are of primary interest in this work due to the behaviour of piezoelectric materials, the reactance is 90° out of phase with the resistive component. As a result, resistance and reactance cannot be combined through arithmetic addition.

Unlike resistance, reactance depends on frequency. For a capacitor, this is referred to as capacitive reactance (X_C), which describes the opposition to AC current and decreases with increasing frequency. The capacitive reactance is given by Equation 2.7 from Electronics Tutorials (2026a):

$$X_C = \frac{1}{2\pi f C} \tag{2.7}$$

Where:

- X_C = Capacitive reactance [Ω]
- f = Frequency [Hz]
- C = Capacitance [F].

As shown in Equation 2.7, the reactance is inversely proportional to both frequency and capacitance.

Accordingly, the total impedance is obtained from the vector combination of resistance and reactance:

$$Z_C = \sqrt{R_C^2 + X_C^2} \tag{2.8}$$

The phase angle (ϕ) describes the angular relationship between the impedance vector and the resistive component. It can be expressed through the following trigonometric relations (Electronics Tutorials, 2026c):

$$\tan \phi = \frac{X_C}{R_C} \tag{2.9}$$

$$\sin \phi = \frac{X_C}{Z_C} \tag{2.10}$$

$$\cos \phi = \frac{R_C}{Z_C} \tag{2.11}$$

These relationships can also be visualized using an impedance triangle, as illustrated in Figure 2.7.

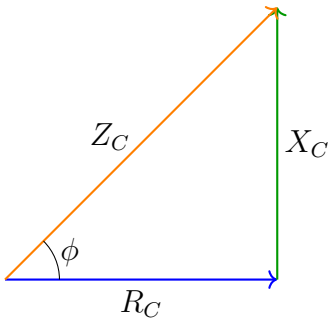

Figure 2.7: Impedance triangle. Inspired by Electronics Tutorials (2026d).

Lastly, in an AC system, the Quality factor (Q or Q-factor), Q_ϕ, describes how efficiently a capacitor stores energy relative to the energy dissipated as heat due to resistance. A higher Q_ϕ indicates lower losses and more efficient energy storage. The quality factor is defined in Equation 2.12 (Electronics Tutorials, 2026b).

$$Q_\phi = \frac{X_C}{R_C} = -\tan(\phi) \tag{2.12}$$

Where:

- Q_ϕ = Quality factor [-]
- X_C = Capacitive reactance [Ω]
- R_C = Resistance [Ω]

- ϕ = Phase angle [°]

The relationship between Q_ϕ and $\tan(\phi)$ becomes evident from the impedance triangle presented in Figure 2.7.

2.8.2 Thermal Effects on Piezoelectric Materials

Soft PZT piezoelectric materials are particularly sensitive to temperature changes. Therefore, the following sections summarise the temperature-dependent behaviour of soft PZT ceramics primarily based on a NASA study investigating how important material properties vary with temperature. This analysis was necessary to identify which properties could be affected during heating and to determine suitable temperature ranges for the ALT.

One of the most important parameter that was considered during the project was the Curie temperature (Azhirnian, 2026; Poggi, 2026). This is the temperature at which a piezoelectric ceramic undergoes a phase change from a ferroelectric state to a paraelectric state. Below the Curie temperature, the PZT ceramic is in the ferroelectric phase, meaning its internal dipoles are aligned in an ordered and polarised structure. This alignment is what enables the material to exhibit piezoelectric behaviour. However, when the temperature rises above the Curie temperature, the PZT ceramic transitions into the paraelectric phase. In this state, the dipoles lose their alignment and become randomly oriented. As a result, the material loses its polarisation, a process commonly referred to as depolarisation (Ling, 2023). For PZT-5A, no Curie temperature was observed within the investigated range, indicating stable ferroelectric behaviour. In contrast, PZT-5H exhibited a Curie temperature around 180°C, beyond which the material transitioned to a paraelectric state and lost its piezoelectric functionality (Hooker, 1998).

Another important parameter is permittivity. It describes how a material responds to an electric field and influences the resulting electric displacement (Ellingson, 2018). The relative permittivity (dielectric constant) is shown in the Equation 2.13 below.

$$\varepsilon_r = \frac{\varepsilon}{\varepsilon_0} \tag{2.13}$$

Where:

- ε = permittivity of the material
- $\varepsilon_0 = 8.854 \times 10^{-12}$ C V^{-1}m^{-1} (permittivity of vacuum (Moldoveanu and David, 2021))

This dimensionless quantity reflects how effectively a material stores electrical energy compared to free space (McKeen, 2012a).

The report by Hooker (1998) showed that the dielectric constant of soft PZT materials increased with temperature. The study evaluated material behaviour in the range of -150 °C to 250 °C and reported that all tested materials exhibited their lowest dielectric constant at approximately -150 °C, followed by a steady increase as temperature increased.

The dissipation factor (tan loss/dielectric loss), ($\tan\delta$), was also investigated in the referenced study. This parameter quantifies the conversion of electrical energy into heat within a dielectric material and is strongly dependent on both temperature and frequency (McKeen, 2012b). It can be calculated using Equation 2.14.

$$\tan\delta = \frac{1}{\tan\phi} = \frac{1}{Q_\phi} \tag{2.14}$$

For PZT-5A, dielectric losses remained relatively constant across low frequencies (100 Hz to 10 kHz), but increased significantly at higher frequencies (100 kHz). In contrast, PZT-5H exhibited peak losses near its Curie temperature, with losses increasing as frequency increased (Hooker, 1998).

Moreover, electrical resistivity was found to decrease with increasing temperature for soft PZT materials. For PZT-5A, this decrease was gradual across the temperature range. In contrast, PZT-5H exhibited a minimum resistivity near its Curie temperature, followed by an increase at higher temperatures (Hooker, 1998). At high power operation, soft PZT materials were also reported to exhibit resistive behaviour, leading to self-heating. This effect could ultimately result in depolarisation and loss of functionality (Yujie, 2025).

Additionally, soft PZT materials were found to be highly polarisable, although their remanent polarisation decreased with increasing temperature. For PZT-5A, polarisation reached its maximum near room temperature and gradually diminished as temperature increased. PZT-5H exhibited a more abrupt transition. Above approximately 170°C, the material became thermally depolarised and no longer exhibited measurable piezoelectric behaviour (Hooker, 1998).

Furthermore, the electromechanical coupling factor describes the efficiency of energy conversion between electrical input and mechanical output (Uchino, 2012). This parameter decreases with increasing temperature. For PZT-5H, the coupling factor decreased rapidly above 150 °C and approached zero near 170 °C due to depolarisation. PZT-5A showed a more gradual reduction, maintaining functionality over a wider temperature range.

The power consumption of a piezoelectric actuator under excitation is another relevant parameter. It is given by:

$$P = \pi C f U^2 \tag{2.15}$$

Where:

- P = power [W]
- C = capacitance [F]
- f = frequency [Hz]
- U = peak-to-peak voltage [V]

This relationship highlights that increasing capacitance or voltage can increase power dissipation, contributing to heating and accelerated degradation (Hooker, 1998).

3

Method

Several methods were used throughout this project. At its core, the work followed a data-driven product development approach based on the methodology described by Ulrich and Eppinger (2015). Building upon this framework, the developed experimental methods for each investigated failure mode (FM) are presented in the following sections. It should be noted that the structure and order of this chapter reflect the chronological order in which the experiments were developed and started.

3.1 Concept Generation

The idea generation phase prioritised early practical testing over a prolonged theoretical phase, given the physical constraints, available resources, and the project's timeline. Concepts were generated by analysing existing tests, combining historical testing methods, and conducting dedicated brainstorming sessions, as well as creating a requirement specification. Each concept was paired with a preliminary measurement method. In total, 26 initial concepts were generated, encompassing both simple design variations and unconventional approaches.

3.2 Iterative Screening and Evaluation

The evaluation process followed an iterative cycle of comparison, refinement, and reassessment, as illustrated in Figure 3.1.

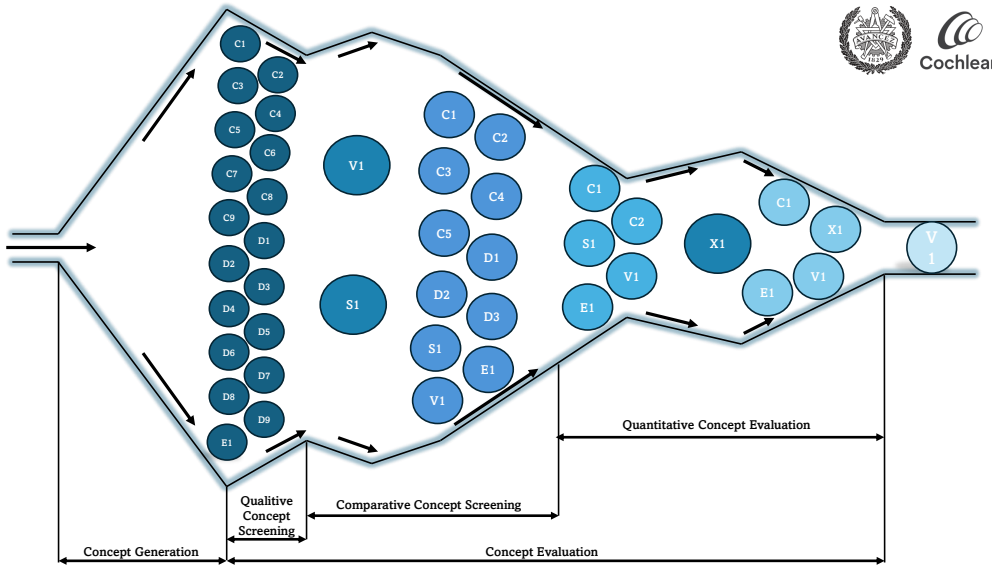

Figure 3.1: Concept evaluation process. Inspired by Ulrich and Eppinger (2015).

3.2.1 Qualitative Concept Screening

An elimination matrix was applied to the 26 concepts using five core criteria:

1. Provides conditions representative of the failure mode causes.
2. Stresses the relevant failure mode.
3. Allows controlled and adjustable test conditions.
4. Enables detection and measurement of failure onset/progression.
5. Can be executed without excessive setup risk or resource demands.

Concepts were marked based on fulfilment (+/-), need for information (?), or need for specification verification (!). The complete elimination matrix is provided in Appendix E.1.

3.2.2 Comparative Concept Screening

A Pugh matrix, see Appendix E.2, was used across three evaluation rounds. Concepts were scored as +1 (better), 0 (equal), or −1 (worse) against a shifting reference point.

- Round 1 Reference: The current 7-year long-term accelerated life testing method.
- Round 2 Reference: A concept that achieved a moderately above-average score in Round 1.
- Round 3 Reference: A concept demonstrating consistently strong performance across both prior rounds.

3.2.3 Quantitative Concept Evaluation

The finalist concepts were evaluated using a Kesselring matrix, see Appendix E.3. The criteria used were*multi-mode efficiency*, *performance for each FM*, *fidelity & validity*, *variance*, and *cost & efficiency*. The weight of each criterion was determined

via a pairwise comparison matrix (scored 1.0 for more important, 0.5 for equal, and 0 for less important). Raw scores were summed and normalised to produce a percentage-based weighting across three refinement iterations, as shown in Table 3.1.

Table 3.1: Pairwise comparison of Kesselring criteria weight.

	Multi-modes efficiency	Performance (FM1)	Performance (FM2)	Performance (FM3)	Performance (FM4)	Fidelity & Validity	Variance	Cost & Efficiency	Score	Weight
Multi-modes efficiency	0,5	0	0	0	0	0	0	1	**1,5**	**0,05**
Performance (FM1)	1	0,5	1	1	0	0,5	1	1	**6**	**0,19**
Performance (FM2)	1	0	0,5	0,5	0	0,5	1	1	**4,5**	**0,14**
Performance (FM3)	1	0	0,5	0,5	0	0,5	1	1	**4,5**	**0,14**
Performance (FM4)	1	1	1	1	0,5	0,5	1	1	**7**	**0,22**
Fidelity & Validity	1	0,5	0,5	0,5	0,5	0,5	1	1	**5,5**	**0,17**
Variance	1	0	0	0	0	0	0,5	1	**2,5**	**0,08**
Cost & Efficiency	0	0	0	0	0	0	0	0,5	**0,5**	**0,02**
									32	

3.3 Data for Failure Modes

To construct a framework for the Accelerated Life Testing (ALT), it was necessary to establish the parameters of the actuator and identify the specific thermodynamic, mechanical and electrical constants of its components.

The data required to calculate the Acceleration Factors (AF) for the FMs fell into two categories:

- **Standard operational inputs:** The normal environmental and electrical conditions the actuator experiences during daily use, including operating temperature (T_{use}), operational voltage (V), and average daily usage hours (h_{use}).
- **Material parameters:** The physical properties of the materials, specifically activation energies (E_a), voltage and mechanical acceleration exponents (n), glass transition temperatures (T_g) and the piezoelectric element's Curie temperature (T_c).

3.4 TU-1000 Skull Simulator Modelling

The limitations presented in Section 2.5 regarding the TU-1000 skull simulator highlighted the need for an alternative mounting model capable of more accurately replicating the boundary conditions of the human head while also tolerating potentially elevated temperatures during ALT experiments. The primary goal of this step was to determine the adequacy of the existing simulator as an environment for ALT.

Specifically, this simulation acted as a decision gate: if the TU-1000 induced internal stress deviations greater than $\approx 3\%$ compared to the 6 kg human skull approximation, it would be deemed insufficient for high-fidelity testing. In such a case, a custom mounting interface would need to be developed to provide the necessary inertial resistance. This ensured that the ALT could be conducted in a stable, repeatable environment that accurately reflected the mechanical loads encountered.

The TU-1000's internal mechanics were approximated using a 50 g central weight supported by a suspension system, as illustrated in Figure 3.2. To reflect the device's internal suspension, the total required stiffness, k_{total}, was derived from the observed natural frequency $f_n \approx 50$ Hz (Cochlear, 2026a) and the active mass $m = 0.05$ kg.

$$k_{total} = m \cdot (2\pi f_n)^2 \tag{3.1}$$

Where:

- k_{total} = Total required stiffness [N/m]
- m = The active mass [kg]
- f_n = Natural frequency [Hz]

$$k_{total} = 0.05 \text{ kg} \cdot (2\pi \cdot 50 \text{ Hz})^2 \approx 4935 \text{ N/m}$$

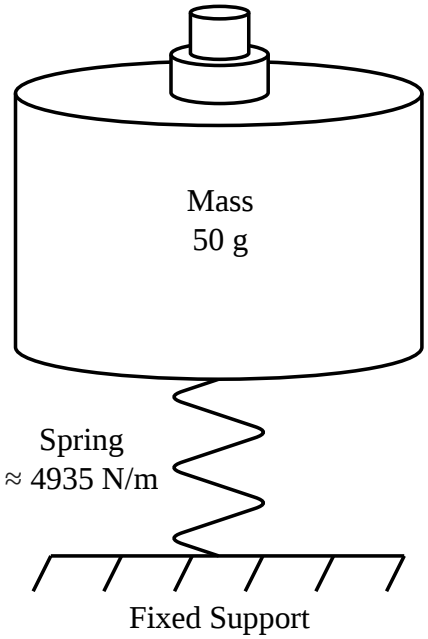

Figure 3.2: Skull simulator spring-mass-damper system.

3.5 Rigid Mounting Modelling

To transition from theoretical skull simulator models to a practical test fixture for the ALT, a series of FEA simulations were conducted to design a rigid mounting

interface. The goal was to identify a mounting configuration that replicated real-world stress conditions while keeping size and scalability in mind.

3.5.1 Volumetric Mass Convergence Study

A parametric study was performed to determine the minimum mass required to achieve stress convergence. Brass was selected as the primary material for the mounting blocks due to its high density ($\rho \approx 8500$ kg/m^3) and machining properties.

The simulation evaluated eight cylindrical geometries, with masses ranging from 25 g to a 6 kg reference. For each configuration, the following metrics were extracted:

1. **First Modal Resonance [Hz]:** To ensure the mounting did not introduce unwanted resonances near the 400 Hz stable frequency.
2. **Peak Equivalent (von Mises) Stress [MPa]:** The absolute maximum stress recorded on the piezoelectric element.
3. **Surface Stress [MPa]:** The stress concentration specifically located at the piezoelectric element's visible top surface.

3.5.2 Comparative Verification

The results from the physical brass mounting simulations were compared against the baseline values established in the skull simulator model (Peak Stress: 1.6528 MPa, Surface Stress: 1.3104 MPa). Convergence was defined as the point where further increases in mass yielded less than a $\approx 3\%$ change in internal stress, ensuring that the selected mounting provides a stable and repeatable environment for long-term evaluation.

3.5.3 Sensitivity Analysis of Boundary Stiffness

Using the established 150 g brass mounting geometry as a baseline, see Section 4.5, the mounting was coupled to the global coordinate system via a spring. Five boundary conditions were simulated at an operational frequency of 400 Hz:

- A theoretical "fixed support" that has infinite stiffness.
- Variable spring constants ranging from high stiffness (60000 N/m) down to low stiffness (60 N/m), including the specific stiffness derived for the skull simulator (4935 N/m).

This analysis aimed to determine whether the mechanical compliance of the fixture's attachment to the test chamber would influence the stress concentrations within the piezoelectric surface.

3.6 Rigid Mounting Solution

The 150 g brass mounting configuration was selected for physical prototyping. This mass was identified as the optimal threshold where the piezoelectric surface stress stabilizes, effectively replicating the boundary conditions while remaining scalable and compatible with the ALT environmental chamber. To support parallel testing of multiple actuators, four mounting units were manufactured.

3.6.1 Design and Manufacturing Process

The mounting solution was designed using a computer-aided design (CAD) program CREO. As shown in Figure 3.3, a height of 15.2 mm and a diameter of 40 mm were selected to achieve the target mass, see Appendix F.1 for technical drawings.

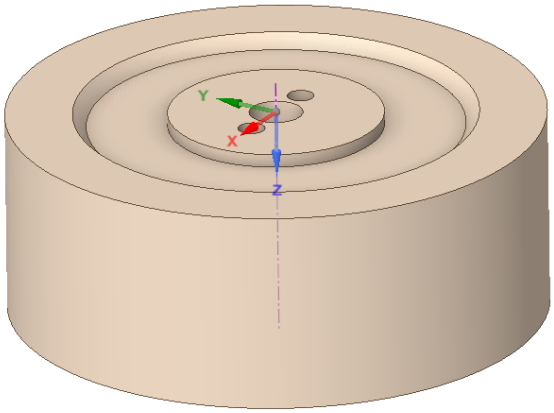

Figure 3.3: CAD design of the rigid mounting solution for actuators $\mathcal{A}_{i,j}$.

The design utilised a stepped-cylindrical geometry. Key features of the design included:

- **Interface Surface:** The top interface featured a recessed ϕ28 mm seating area and a central ϕ16 mm pedestal to ensure uniform stress distribution at the actuator-mounting interface.
- **Mechanical Fastening:** Two ϕ2 mm holes were included to accommodate the actuator base. An M4 threaded bore was machined into the centre of the mounting to secure the actuator via an M4 screw, ensuring a rigid mechanical coupling.

Free-machining brass (C360) was selected as the material. The physical prototypes were manufactured using subtractive manufacturing by the thesis' supervisor (Poggi, 2026):

1. **Turning:** The primary cylindrical profiles were produced on a manual lathe. This process ensured concentricity and allowed for a high-quality surface finish on the mounting face.
2. **Drilling and Tapping:** A vertical drill press was used to create the central hole and the ϕ2 mm accommodation holes, followed by creating the internal

threads required for actuator coupling.

3.6.2 Accelerometer Integration

To be able to monitor an actuator performances during testing, an accelerometer was required. A Dytran 3055D3 accelerometer with a removal base was picked due to performance and availability, see Figure 3.4. The geometry of the mounting also had to be changed to accommodate the sensor, see Appendix F.2 for technical drawings.

Figure 3.4: Dytran 3055D3 accelerometer with its base.

Furthermore, the raw data acquired from the accelerometer needs to be derived into the Output Force Level (OFL). This conversion accounts for the accelerometer having a sensitivity of 0.5 V/g and the mass of the active weight being 250 g (0.25 kg). The OFL is calculated as follows (Azhirnian, 2026):

$$\text{OFL} = \text{dBV} + 20 \cdot \log_{10}\left(\frac{0.25 \cdot 9.81}{0.5}\right) \tag{3.2}$$

Where:

- OFL = Output Force Level [dB]
- dBV = Raw accelerometer output voltage level [dBV]
- 0.25 = Mass of the active weight [kg]
- 9.81 = Acceleration due to gravity [m/s^2]
- 0.5 = Accelerometer sensitivity [V/g]

Note that the multiplier of 20 in Equation 3.2 is standard for amplitude quantities like voltage and force. Because physical power is proportional to the square of the amplitude, the traditional decibel multiplier of 10 is mathematically doubled when measuring amplitude ($10 \cdot \log_{10}(x^2) = 20 \cdot \log_{10}(x)$).
This calculation simplifies to adding a constant system gain to the raw signal:

$$\text{OFL} = \text{dBV} + 13.8116 \tag{3.3}$$

Where:
- 13.8 = Derived constant gain factor [dB]

To quantify the mounting's performance difference, the absolute difference in OFL is calculated, denoted as ΔOFL. This metric evaluates the physical deviation from a baseline state by normalising the TU-1000 measurements to zero across the entire frequency spectrum, making it easier to isolate and observe relative performance shifts.

3.7 Piezoelectric Element Overstress Limit Test (FM4)

The purpose of this experiment was to evaluate how heat affects the polarisation of the piezo and to identify the temperatures at which these changes occur by analysing its impedance and capacitance. The results will be used as input parameters for the subsequent ALT.

3.7.1 Design and Planning

The primary objective of this experiment was to investigate the effect of temperature on piezoelectric elements in practice, building on the theoretical framework presented in Section 2.8.2. By combining experimental observations with theory, the aim was to determine an appropriate temperature range for the ALT.

Temperature was identified as a critical test parameter. It needed to be sufficiently high to accelerate ageing, while remaining below levels that would cause significant depolarisation and degrade piezoelectric performance. Establishing this balance was therefore essential.

Three piezos were provided for the study. These samples were equipped with heat-resistant wiring and soldered connections, allowing them to withstand elevated temperatures during testing. The experimental procedure involved initially measuring the piezoelectric elements before heating, followed by controlled heating in an oven for specified time intervals. After each heating cycle, impedance and capacitance measurements were recorded, as these parameters are directly related to the polarisation state of the material.

The result gathered in this test was averaged for each measuring temperature and presented as a percentage of change relative to the baseline (RT) and was calculated using Equation 3.4-3.5.

$$Z_{\mathrm{RT_{avg}}} = \frac{Z_{avg} - Z_{\mathrm{RT_{avg}}}}{Z_{\mathrm{RT_{avg}}}} \times 100 \tag{3.4}$$

$$C_{\mathrm{RT_{avg}}} = \frac{C_{avg} - C_{\mathrm{RT_{avg}}}}{C_{\mathrm{RT_{avg}}}} \times 100 \tag{3.5}$$

3.7.2 Measuring Instrument

The impedance measurements were conducted using the KEYSIGHT E4990A impedance analyser. A frequency sweep from 100 Hz to 10 kHz was applied. Although this interval does not cover the full human auditory range, it was considered sufficient to capture the general behaviour of heat on the piezos. Restricting the range also reduced the measurement time, which was advantageous for the repeated test procedure. A linear sweep with 250 measurement points was used throughout the measurements. The excitation signal was set to 0.5 V_{RMS}. For each measurement point, the instrument recorded capacitance, impedance, and phase angle to see how the polarisation is changed.

3.7.3 Testing

A group of three piezos was used for each test phase to ensure statistical consistency, denoted as K1, K3, and K4 based on the samples provided. Following an initial phase, called iteration one, the methodology was refined to improve consistency and the methodology. Each piezo was measured "in situ" while still inside the oven at the test temperature, then removed and allowed to cool to room temperature before being measured again for each temperature step. This was the second iteration of the experiment.

The final testing protocol is presented below:

1. **Pre-test measurement:** Each piezo's electrical properties were measured to establish an initial baseline at room temperature.

2. **Thermal exposure:** All three piezos were placed in the oven simultaneously for a duration of 1 hour. This process was repeated across discrete temperature levels: 37 °C, 100 °C, 140 °C, 180 °C, and 220 °C.

3. **In situ measurement:** Immediately after the one hour exposure, measurements were taken while the piezos remained in the oven at the specified temperature, see Figure 3.5 for the in situ measurement setup.

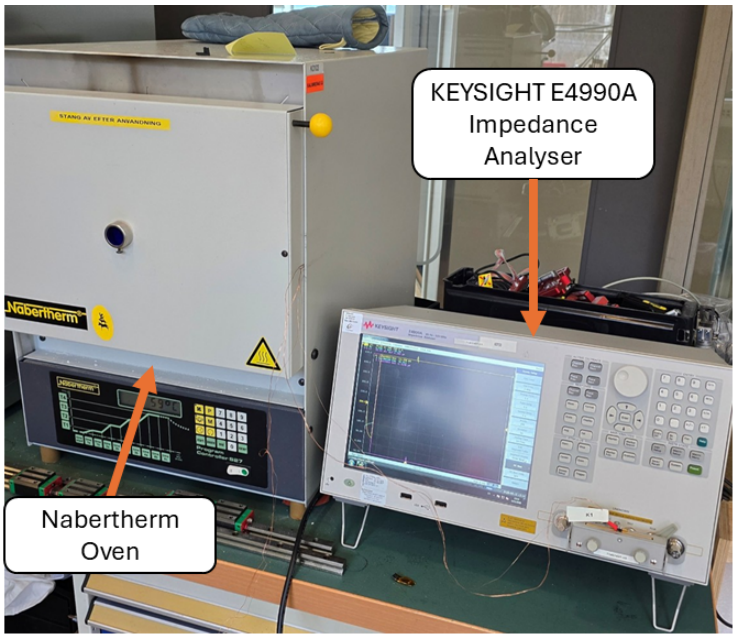

Figure 3.5: In situ measurement setup.

4. **Post-test measurement:** After the in-situ measurements, the piezos were removed from the oven and allowed to cool to room temperature (approximately 20-30 min), after which a final measurement was recorded.

To investigate the effect of increased electrical stimulus under thermal conditions, the K1 piezo was additionally tested at 100 °C with an applied excitation of 1 V_{RMS}, corresponding to the maximum output of the measurement equipment, in a separate experiment.

3.7.4 Pass/Fail Criteria

The pass criterion was defined as maintaining the measured capacitance within -5% and the impedance within $+5\%$ of their respective room-temperature baseline values after the piezos had cooled back to room temperature (RT After). Any sample outside these limits was considered to have been overstressed.

3.8 Nylon Thread-locker Element Overstress Limit Test (FM3)

The primary objective of this study was to evaluate the functional integrity of a nylon locking element under accelerated ageing conditions. Specifically, the test aimed to establish a baseline for prevailing torque loss and determine if the average glass transition temperature (T_g = 90–100 °C) (Cochlear, 2026a) of the nylon (PPA) material imposes a limit on subsequent full-actuator ALT. While the operational range is around 37 °C (Cochlear, 2026a), this empirical validation investigated if no critical loss of torque occurred at elevated temperatures.

3.8.1 Design and Planning

Test samples consisted of screws with pre-applied nylon thread-locker threaded into two components. All screws were tightened to a baseline seating torque of 10 ± 0.3 Ncm to ensure full engagement of the locking element.

To maintain consistency and prevent structural warping, screws were tightened using a cross-pattern sequence (1-4, 6-3, 5-2) as illustrated in Figure 3.6. Between test iterations, the components were immersed in acetone for a minimum of one hour with agitation to remove any residual nylon debris from the internal threads, and new screws with pre-applied nylon were installed before every test.

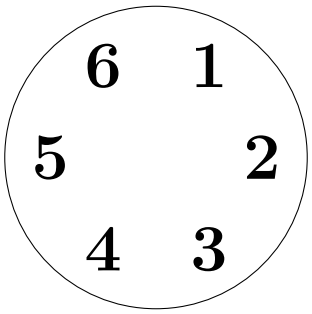

Figure 3.6: Screw order numbers.

3.8.2 Measuring Instrument

Following thermal exposure, samples were allowed to cool to room temperature for 30 minutes. The prevailing torque was measured using a micro torque wrench, see Figure 3.7 utilising a consecutive disassembly order (1–6).

Figure 3.7: Micro torque wrench.

3.8.3 Testing

The thermal endurance was evaluated at 37 °C, 70 °C, 100 °C and 150 °C through two testing phases:

3.8.3.1 Phase 1: Short-Term Cumulative Time-scale Stability

This phase observed rapid torque degradation at 100 °C. Six screws were subjected to thermal stress and sampled at cumulative intervals:

- **Baseline:** Initial average prevailing torque.
- **Intervals:** Individual measurements at 1.5, 2.5, and 3.5 hours.
- **End State:** Simultaneous measurement of the remaining three screws at 4.5 hours.

3.8.3.2 Phase 2: Logarithmic Time-scale Stability

To accurately characterise the degradation curve over extended periods, structural endurance was evaluated using fresh samples across an exponential timeline (10 to 10,000 minutes) at three primary temperature set points: 37 °C, 70 °C, and 100 °C. To capture long-term behavioural trends, the testing duration for both the 70 °C and 100 °C profiles was further extended to 40,000 minutes ($\approx$ 4 weeks). Additionally, an overstress condition at 150 °C was evaluated at 1,000 ($\approx$ 17 hours) and 10,000 minutes ($\approx$ 1 week) to determine whether excessive thermal loads would induce a shift in the primary failure mode.

3.8.4 Pass/Fail Criteria

A statistical framework was established with performance benchmarked against a room-temperature baseline. Using the mean (μ) and standard deviation (σ) of these baselines, results were categorised into performance zones:

- **Invalid:** Residual torque exceeds 2σ above the mean ($> \mu + 2\sigma$). This indicates a transition to non-representative failure mechanisms.
- **Pass:** Residual torque remains within 2σ of the baseline mean ($\mu \pm 2\sigma$).
- **Marginal:** Residual torque falls between 2σ and 3σ below the mean.
- **Fail:** Residual torque drops more than 3σ below the mean ($< \mu - 3\sigma$).

This approach justifies an allowable degradation of approximately 15–20%, ensuring that despite stress relaxation, the nylon retains sufficient friction to prevent vibration-induced loosening. Furthermore, the upper "Invalid" threshold prevents the over-acceleration of non-representative failure mechanisms.

3.9 Adhesive Element Overstress Limit Test (FM2)

The primary goal of this test was to evaluate the structural integrity of the adhesive under accelerated ageing conditions. In particular, the objective was to determine whether the glass transition temperature (T_g = 75–85 °C, Table D.2 in Appendix D) of the adhesive would act as a limiting threshold for the subsequent ALT.

3.9.1 Design and Planning

To prepare the test samples, a circular aluminium rod was machined into two smaller cylindrical components (Poggi, 2026), as shown in Figure 3.8 and Appendix F.5.

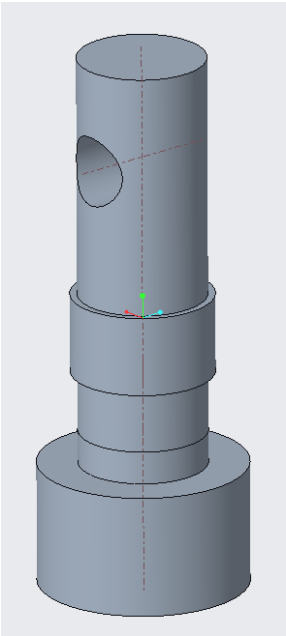

(a) CAD geometry of the components.

(b) Manufactured test component.

Figure 3.8: Adhesive test component designed for thermal stability evaluation.

The components were bonded together using the adhesive and cured in an oven according to the process specifications. During the curing cycle, a static brass weight of 320 g was applied vertically to ensure uniform adhesive distribution across the bonding interfaces and to restrict the component's movement.

Three design iterations were developed for this study. The first two iterations exhibited mechanical instability during the curing process, resulting in uneven surface contact. Furthermore, the contact area in these initial designs was excessively large, introducing a risk that the force required to separate the components would exceed the maximum load capacity of the tensile testing machine. To mitigate these risks, a third and final prototype was designed with a lower centre of gravity, see Figure 3.8.

3.9.2 Measuring Instrument

To quantify the remaining bond strength after testing, an Instron Bluehill Testing Machine 5543 tensile testing machine was used. This instrument performs a uniaxial tension test to separate the adhered components, actively recording the applied load in newtons and the corresponding extension in millimetres. The equipment setup used for these measurements is shown in Figure 3.9.

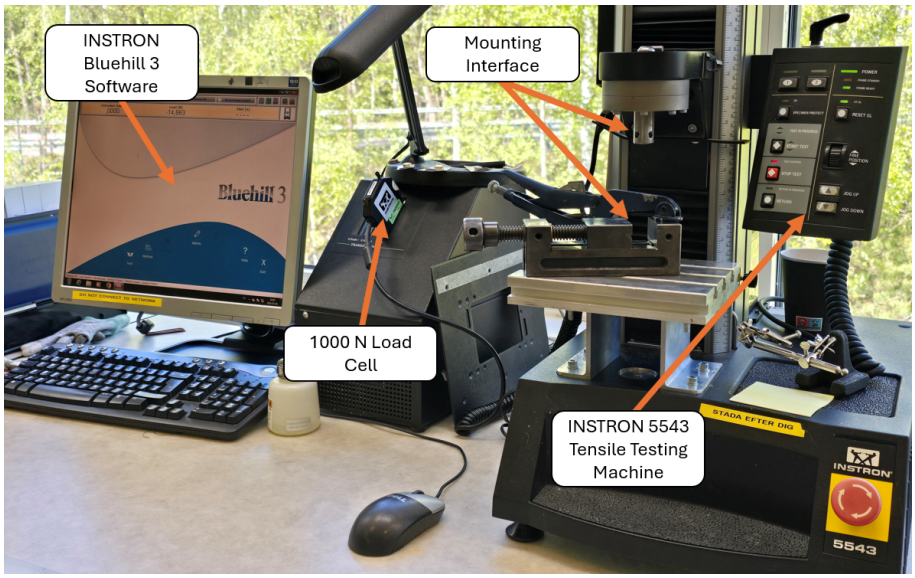

Figure 3.9: Tensile testing machine setup.

3.9.3 Testing

Before testing at elevated temperatures, the samples first had to be bonded together by curing the adhesive in an oven as described earlier, see Figure 3.10 and then rested for 24 hours. To establish a baseline, samples were tested after being cured and rested. To evaluate how the adhesive performed under thermal overstress, additional samples were subjected to a 24-hour thermal exposure in an oven at 70 °C, and 100 °C. Following the thermal exposure, these samples were allowed to cool at room temperature for at least 24 hours prior to being tested.

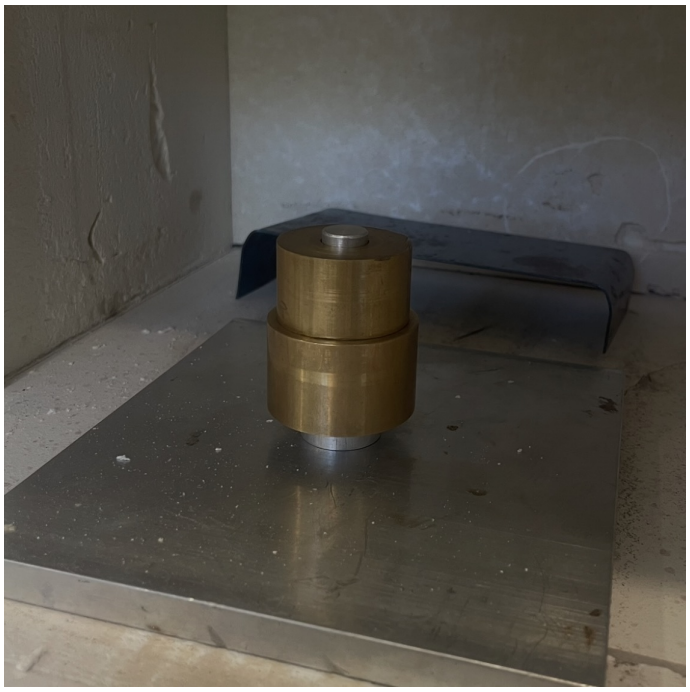

Figure 3.10: Test setup curing in the oven.

3.9.4 Pass/Fail Criteria

To evaluate the structural integrity of the adhesive, both the maximum load and the extension prior to failure was measured and benchmarked against the baseline samples. Together, these two metrics characterise the adhesive's bond strength and its ductility. The thermal overstress temperature was categorised based on the following criteria:

- **Pass:** The sample has none to moderate degradation in either the maximum load capacity or the extension profile, the material must maintain its fundamental mechanical behaviour.
- **Fail:** The sample exhibits a 40% reduction in either its maximum load capacity or its extension prior to failure. A severe drop in load capacity signifies an unacceptable deterioration of bond strength, while a drastic reduction in extension indicates thermal embrittlement.

3.10 atBCD Actuator Overstress Limit Test

The purpose of this test was to find out how much the OFL of the actuator changed given increased voltage or temperature; the results were later used as input parameters in the ALT.

3.10.1 Design and Planning

The testing methodology was divided into four stages: measurement variation, voltage limit testing, endurance under electrical stress, and thermal degradation. This section describes both the experimental procedure and the mathematical methods used to evaluate the collected data.

To ensure that the observed variations were not caused by the measurement setup itself, Phase 1 first evaluated the baseline variation of the interface. Five independent measurements were performed at each frequency f to estimate the measurement noise. The inherent variation was then defined as the largest signed deviation from the median value. This made it possible to identify the worst-case measurement error while also preserving whether the deviation was positive or negative.

Mathematically, if $M(f)$ represents the set of five repeated measurements at a given frequency, and $\tilde{m}(f)$ represents the median of that set, the baseline measurement noise $\Delta\text{OFL}_{\text{noise}}(f)$ is calculated as:

$$\Delta\text{OFL}_{\text{noise}}(f) = m_{\text{extreme}}(f) - \tilde{m}(f) \tag{3.6}$$

Where:

- $m_{\text{extreme}}(f)$ = Measurement at frequency f with the largest deviation from the median
- $M(f)$ = Set of all measurements at frequency f
- $\tilde{m}(f)$ = Median measurement at frequency f

In practice, this was evaluated by comparing the absolute differences between the maximum and minimum measured values and the median. The signed deviation corresponding to the largest absolute difference was then retained.

3.10.2 Measuring Instrument

The OFL of the actuator was measured while attached to a TU-1000 skull simulator. This simulator was connected to Cochlear's Actuator Characterisation Tool (ACT), which determines sensitivity via the skull simulator's built-in accelerometer. The resulting data were then extracted and used to plot the ΔOFL after each test.

The metric used to quantify actuator performance change across Phases 2 through 4 was the absolute difference in OFL, denoted as $\Delta\text{OFL}(f)$. This approach normalised the baseline (pre-test) measurement to zero across the full frequency spectrum. The analysis isolated two stable frequencies of interest found in Phase 1. The plotted data in Section 4.10 therefore represent the physical deviation from this baseline across all frequencies, calculated using Equation 3.7 below.

$$\Delta\text{OFL}(f) = \text{OFL}_{\text{24 recovery}}(f) - \text{OFL}_{\text{baseline}}(f) \tag{3.7}$$

3.10.3 Testing

A set of six actuators, denoted as $\mathcal{A}_i$, was initially allocated for this testing. Two of these actuators ($\mathcal{A}_4$ and $\mathcal{A}_5$) were found to be non-functional and were excluded. Additionally, three other actuators of batch $\mathcal{A}_j$, designated as $\mathcal{A}_B$, $\mathcal{A}_C$ and $\mathcal{A}_F$, were used for the thermal exposure and repeatability phases.

The experimental setup consisted of a TU-1000 skull simulator, function generator, amplifier, and multimeter. During the active electrical testing phases, a function generator was configured to produce a sinusoidal frequency sweep from 200 Hz to 8 kHz. This signal was amplified and applied to the actuator, while the input voltage was monitored using a multimeter. The complete experimental setup is illustrated in Figure 3.11.

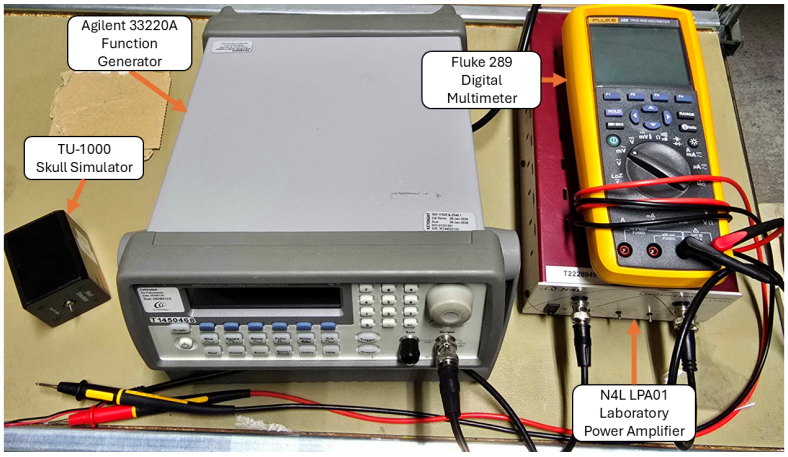

Figure 3.11: Actuator voltage test setup.

Prior to any testing, each actuator's OFL was measured while mounted to the skull simulator to establish an initial performance baseline.

3.10.3.1 Phase 1: OFL Repeatability Study and Pass/Fail Criteria

Because the project aimed to detect small actuator performance changes, it was important to first determine how much variation was caused by the measurement setup itself. This made it possible to distinguish actual actuator degradation from normal measurement noise.

The objective of this phase was therefore to quantify the inherent variation of the measurement system and use it to establish pass/fail criteria for actuator signal stability. To achieve this, the largest directional deviation from the median value was calculated across five repeated installations.

As operator-induced variation is recognised as a major source of measurement variation (Sittsamer, 2022), all measurements were performed by a single operator to minimise operator-related inconsistencies. Five repeated OFL measurements were conducted on two separate actuators, designated as $\mathcal{A}_B$ and $\mathcal{A}_C$.

Based on the measured system variation, evaluation limits were then established for the following test phases. Small deviations were classified as a Pass, moderate deviations as Marginal, and large deviations exceeding the acceptable system variation as a Fail.

3.10.3.2 Phase 2: Increasing Voltage Test

This phase served as a screening test to identify the voltage threshold for actuator failure under short-term excitation. The testing protocol was as followed:

1. **Initial reference measurement:** Actuator $\mathcal{A}_1$ was operated at its operating voltage for 1 minute to confirm stable baseline behaviour. The voltage supplied to the actuator was continuously monitored using a multimeter.
2. **Step-stress excitation:** After recording the OFL at the operating voltage, the test was repeated at increasing voltage increments (4, 6, 7.5, 11, and 12 V_{RMS}). The actuator was excited for 1 minute at each level, with an OFL measurement taken immediately after each interval. Testing was terminated once the OFL exhibited out-of-specification behaviour at frequencies of interest.

3.10.3.3 Phase 3: Voltage Endurance Test

Following the establishment of the upper voltage limit in Phase 2, Phase 3 evaluated the performance of the actuators ($\mathcal{A}_{2,3,6}$ and $\mathcal{A}_{D,G}$) under prolonged electrical stress.

1. **Long-term excitation:** The actuators were initially subjected to a continuous 1-hour excitation at the maximum allowable voltage determined in Phase 2 (7 V_{RMS}).
2. **Performance evaluation:** An OFL measurement ("Immediate") was recorded directly after the 1-hour stimulation. The actuator was then allowed to rest, and a second measurement ("24h Recovery") was taken 24 hours later to evaluate degradation after relaxation.
3. **Decreasing voltage sweep:** This 1-hour excitation and recovery method was repeated at decreasing voltage levels (6, 5, and 4 V_{RMS}) using the same procedure.
4. **24-hour rigid mounting endurance test:** Lastly, to evaluate long-term stability with the actuator mounted on the manufactured rigid mounting solution, two ($\mathcal{A}_{D,G}$) 24-hour endurance tests were conducted at 5 V_{RMS} and 7 V_{RMS}.

3.10.3.4 Phase 4: Thermal Exposure Test

To evaluate the effects of elevated temperature on actuator performance, a thermal exposure test was conducted. Actuators $\mathcal{A}_B$ and $\mathcal{A}_C$ were exposed to both rapid and prolonged thermal loading without electrical excitation to isolate the effect of heat on the actuator components.

Prior to thermal exposure, an initial baseline OFL measurement was recorded for

each actuator at ambient room temperature. The testing protocol was then conducted as followed:

1. **Rapid heating using heat gun:** The actuators were rapidly heated using a heat gun, while the actuator temperature was monitored using a Type K thermocouple. An OFL measurement was recorded immediately after the target temperature was reached to evaluate the effects of short-term thermal expansion and material softening.
2. **24-hour prolonged heating using oven:** The actuators were subsequently placed in an oven and subjected to a continuous, sustained temperature for 24 hours. Another OFL measurement was taken immediately upon their removal to assess sustained thermal degradation while the actuators were still hot.
3. **24-hour recovery:** Finally, the actuators were allowed to cool and rest at room temperature for 24 hours. A final measurement was taken to determine whether the thermal exposure caused permanent structural changes or if the materials recovered to their baseline state.

3.11 Accelerated Life Testing

To design the ALT methodology, several specific input parameters were established:

- **Baseline operating conditions:** The standard voltage, temperature, and mechanical load the actuator experiences during typical use.
- **Overstress limits:** The maximum stress thresholds before unnatural failure mechanisms, such as melting or catastrophic piezo failure.
- **Activation energies & constants:** Material-specific constants required to calculate the theoretical acceleration factor.

3.11.1 Input Parameters

The input parameters for the ALT were derived through data gathering and testing phases detailed in previous sections. Thermal inputs were determined by the lowest degradation threshold among the adhesive, nylon thread-locker, and the piezo. Voltage inputs were constrained by the actuator failure threshold (ΔOFL failure limit). Finally, the mechanical load was derived from the physical constraints of the rigid mounting solution compared to the TU-1000 skull simulator.

3.11.2 System Design

Performing the ALT required an environment capable of delivering sustained simultaneous stressors. The system design balanced two priorities: capturing real-time degradation data and testing a sufficiently large sample size for statistical significance. The main performance measurement system used throughout the ALT was the actuator OFL. Two architectural configurations were developed, Option A: Integrated Solution and Option B: Modular Solution.

The primary configuration, the Integrated Solution, utilised an audio analyser to

combine signal generation, amplifier, equaliser, and data logging into a single workflow. This allowed autonomous monitoring of performance throughout the duration of the test. However, this precision came at the cost of scalability. The analyser was limited to a maximum of two test samples at a time. The logical flow for this architecture is illustrated in Figure 3.12.

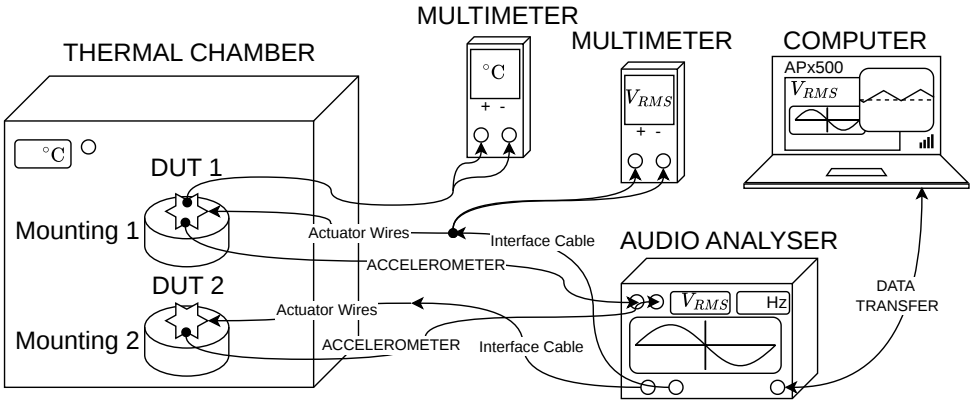

Figure 3.12: Option A: Integrated Solution block diagram illustrating the automated signal generation and data gathering architecture.

Alternatively, a Modular Solution was developed using a stand-alone function generator and power amplifier. While this setup lacked automated performance logging, it offered significantly higher output, with the amplifier capable of driving up to twelve test samples simultaneously. Unlike Option A, this configuration could not utilise an inbuilt equaliser if required. The configuration also required manual OFL checks, which necessitated removing the actuator from the thermal chamber and potentially introduced thermal cycling variables. This architecture is shown in Figure 3.13.

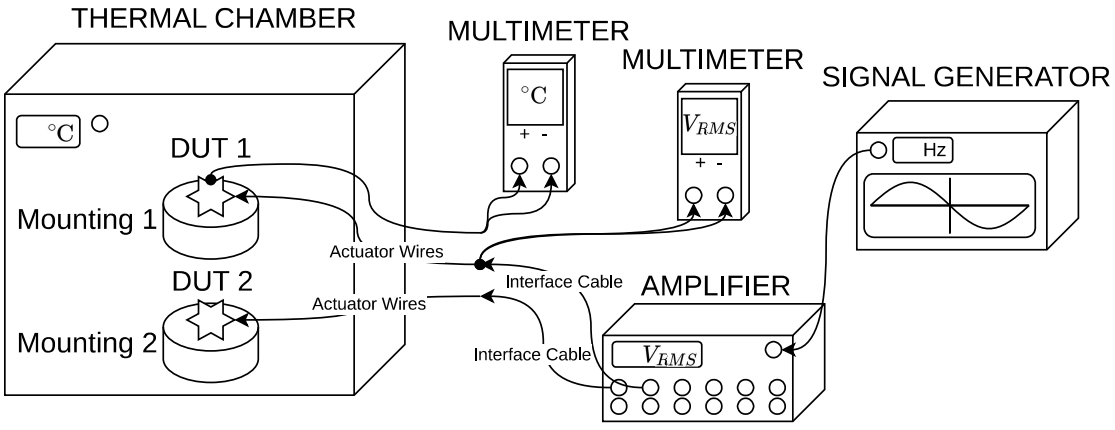

Figure 3.13: Option B: Modular Solution block diagram utilising separate components for power and signal delivery.

To achieve the best of both worlds, the two configurations could be operated simultaneously under identical voltage and temperature conditions. In this hybrid

approach, Option A could be used to provide real-time monitoring and data for one or two actuators to capture degradation behaviour, while Option B could be utilised solely for acceleration to increase the total sample size. This parallel operation ensures that the experiment maintains high statistical significance without sacrificing data logging. The specific hardware utilised for both configurations is detailed in Table 3.2.

Table 3.2: Components of the ALT setup.

Component	Qty	Hardware Used	Function
Option A: Integrated Solution			
Audio Analyser	1	APx517B Acoustic Analyzer	Synthesizes 100 Hz – 10 kHz sweep and scales output to target V_{RMS}.
Interface Cable	2	Speakon (M) to Dupont (F)	Transmits drive signal from analyser to the chamber boundary.
Accelerometer	2	Dytran 3055D3 accelerometer	Records continuous mechanical performance of the DUT.
Data transfer	1	Computer with APx500 Software	Controls signal parameters and logs real-time performance data.
Option B: Modular Solution			
Signal Generation	1	Agilent 33220A Function Generator	Synthesizes 100 Hz – 10 kHz sweep.
Amplification	1	ATI AT6012 Power Amplifier	Scales signal to target V_{RMS} limit.
Interface Cable	12	BNC (M) to Dupont (F)	Transmits drive signal from amplifier to the chamber boundary.
Common Components			
Thermal Chamber	1	Froilabo climate chamber	Maintains elevated target temperature for accelerated ageing.
Mounting	14	Rigid solution	Secures DUTs to ensure consistent mechanical stress.
Device Under Test	14	Cochlear actuator	Active test sample undergoing life cycle testing.
Actuator Wires	14	2-pin (M) to 0.2 mm copper	Soldered directly to actuator; delivers voltage within the thermal chamber.
Multimeters	2	Fluke 289 DMM	Monitors temperature (°C) and terminal voltage (V_{RMS}).
Voltage Probe	1	Test Leads	Provides voltage feedback outside the chamber to the multimeter
Temp. Sensor	1	Type K Thermocouple	Provides thermal feedback from the chamber to the multimeter.

3.11.3 ALT Durations

Based on the established acceleration models and safe component testing limits, the physical test durations required to simulate a 10-year operational lifespan were calculated across a range of safe voltage and temperature combinations. To ensure that all subcomponents achieved the required simulated 10-year lifespan, the overall ALT duration was dictated by the slowest-accelerating component.

To accurately reflect real-world ageing, the calculation accounted for the difference between a user's daily usage profile (assumed to be 16 active hours per day (Cochlear, 2026a)) and the continuous 24-hour nature of the physical ALT environment (168 hours per week). The required physical test time in weeks (t_{test}) is defined in Equation 3.8:

$$t_{test} = \frac{Y_{sim} \times d_{year} \times h_{use}}{AF_{Total} \times h_{week}} \tag{3.8}$$

Where:

- t_{test} = Required physical test duration [weeks]
- Y_{sim} = Target simulated lifespan [years]
- d_{year} = Number of days per year [days]
- h_{use} = Daily device usage time [hours/day]
- AF_{Total} = Total acceleration factor [-]
- h_{week} = Continuous weekly ALT operating time [hours/week]

Substituting the constant values into Equation 3.8 yields:

$$t_{test} = \frac{58400}{AF_{Total} \times 168} \tag{3.9}$$

3.11.4 Pass/Fail Criteria

Same criteria as atBCD Actuator Overstress Limit Test, see Table 4.14 in Section 4.10.1.

3.11.5 Procedure Validation

To validate the testing procedure before the full-duration ALT was initiated, a pre-test protocol was conducted. First, a baseline OFL was measured for each actuator at room temperature. The actuators were then secured in the rigid mounting fixtures, placed inside the thermal chamber at 70 °C, and subjected to an electrical excitation of 4.3 V_{RMS}.

To monitor degradation after the test had been completed, the actuators were removed from the chamber and ΔOFL was measured. This evaluation was repeated 24 hours after the initial post-test measurement. The primary metric for analysis was the shift in ΔOFL at the 400 Hz and 3000 Hz.

3.11.5.1 Phase 1: Initial System Validation

This phase consisted of a short preliminary run using a single actuator. The primary objective was to verify that the method could reliably reach and maintain the target electrical and thermal stresses over a 9 days without causing overstress induced failures in the components.

3.11.5.2 Phase 2: System Scaling

This phase utilised two actuators to validate the scalability and compatibility of the ALT system over a target duration of 2 hours, operating at an applied voltage of 2 V_{RMS} at room temperature, while continuously logging data from the accelerometers. To enable long-term continuous testing, a custom Python script was developed using the APx500 API. The script automated the entire measurement sequence, alternating between normal sweeps and data export sequences of time-stamped OFL measurements without manual intervention, see Appendix G. Furthermore, the script was configured to save the exported CSV files 10 times during the test directly to a shared Cochlear network drive. This allowed the data to be accessed securely from any authorized computer within the Cochlear network, enabling real-time remote monitoring of the test progression without the need to physically visit the ALT setup in the basement.

3.11.5.3 Phase 3: APx vs ACT ΔOFL Test

Phase 3 was designed to verify the fidelity of the automated APx measurements against the established Actuator Characterisation Tool (ACT). The primary objective was to ensure that the continuous in situ monitoring accurately reflected the true OFL deviations (ΔOFL) of the devices under test.

To achieve this, sample actuators (including $\mathcal{A}_A$ and $\mathcal{A}_B$) were subjected to elevated stress conditions of 4.3 V_{RMS} at 70 °C inside an oven for a duration of 5 days. During this period, the APx automated script logged the OFL deviations continuously, with key data milestones evaluated at 3720 sweeps (midway) and 7440 sweeps (end of test).

To validate the APx exports, the test sequence included a secondary verification using the ACT. Upon completing the 7440 sweeps, the actuators were evaluated in the ACT immediately to capture their post-stress state. Furthermore, to account for thermal and mechanical relaxation, a subsequent ACT measurement was taken after a 24-hour recovery period at ambient conditions. The ΔOFL was explicitly tracked at key frequencies of 400 Hz and 3000 Hz across both the APx and ACT setups to confirm that the automated method provided reliable tracking of performance degradation under prolonged operational stress.

3.11.5.4 Phase 4: Stress Influence

Phase 4 isolated the independent effects of electrical and thermal stresses on actuator performance.

Utilising the automated APx500 script and environmental oven established in prior phases, actuator $\mathcal{A}_A$ underwent two testing profiles:

- Voltage Variation: To assess electrical stress under a high thermal load, the oven was held at a 70 °C while the drive voltage was stepped through 0.5, 1.075, 2.15, and 4.3 V_{RMS}. The 0.5 V_{RMS} measurement served as the baseline.
- Temperature Variation: To assess thermal stress under a high electrical load, the drive voltage was fixed at 4.3 V_{RMS} while the oven temperature was stepped through 37 °C, 53.5 °C, and 70 °C. The 37 °C served as baseline as the reference.

Throughout both profiles, the automated script continuously logged OFL measurements. Consistent with Phase 3, the ΔOFL was explicitly tracked at 400 Hz and 3000 Hz to precisely characterise how isolated increases in voltage and temperature impact degradation across the frequency spectrum.

3.11.6 ALT Inspection

To monitor failure modes without compromising test validity, a routine physical inspection protocol was established alongside continuous automated data logging. Because t_{test} varied dynamically based on the selected stress factors, the physical inspection intervals were normalised as a function of target simulated years (Y_{sim}) by using Equation 3.8

- **Visual inspections ($Y_{sim} = 1.0$):** Conducted every 1 simulated year to confirm the test is running at the correct voltage and temperature, and to check for early mechanical anomalies such as adhesive failure, nylon threadlocker loosening, and general fractures.
- **Full inspections ($Y_{sim} = 5.0$):** Conducted every 5 simulated years to evaluate performance drift over extended simulated lifespans when only option B is used.

During inspection, it is recommended that the system should be be powered down and that the actuators should be allowed to cool to room temperature. The actuators' ΔOFL should be recorded at 400 Hz and 3000 Hz.

3.11.7 Requirement Specification Compliance

Before the ALT could be operated long-term, the system had to be verified. This was done by evaluating the physical setup and its initial operational performance against the requirement specification to ensure that all functional, safety, and reliability requirements were fulfilled, see Appendix C.

4
Results

After developing the experimental methods, the corresponding results obtained from the selected approaches are presented in this chapter in the form of tables and figures. It should be noted that the structure and order of this chapter follow the chronological order in which the experiments were started. Due to confidentiality agreements and NDAs, the raw data from certain experiments cannot be presented directly. Instead, the results are shown relative to a baseline reference, which differs depending on the specific test and experiment.

4.1 Concept Evaluation

The multi-staged screening process successfully screened the initial idea pool into a single test concept:

- **Elimination Matrix:** Reduced the initial 26 generated concepts to 12 viable candidates, see Appendix E.1.
- **Pugh Matrix:** Progressively narrowed the field from 12 concepts down to 8 in the first round, to 4 in the second, and finally to 3 in the third round, see Appendix E.2.
- **Kesselring Matrix:** The three finalist concepts were quantitatively scored out of a maximum of 40 points. The selected concept, **FM0.3**, scored 35 points, outperforming the runner-up, which scored 28 points, see Appendix E.3.

4.2 The Final Concept

Concept FM0.3 accurately simulates realistic operating conditions while achieving high acceleration factors. The methodology involved exposing the fully assembled actuator to elevated temperatures and increased voltage across the standard operational frequency range of 100–10000 Hz (Cochlear, 2026a). This setup enables simultaneous monitoring of the actuator's overall output performance and the degradation behaviour of its individual components. Lastly, the major strength of the chosen concept is its adaptability and scalability.

4.3 Data for Failure Modes

The data collection phase was successfully completed and provided the thermodynamic constants, exponents, and operational baseline values required for the ALT

predictive models. All standard operating parameters and material-specific constants for failure modes (FM) 2, 3, and 4 were compiled and are presented in Appendix D.

4.4 TU-1000 Skull Simulator Modelling

The simulation results comparing the TU-1000 skull simulator to the 6 kg human skull approximation are summarised in Table 4.1.

Table 4.1: Skull simulator piezoelectric model resonance and stress at 400 Hz with % difference from 6 kg reference

Model	**Resonance [Hz]**	**Peak Stress [MPa]**	**Surface Stress [MPa]**
TU-1000	880.93 (+9.56%)	1.6528 (−0.45%)	1.3104 (−6.93%)
6kg Approx	804.03 (Ref)	1.6603 (Ref)	1.4079 (Ref)

A direct comparison revealed varying levels of deviation across the measured parameters. The primary internal peak stress recorded for the TU-1000 skull simulator (1.6528 MPa) closely matched the 6 kg reference model (1.6603 MPa), corresponding to a minor deviation of −0.45%. However, larger differences were observed in both the resonance frequency and the surface stress. The resonance frequency of the skull simulator was 9.56% higher than that of the 6 kg reference model. In addition, the surface stress, representing the mechanical load at the top surface, was measured at 1.3104 MPa in the simulator, corresponding to a deviation of −6.93% compared to the reference value of 1.4079 MPa.

4.5 Rigid Mounting Modelling

The simulation results evaluating various physical brass mounting masses against the 6 kg reference are presented in Table 4.2 and visualised in Figure 4.1. The data revealed a clear logarithmic stabilisation in mechanical stress as the mounting mass increased, with the deviation falling within the $\approx 3\%$ limit at 150 g.

Table 4.2: Rigid brass mounting: stress at 400 Hz with % difference from 6 kg reference

Mass [kg]	**Ø × h [mm]**	**Resonance [Hz]**	**Peak Stress [MPa]**	**Surface Stress [MPa]**
0.025	30 × 4	961.17 (+19.54%)	1.6480 (−0.74%)	1.2405 (−11.89%)
0.050	40 × 5	880.85 (+9.55%)	1.6528 (−0.45%)	1.3108 (−6.90%)
0.100	40 × 10	843.64 (+4.93%)	1.6558 (−0.27%)	1.3530 (−3.90%)
0.150	40 × 15	830.55 (+3.30%)	1.6570 (−0.20%)	1.3699 (−2.70%)
0.450	60 × 20	803.78 (−0.03%)	1.6568 (−0.21%)	1.3647 (−3.07%)
0.675	60 × 30	800.72 (−0.41%)	1.6571 (−0.19%)	1.3694 (−2.73%)
0.900	60 × 40	807.92 (+0.48%)	1.6597 (−0.04%)	1.4019 (−0.43%)
6.000	100 × 94	804.03 (Ref)	1.6603 (Ref)	1.4079 (Ref)

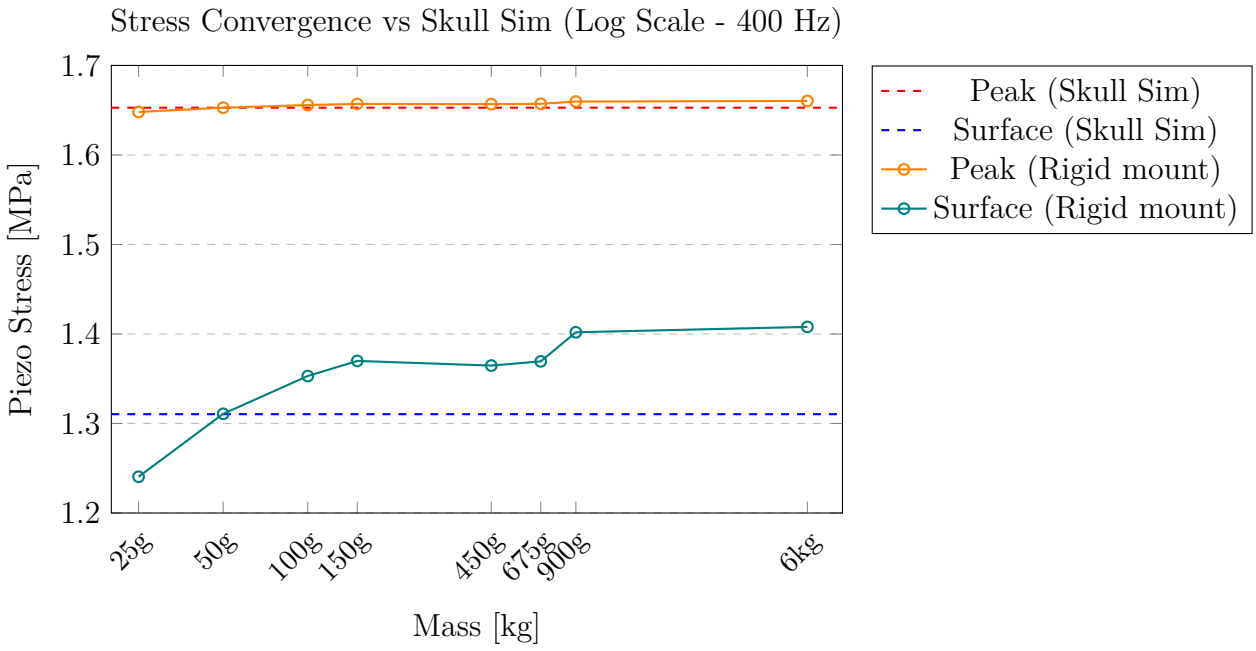

Figure 4.1: Stress convergence (log scale) showing comparison against Skull sim reference.

Additionally, an assessment was conducted to determine the impact of external spring stiffness on the internal stress profile of the 150 g model. As shown in Table 4.3, varying the spring stiffness across multiple orders of magnitude yielded a negligible effect on both the peak and surface stresses.

Table 4.3: Spring study: 150 g rigid brass mounting stress at 400 Hz

Springs [N/m]	**Resonance [Hz]**	**Peak stress [MPa]**	**Surface stress [MPa]**
Fixed Support	830.22	1.6599	1.4089
60000	830.91	1.6568	1.3678
4935 (TU-1000)	830.56	1.6570	1.3698
3198 (Mounting)	830.55	1.6570	1.3699
60	830.53	1.6570	1.3700

4.6 Rigid Mounting Fabrication

Following fabrication, physical validation was conducted on the prototypes. As shown in Figure 4.2, the finished components exhibited a visibly smooth surface finish on the primary mounting face. Each of the mounts were weighed to verify compliance, confirming that all four manufactured units were above the target weight of 150 g mass. Furthermore, the central threaded bore was verified for mechanical compatibility with the actuator's mounting. It should be noted that the second mounting configuration was designed for a different actuator ($\mathcal{A}_k$), which utilised a smaller screw and did not require the recessed area, as depicted in Figure 4.2b.

(a) Rigid mounting solution for $\mathcal{A}_{i,j}$.

(b) Rigid mounting solution for $\mathcal{A}_k$.

Figure 4.2: Manufactured standard rigid mounting solutions.

4.6.1 Accelerometer Integration

The Dytran 3055D3 accelerometer was integrated into two rigid mounting solutions by attaching its removable base to the rear of the mount using epoxy. To ensure stability when laid flat, material was removed to create a symmetrical profile. To

compensate for this mass reduction, the overall length of the mount was increased to maintain the target weight, see Figure 4.3.

(a) Front view ($\mathcal{A}_{i,j}$).

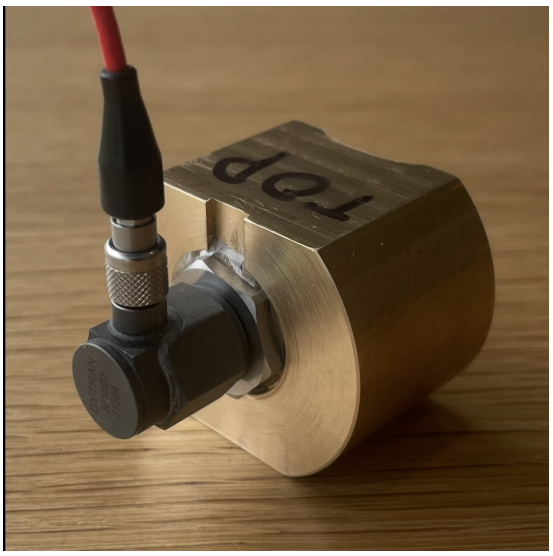

(b) Rear view ($\mathcal{A}_{i,j}$).

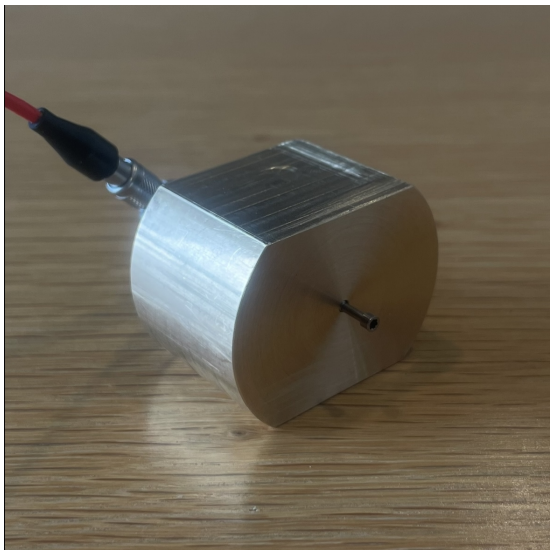

(c) Front view ($\mathcal{A}_k$).

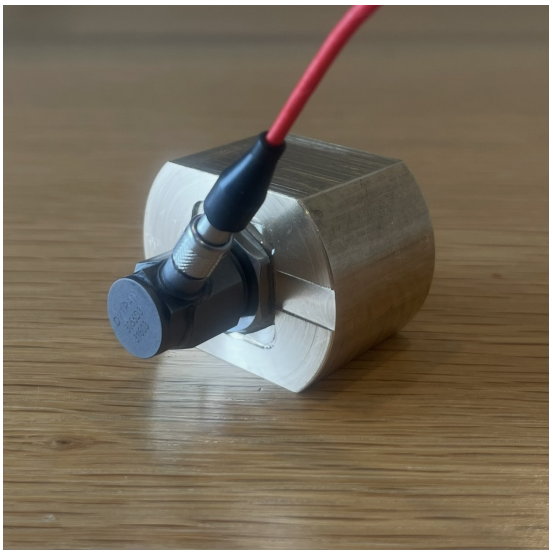

(d) Rear view ($\mathcal{A}_k$).

Figure 4.3: Rigid mounting solutions with accelerometers for $\mathcal{A}_{i,j}$ (top row) and $\mathcal{A}_k$ (bottom row).

4.6.2 Measurement Setup Comparison

The measurement capabilities of the final mounting solution were compared against the TU-1000 skull simulator baseline in Figure 4.4. It illustrates the relative deviation Output Force Level (ΔOFL) introduced by the new mount. A gain of 17.1 dB was found to give the most similar ΔOFL results to the ACT for sample $\mathcal{A}_H$ instead of the calculated standard gain of 13.8 dB.

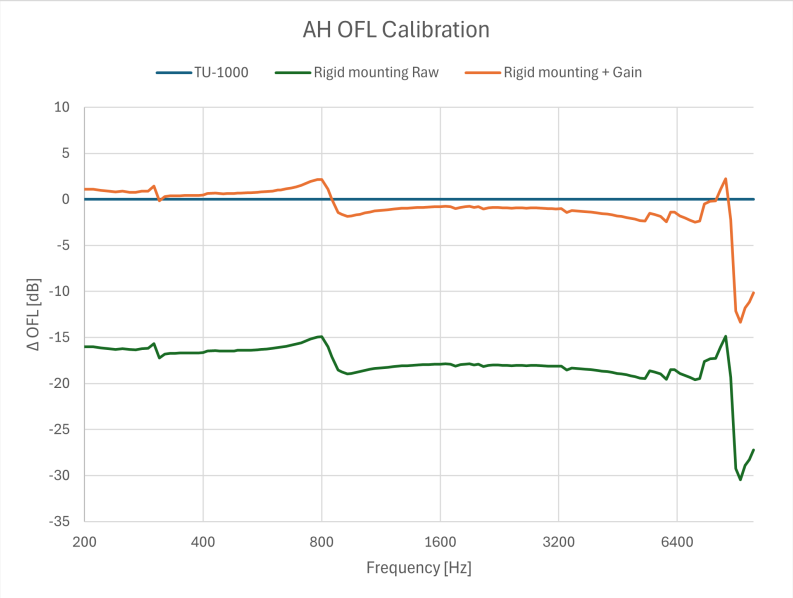

Figure 4.4: ΔOFL for sample $\mathcal{A}_H$ when using the rigid mounting solution with accelerometer compared to the TU-1000 baseline.

4.7 Piezoelectric Element Overstress Limit Test (FM4)

Individual thermal tests were performed on the piezos to determine the temperature range over which the piezoelectric behaviour changed and find its overstress limit, see Section 3.7. The results of the capacitance and impedance measurements are presented below in Table 4.4 using Equations 3.4-3.5. The results of the table were plotted in Figures 4.5-4.6 for the K4 piezo.

Table 4.4: Percentage change in capacitance and impedance relative to individual RT baselines.

Temp (°C)	**K1**		**K3**		**K4**		**Status**
	Cap (%)	**Imp (%)**	**Cap (%)**	**Imp (%)**	**Cap (%)**	**Imp (%)**	
220	343.73	-74.98	-	-	482.52	-81.55	-
RT After 220 Test	-35.48	53.19	-	-	-24.32	29.36	Fail
180	593.88	-83.40	770.21	-86.72	675.68	-86.00	-
RT After 180 Test	-31.35	43.23	-19.55	21.42	-18.92	20.38	Fail
140	106.42	-50.72	153.70	-60.63	147.21	-59.59	-
RT After 140 Test	-7.80	8.00	4.17	-5.34	3.60	-4.89	Marginal
100	49.08	-33.02	97.35	-49.49	100.54	-50.47	-
100 (ii)	-	-	-	-	82.16	-44.94	-
RT After 100 (ii) Test	-	-	-	-	11.17	-11.56	Pass
100 1 V_{RMS}	777.52	-9.19	-	-	-	-	-*
RT After 100 1 V_{RMS} Test	0.92	-1.28	-	-	-	-	Pass
70	22.60	-18.58	-	-	41.58	-30.36	-
RT After 70 Test	-2.04	2.20	-	-	7.40	-7.69	Pass
37	6.42	-6.38	-	-	19.64	-17.73	-
RT After 37 Test	1.22	-1.70	-	-	12.25	-12.49	Pass
RT	0.00	0.00	0.00	0.00	0.00	0.00	-

* partially corrupted data.
- data missing due to faulty wires.

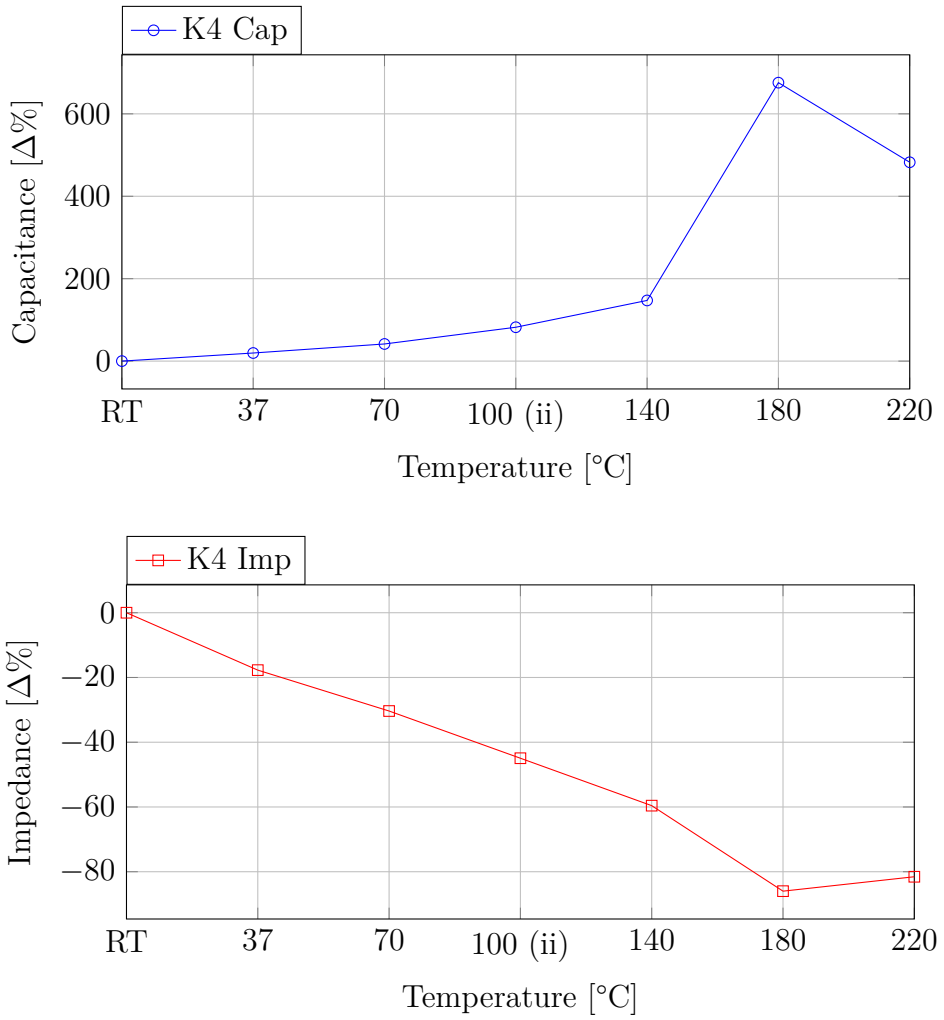

Figure 4.5: Capacitance and impedance change relative to RT for K4.

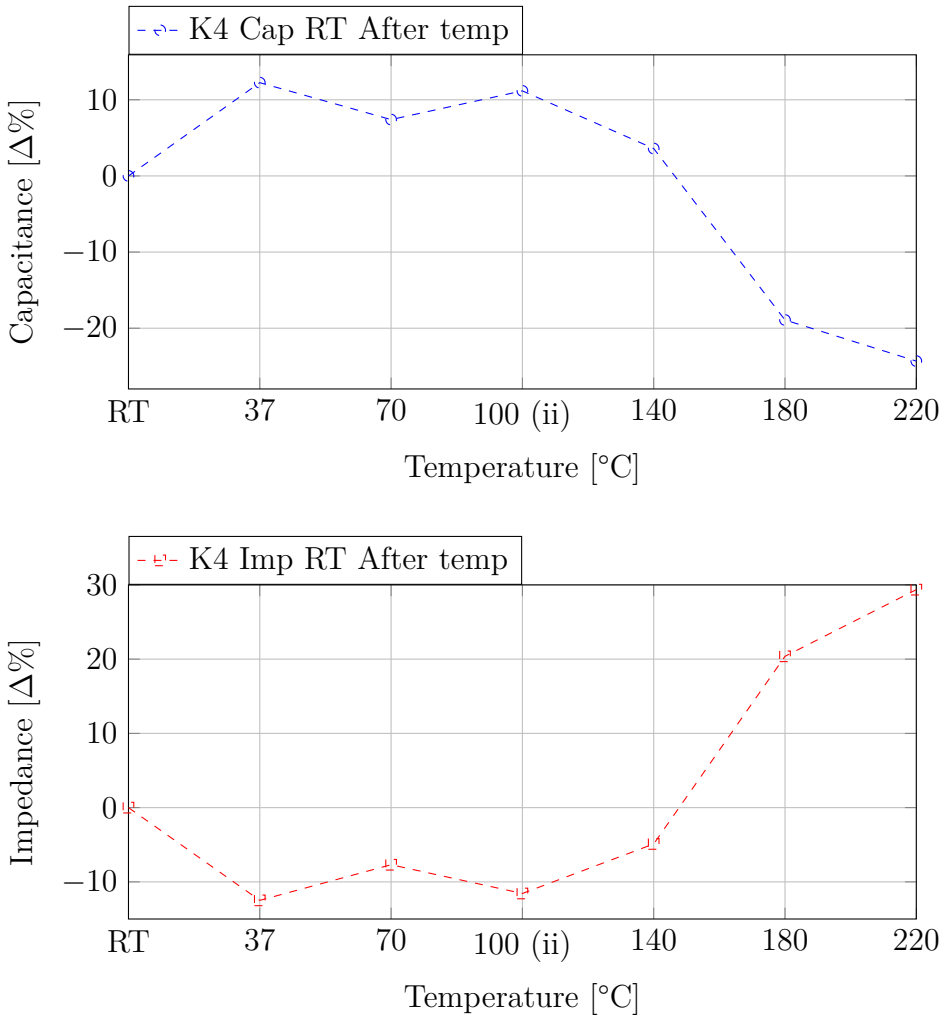

Figure 4.6: Capacitance and impedance change relative to RT for K4 after temperature exposure.

4.7.1 Quality Factor and Loss Tangent

Quality factor and loss tangent were calculated and plotted for K1 for a high temperature as well as temperatures of interest, see Figure 4.7, in order to evaluate whether the experimental results were consistent with the theoretical expectations written in Section 2.8.2.

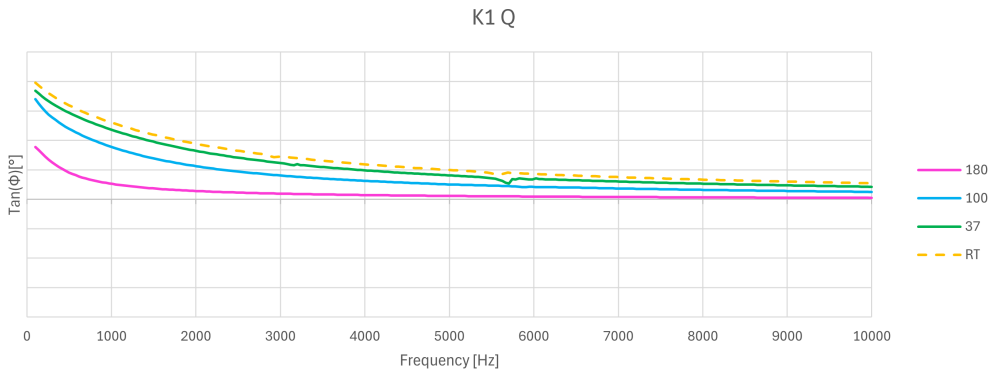

(a) Q-Factor.

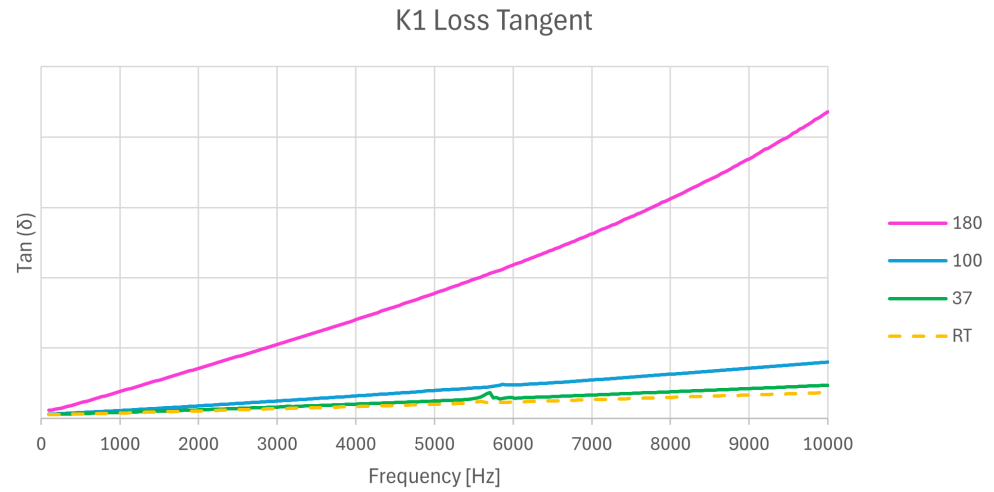

(b) Loss tangent.

Figure 4.7: Q-value and loss tangent of the K1 Piezo.

4.8 Nylon Thread-locker Element Overstress Limit Test (FM3)

Initial baseline torque measurements were established across three baseline assemblies and six screw positions, yielding a mean residual torque (μ) of 5.80 Ncm with a standard deviation (σ) of 0.31 Ncm (see Tables 4.5 and 4.6). These baseline statistics were used to define the performance and pass/fail criteria for all subsequent thermal degradation tests, which are detailed in Table 4.7.

Table 4.5: Baseline torque measurement raw data.

Baseline	Screw Position [Ncm]						Δ Residual
	S1	S2	S3	S4	S5	S6	[Ncm]
Baseline 1	5.6	5.9	6.1	5.6	5.6	6.3	5.85
Baseline 2	6.0	6.0	6.0	5.7	5.4	5.8	5.82
Baseline 3	5.7	5.7	5.2	6.2	6.0	5.5	5.72

Table 4.6: Statistical summary of baseline results.

Metric	Screw Position [Ncm]						Average
	S1	S2	S3	S4	S5	S6	[Ncm]
Mean (μ)	5.77	5.87	5.77	5.83	5.67	5.87	**5.80**
Sigma (σ)	0.21	0.15	0.49	0.32	0.31	0.40	**0.31**

Table 4.7: Torque pass/fail criteria ($\mu = 5.8, \sigma = 0.31$)

Status	Statistical Basis	Residual Torque [Ncm]
Invalid	$> \mu + 2\sigma$	> 6.4
Pass	$\mu \pm 2\sigma$	$5.2 - 6.4$
Marginal	3σ to 2σ	$4.9 - 5.2$
Fail	$< \mu - 3\sigma$	< 4.9

4.8.1 Phase 1: Short-Term Cumulative Time-scale Stability

The results of the initial short-term torque degradation tests at 100 °C are summarised in Table 4.8. The "Δ Residual" represents the average residual torque of the whole assembly for that specific sample.

Table 4.8: Short-term cumulative time-scale torque results at 100 °C.

Time	Screw Position [Ncm]						Δ Residual	Status
[hours]	S1	S2	S3	S4	S5	S6	[Ncm]	
1.5	5.0	—	—	—	—	—	5.00	Marginal
2.5	—	4.0	—	—	—	—	4.00	Fail
3.5	—	—	5.3	—	—	—	5.30	Pass
4.5	—	—	—	6.7	5.0	5.9	5.87	Pass

4.8.2 Phase 2: Logarithmic Time-scale Stability

Logarithmic time-scale testing was conducted across distinct temperature profiles to capture degradation trends. The results for the 100 °C, 70 °C, and 37 °C tests

are presented in Tables 4.9, 4.10, and 4.11, respectively.

Table 4.9: Logarithmic time-scale torque results at 100 °C.

Time	Screw Position [Ncm]						Δ Residual	Status
[min]	S1	S2	S3	S4	S5	S6	[Ncm]	
10	4.9	5.1	4.8	4.5	5.5	5.1	4.98	Marginal
100	4.5	4.7	5.4	4.4	6.3	5.4	5.12	Marginal
1000	4.9	5.6	5.8	4.9	4.8	4.9	5.15	Marginal
10000	5.6	5.4	5.2	6.0	5.9	5.5	5.60	Pass
60000	5.0	6.1	7.3	6.1	7.2	6.8	6.42	Invalid

Table 4.10: Logarithmic time-scale torque results at 70 °C.

Time	Screw Position [Ncm]						Δ Residual	Status
[min]	S1	S2	S3	S4	S5	S6	[Ncm]	
10	5.5	5.1	5.1	5.8	5.5	5.7	5.45	Pass
100	5.3	5.8	6.1	6.0	5.7	6.1	5.83	Pass
1000	4.9	5.9	4.3	3.9	4.8	3.7	4.58	Fail*
1000	5.5	5.1	5.1	5.3	5.7	5.2	5.32	Pass
10000	5.6	5.6	5.1	5.6	5.2	5.4	5.42	Pass
60000	5.8	5.5	4.6	6.2	6.0	6.1	5.70	Pass

* excluded due to assembly error.

Table 4.11: Logarithmic time-scale torque results at 37 °C.

Time	Screw Position [Ncm]						Δ Residual	Status
[min]	S1	S2	S3	S4	S5	S6	[Ncm]	
10	5.5	5.4	5.1	6.1	5.9	5.4	5.57	Pass
100	5.8	5.6	5.8	5.5	6.3	5.6	5.77	Pass
1000	4.8	5.6	5.9	5.3	6.4	5.9	5.65	Pass
10000	6.1	6.2	5.8	5.3	6.3	6.2	5.98	Pass

Results for the additional elevated temperature evaluation performed at 150 °C are detailed in Table 4.12.

Table 4.12: Logarithmic time-scale torque results at 150 °C.

Time	Screw Position [Ncm]						Δ Residual	Status
[min]	S1	S2	S3	S4	S5	S6	[Ncm]	
1000	4.9	6.2	6.5	5.2	5.9	6.9	5.93	Pass
10000	7.3	6.7	7.0	7.0	6.1	6.3	6.73	Invalid

Figure 4.8 displays the logarithmic time-scale data, plotting the average residual torque degradation over time against the baseline mean of 5.80 Ncm.

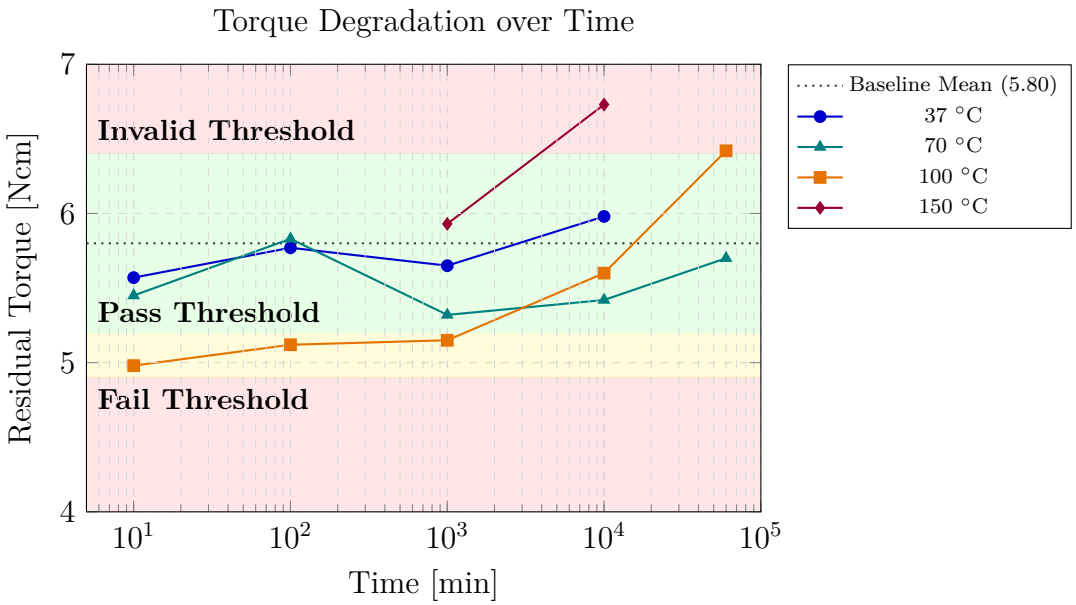

Figure 4.8: Measured residual torque across temperatures over time..

4.9 Adhesive Element Overstress Limit Test (FM2)

Individual thermal tests were performed on the adhesive samples to determine the temperature range over which the mechanical behaviour changed and find its overstress limit. The results of the measured maximum mechanical loads and subsequent extension are presented below in Table 4.13. The experimental load versus extension curves are plotted in Figure 4.9.

Table 4.13: 24-hour experimental mechanical testing data.

Test Sample	Max Load [N]	Extension [mm]	Status
Baseline (1)	229.45	0.27	Reference
Baseline (2)	462.88	0.28	Reference
70 °C	179.95	0.27	Pass
100 °C (1)	275.43	0.17	Fail
100 °C (2)	294.87	0.31	Fail

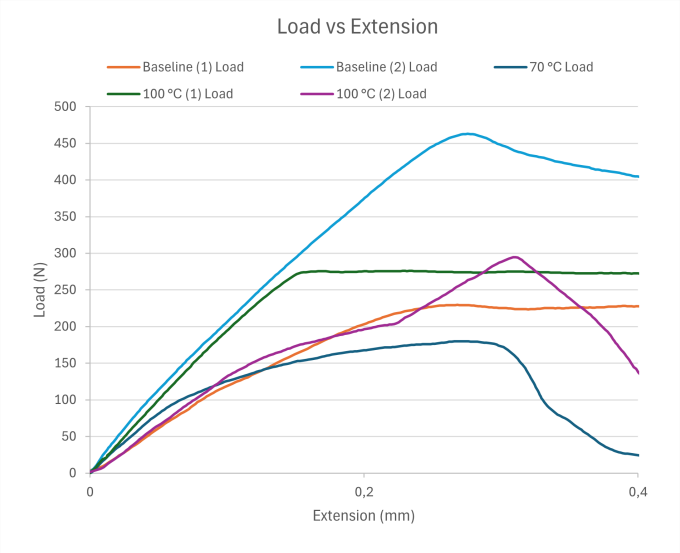

Figure 4.9: Experimental load versus extension curves.

4.10 atBCD Actuator Overstress Limit Test

This section presents the performance deviation results across the four phases outlined in Section 3.10 to find the actuators' overstress limits. To reflect both the physical changes in the actuators and the inherent system variation, all results are visualised using the absolute difference metric, $\Delta\mathrm{OFL}(f)$.

4.10.1 Phase 1: OFL Repeatability Study and Pass/Fail Criteria

This study evaluated system variation and used that data to establish empirical pass/fail criteria for the actuator. Figure 4.10 illustrates this measurement spread across the frequency spectrum.

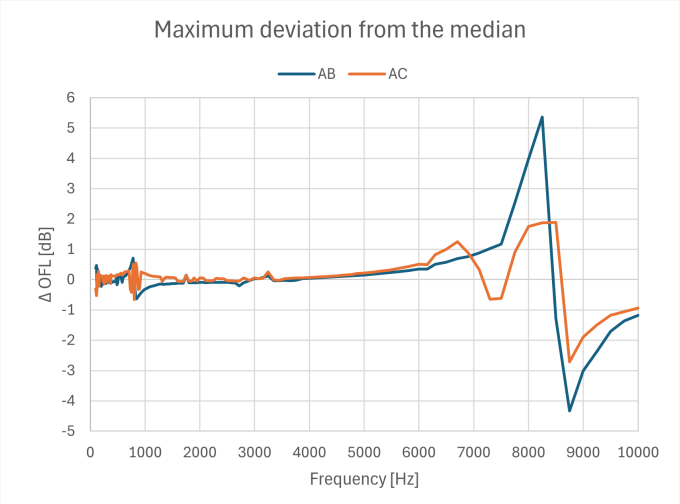

Figure 4.10: Maximum directional deviation in ΔOFL from the median across the five repeated measurements for actuators $\mathcal{A}_B$ and $\mathcal{A}_C$.

The deviation remained highly stable at lower and mid-frequencies; notably, around 400 Hz and 3 kHz, inherent system variation was minimal and contained within approximately ±0.25 dB. However, significant measurement variation emerged at higher frequencies. Specifically, actuator $\mathcal{A}_B$ exhibited a maximum directional deviation of approximately +5.3 dB around 8.2 kHz, while actuator $\mathcal{A}_C$ showed a maximum deviation of approximately -2.7 dB near 8.8 kHz.

By analysing these observations, standard tolerance thresholds were defined for the full frequency spectrum, as detailed in Table 4.14.

Table 4.14: Actuator pass/fail criteria based on maximum directional deviation.

Status	**Condition**	**Maximum ΔOFL [dB]**
Pass	Minimal variation	$\leq \pm 1.0$
Marginal	Moderate variation	± 1.0 to ± 2.0
Fail	Significant variation	$> \pm 2.0$

The stable 400 and 3000 Hz band (±0.25 dB) was utilised as the baseline for normal operation. Consequently, a maximum deviation of $\leq \pm 1.0$ dB was classified as a pass. Conversely, any variation greater than ±2.0 dB was considered a failure.

4.10.2 Phase 2: Increasing Voltage Test

The results of the voltage screening test, consisting of 1-minute step increments up to 12 V_{RMS}, are shown in Figure 4.11.

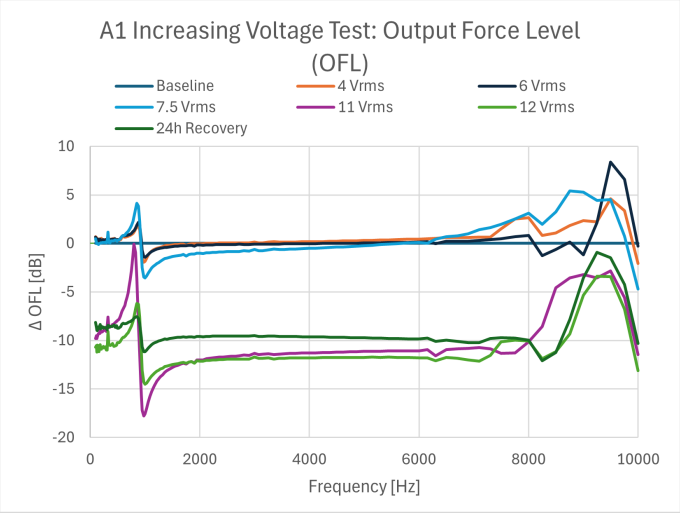

Figure 4.11: ΔOFL for sample $\mathcal{A}_1$ subjected to increasing voltage screening.

4.10.3 Phase 3: Voltage Endurance Test

This section covers the result of Phase 3 and the "long-term" stimulation test covered in Section 3.10.3.3.

4.10.3.1 7 V_{RMS} Endurance Test

The following data, see Figure 4.12, illustrates an actuator's OFL performance deviation following a continuous 1-hour exposure at 7 V_{RMS}.

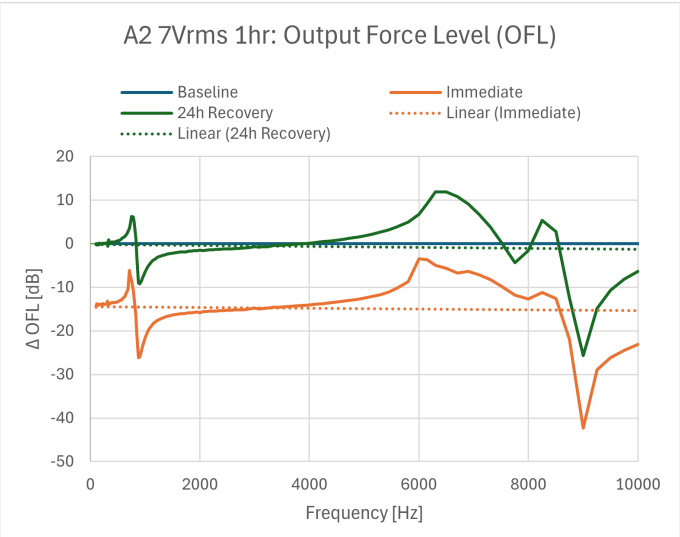

Figure 4.12: ΔOFL for sample $\mathcal{A}_2$ subjected to 7 V_{RMS} for 1 hour.

4.10.3.2 6 V_{RMS} Endurance Test

The OFL performance deviation of an actuator following a continuous 1-hour exposure at 6 V_{RMS} is shown below in Figure 4.13.

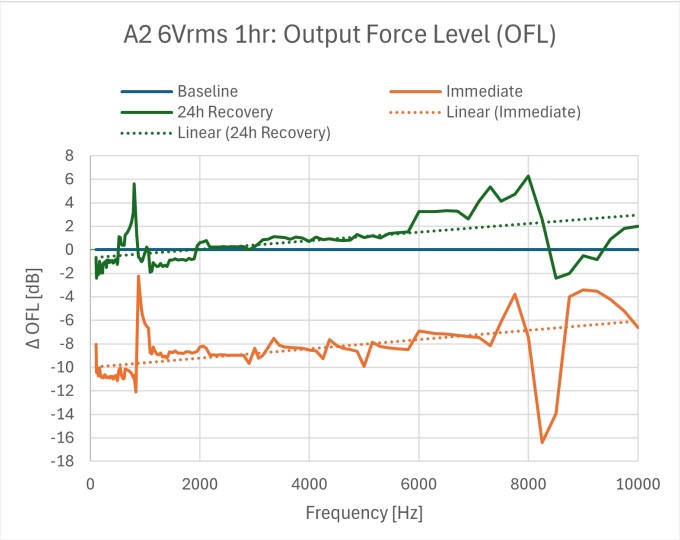

Figure 4.13: ΔOFL for sample $\mathcal{A}_2$ subjected to 6 V_{RMS} for 1 hour.

4.10.3.3 5 V_{RMS} Endurance Test

The following data illustrates the actuator OFL performance deviation following a continuous 1-hour exposure at a reduced amplitude of 5 V_{RMS}, see Figure 4.14.

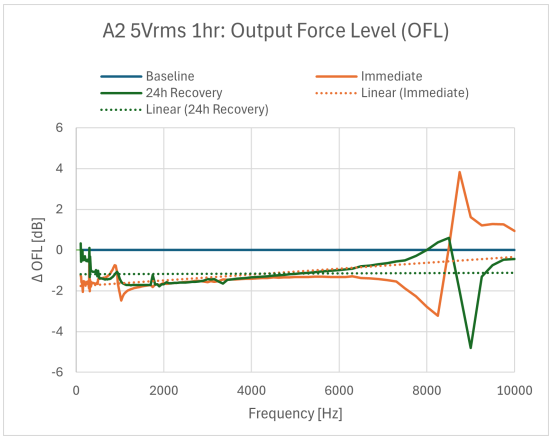

(a) ΔOFL for sample $\mathcal{A}_2$ subjected to 5 V_{RMS} for 1 hour.

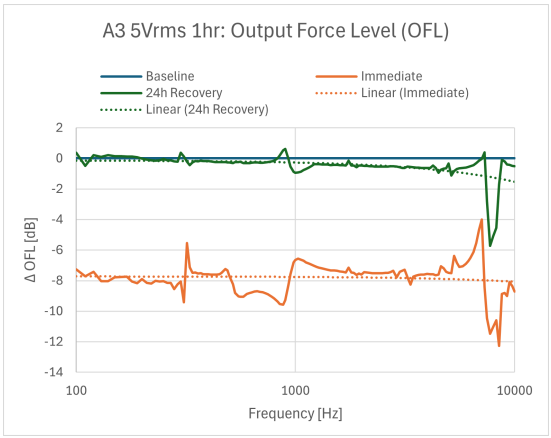

(b) ΔOFL for sample $\mathcal{A}_3$ subjected to 5 V_{RMS} for 1 hour.

Figure 4.14: 5 V_{RMS} endurance test.

.

4.10.3.4 4 V_{RMS} Endurance Test

Lastly, the performance deviation following the lowest amplitude endurance test at 4 V_{RMS} is presented below, see Figure 4.15

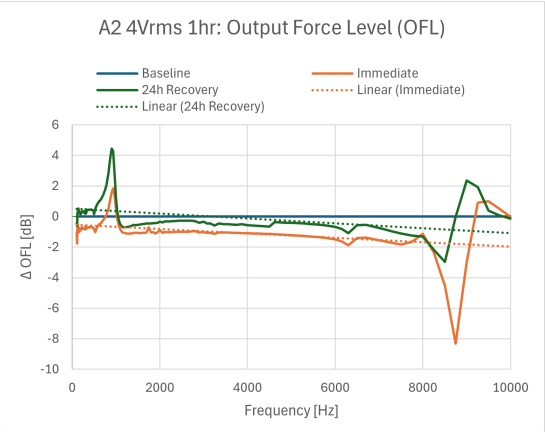

(a) ΔOFL for sample $\mathcal{A}_2$ subjected to 4 V_{RMS} for 1 hour.

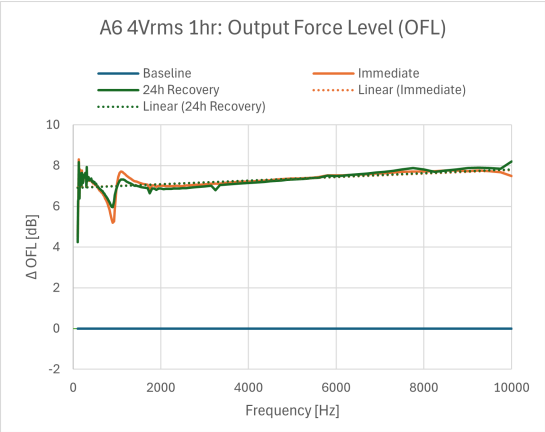

(b) ΔOFL for sample $\mathcal{A}_6$ subjected to 4 V_{RMS} for 1 hour.

Figure 4.15: 4 V_{RMS} endurance test.

.

4.10.3.5 24 Hour Rigid Mounting Endurance Test

Lastly, the long-term performance deviation under structurally constrained conditions was evaluated. The resulting physical deviations from the baseline for sample $\mathcal{A}_G$ subjected to 5 V_{RMS} and sample $\mathcal{A}_F$ subjected to 7 V_{RMS} are presented below, see Figures 4.16 and 4.17.

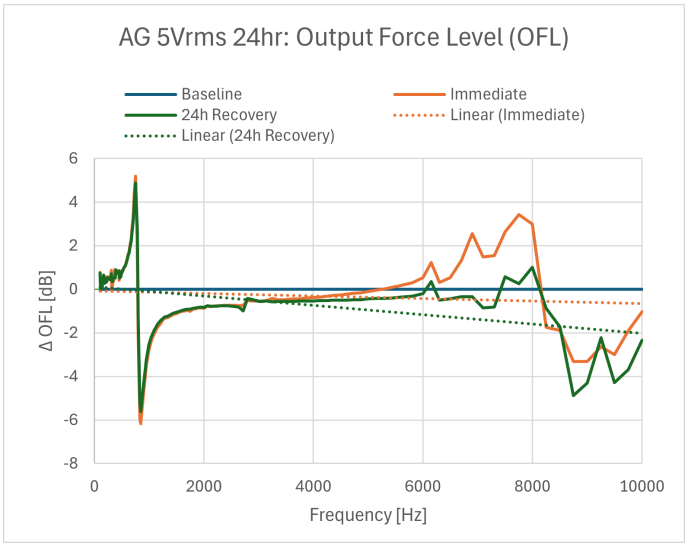

Figure 4.16: ΔOFL for sample $\mathcal{A}_G$ subjected to 5 V_{RMS} for 24 hours.

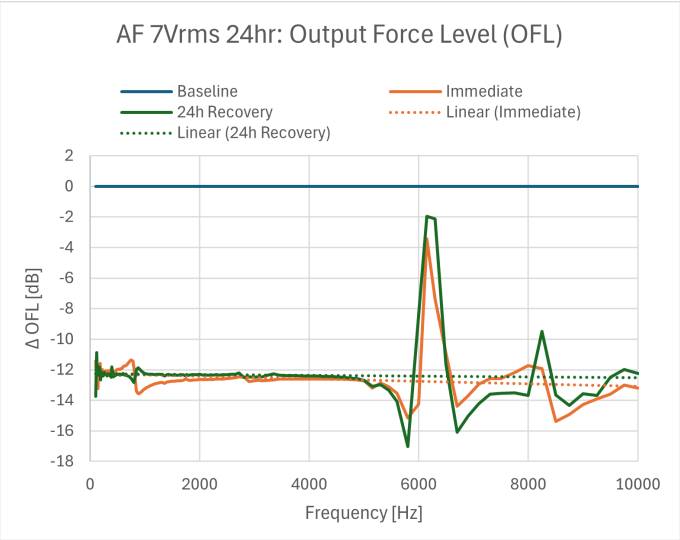

Figure 4.17: ΔOFL for sample $\mathcal{A}_F$ subjected to 7 V_{RMS} for 24 hours.

4.10.4 Phase 4: Thermal Exposure Test

Figures 4.18-4.19 and Table 4.16 present ΔOFL for samples $\mathcal{A}_B$ and $\mathcal{A}_C$ throughout the thermal test. The data illustrate performance shifts immediately following rapid heating (Heat Gun), after sustained exposure (24h Oven), and after a cooling period (24h Recovery).

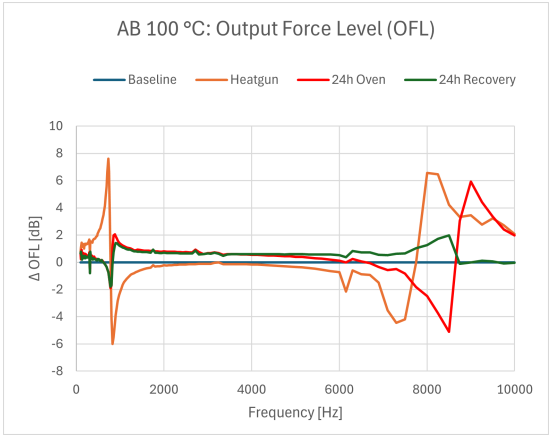

(a) ΔOFL for $\mathcal{A}_B$.

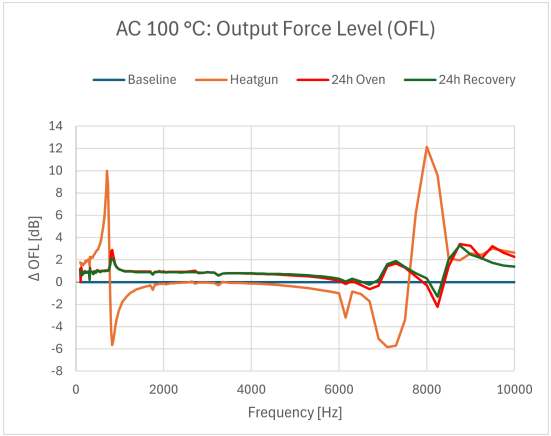

(b) ΔOFL for $\mathcal{A}_C$.

Figure 4.18: 100 °C thermal exposure test.

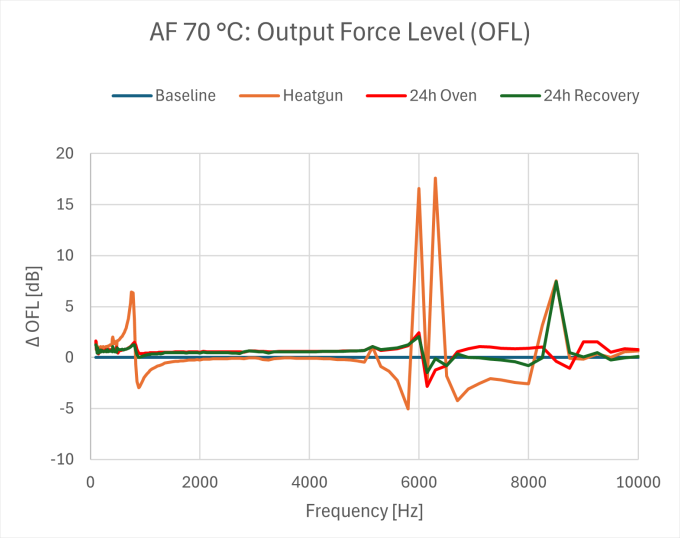

Figure 4.19: 70 °C thermal exposure test (ΔOFL for $\mathcal{A}_F$).

4.10.5 Summary of Actuator Test

The following section aggregates the post-test evaluation data across all four actuator test phases. As established in Phase 1, the inherent baseline variation of the system dictated a strict pass threshold of ± 1.0 dB and a failure limit of ± 2.0 dB for evaluating signal and structural stability. Table 4.15 details the physical deviation from the baseline (ΔOFL) at low (400 Hz) and mid (3000 Hz) frequencies for each tested voltage level in Phases 2 and 3, encompassing both immediate and 24-hour recovery measurements.

Table 4.15: Summary of voltage ΔOFL tests.

$\mathcal{A}_i$	**Voltage**	**Duration**	**Phase**	**ΔOFL @ 400 Hz [dB]**	**ΔOFL @ 3000 Hz [dB]**	**Status**
$\mathcal{A}_1$	4 V_{RMS}	1 min	Immed.	+0.45	+0.15	Pass
$\mathcal{A}_1$	6 V_{RMS}	1 min	Immed.	+0.42	-0.05	Pass
$\mathcal{A}_1$	7.5 V_{RMS}	1 min	Immed.	+0.25	-0.64	Pass
$\mathcal{A}_1$	11 V_{RMS}	1 min	Immed.	-8.42	-11.31	Fail
$\mathcal{A}_1$	12 V_{RMS}	1 min	Immed. 24h Recov.	-10.38 -8.57	-11.71 -9.52	Fail Fail
$\mathcal{A}_2$	4 V_{RMS}	1 hour	Immed. 24h Recov.	-0.69 +0.45	-1.01 -0.35	Marginal Pass
$\mathcal{A}_6$	4 V_{RMS}	1 hour	Immed. 24h Recov.	+7.26 +7.29	+7.08 +6.98	Fail Fail*
$\mathcal{A}_2$	5 V_{RMS}	1 hour	Immed. 24h Recov.	-1.63 -1.07	-1.57 -1.43	Marginal Marginal
$\mathcal{A}_3$	5 V_{RMS}	1 hour	Immed. 24h Recov.	-7.58 -0.18	-7.43 -0.59	Fail Pass
$\mathcal{A}_2$	6 V_{RMS}	1 hour	Immed. 24h Recov.	-10.75 -0.92	-8.36 +0.28	Fail Pass
$\mathcal{A}_2$	7 V_{RMS}	1 hour	Immed. 24h Recov.	-13.54 +0.35	-14.78 -0.67	Fail Pass
$\mathcal{A}_G$	5 V_{RMS}	24 hour	Immed. 24h Recov.	+0.86 +0.89	-0.55 -0.55	Pass Pass
$\mathcal{A}_F$	7 V_{RMS}	24 hour	Immed. 24h Recov.	-11.99 -11.81	-12.73 -12.50	Fail Fail
$\mathcal{A}_D$	7 V_{RMS}	24 hour	Immed.	–	–	Fail*

*Samples $\mathcal{A}_6$ and $\mathcal{A}_D$ were excluded due to failure in testing setup.

To visualise the trend, the shift in ΔOFL at 400 Hz and 3000 Hz across the 1-hour tests (excluding sample $\mathcal{A}_6$) is plotted as a function of applied voltage in Figure 4.20.

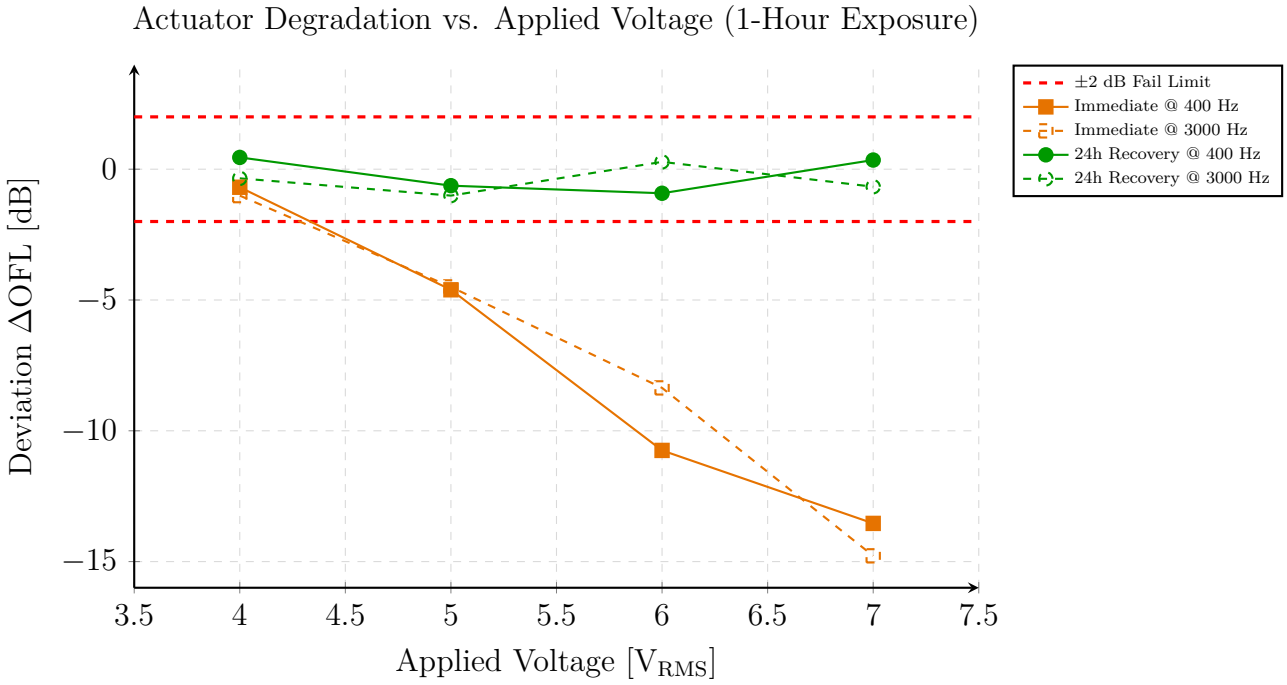

Figure 4.20: Shift in ΔOFL at 400 Hz and 3000 Hz as a function of applied voltage following a 1-hour exposure.

Finally, Table 4.16 presents the findings from the Phase 4 thermal exposure tests. Applying the pass/fail criteria from Phase 1.

Table 4.16: Summary of thermal ΔOFL tests.

$\mathcal{A}_j$	**Condition**	**Duration**	**Phase**	**ΔOFL @ 400 Hz [dB]**	**ΔOFL @ 3000 Hz [dB]**	**Status**
$\mathcal{A}_B$	Heat Gun (100 °C*)	Rapid	Immed.	+1.69	-0.11	Pass
$\mathcal{A}_B$	Oven (100 °C)	24 hours	Immed.	+0.39	+0.66	Pass
			24h Recov.	+0.30	+0.64	Pass
$\mathcal{A}_C$	Heat Gun (100 °C*)	Rapid	Immed.	+2.38	-0.06	Fail
$\mathcal{A}_C$	Oven (100 °C)	24 hours	Immed.	+0.71	+0.88	Pass
			24h Recov.	+0.73	+0.90	Pass
$\mathcal{A}_F$	Heat Gun (70 °C*)	Rapid	Immed.	+1.84	-0.02	Marginal
$\mathcal{A}_F$	Oven (70 °C)	24 hours	Immed.	+0.76	+0.65	Pass
			24h Recov.	+0.55	+0.59	Pass

*Due to the heat gun rapid heating rate, the actual peak temperatures frequently exceeded the targets significantly (≈ 20 °C).

4.11 Accelerated Life Testing

This section details the physical realisation of the ALT system in accordance with the defined parameters. It presents the finalised input data, the initial operational test, and a verification against the project's requirements, see Appendix C.

4.11.1 Input Parameters

Based on the overstress limit testing conducted previously, the parameters in Table 4.17 show the overstress and safe limits for the ALT.

Table 4.17: Overstress and safe limits for each component.

Component	Overstress	Safe Limit
Adhesive Element (FM2)	75 °C	70 °C
Nylon Thread-locker Element (FM3)	100 °C	70 °C
Piezoelectric Element (FM4)	140 °C	100 °C
atBCD Actuator	7 V_{RMS}	5 V_{RMS}

4.11.2 ALT Durations

The resulting test durations for the individual components are presented in Tables 4.18–4.20. To match the requirement specification in Appendix C, the matrices are colour-coded: green indicates combinations with test durations below 15 weeks (meeting the preferred target), while red indicates combinations exceeding the maximum allowed limit of 26 weeks.

Among all evaluated conditions, the nylon thread-locker was consistently the most limiting component and therefore determined the total required test duration for the complete assembly.

Table 4.18: Adhesive element's required test duration to simulate 10 years in weeks.

	70 °C	**60 °C**	**50 °C**	**40 °C**
5 V_{RMS}	0,54	2,01	8,02	34,99
4 V_{RMS}	0,85	3,13	12,52	54,67
3 V_{RMS}	1,51	5,57	22,26	97,20
2 V_{RMS}	3,40	12,54	50,10	218,70

Table 4.19: Nylon thread-locker element's required test duration to simulate 10 years in weeks.

	70 °C	60 °C	50 °C	40 °C
5 V_{RMS}	13,80	20,43	31,00	48,29
4 V_{RMS}	21,56	31,93	48,43	75,45
3 V_{RMS}	38,34	56,76	86,10	134,14
2 V_{RMS}	86,26	127,71	193,73	301,81

Table 4.20: Piezoelectric element's required test duration to simulate 10 years in weeks.

	70 °C	60 °C	50 °C	40 °C
5 V_{RMS}	5,26	7,89	12,15	19,22
4 V_{RMS}	10,27	15,42	23,73	37,54
3 V_{RMS}	24,35	36,55	56,25	88,99
2 V_{RMS}	82,18	123,34	189,84	300,35

4.11.3 Phase 1: Initial System Validation

To confirm most ALT requirements, an initial run was conducted to check system stability under safe conditions. The system was turned on and ran for 9 days using a single actuator. At startup, the voltage was measured, and the thermal chamber reached its target temperature, see Figure 4.21.

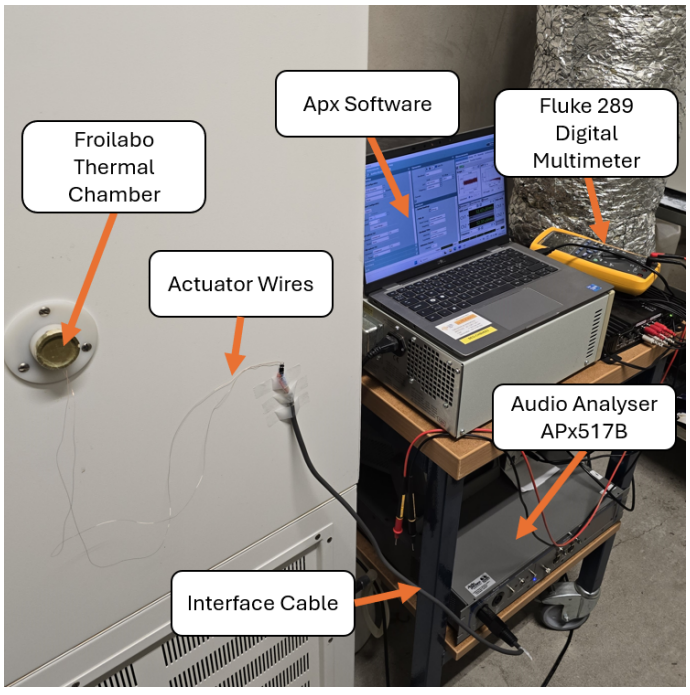

Figure 4.21: Physical installation of the initial ALT setup.

After this initial test, the OFL of the test actuator ($\mathcal{A}_A$) was measured using Cochlear's Actuator Characterisation Tool (ACT). This confirmed that the setup was causing measurable, but not destructive, wear. The observed changes ΔOFL for this sample are shown in Figure 4.22.

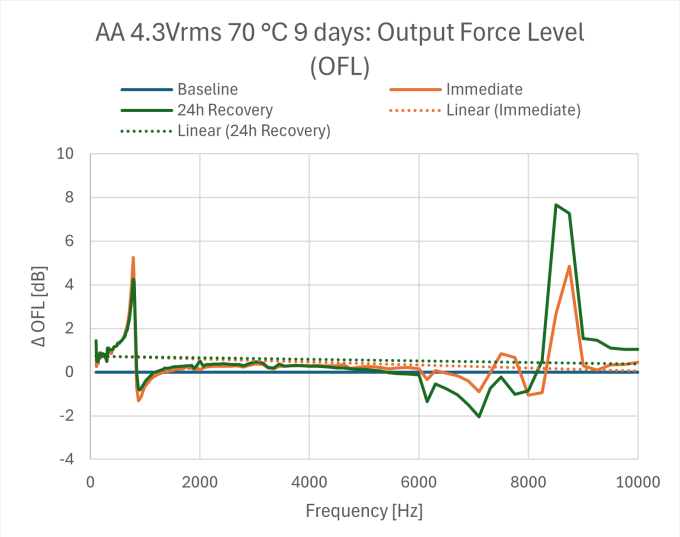

Figure 4.22: ΔOFL for sample $\mathcal{A}_A$ subjected to 4.3 V_{RMS} and 70 °C for 9 days.

4.11.4 Phase 2: System Scaling

The setup for the second test run, conducted to verify system scalability, compatibility, and continuous automated logging, is shown in Figure 4.23. The system operated for a continuous duration of 2 hours and 17 minutes utilising two different actuator variants.

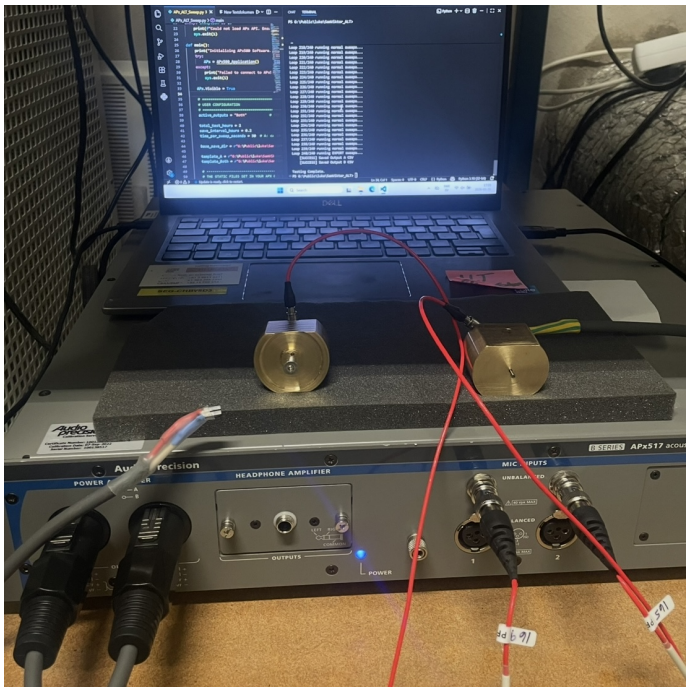

Figure 4.23: Physical installation of the scaled ALT setup.

The test was automated using the Python script detailed in Appendix G. During this phase, both actuators received a constant applied voltage of 2 V_{RMS} and completed a total of 240 frequency sweeps. Accelerometer performance was successfully logged 10 times throughout the duration of the test, and uploaded to the network drive folder.

4.11.5 Phase 3: APx vs ACT ΔOFL Test

Following the 5 day test, the results from the APx exports of actuator $\mathcal{A}_A$ was then verified using the ACT to confirm that both systems showed similar OFL deviations, see Figure 4.24 and Table 4.21.

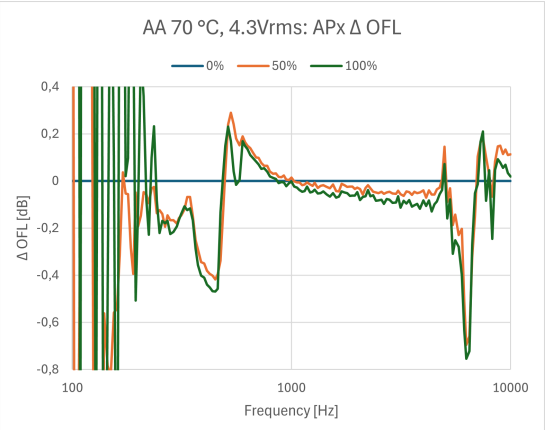

(a) APx ΔOFL.

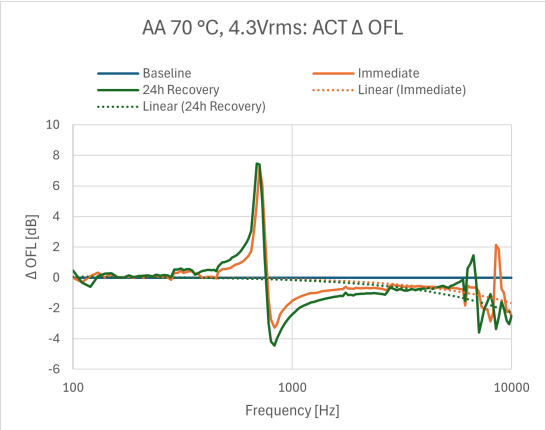

(b) ACT ΔOFL.

Figure 4.24: ΔOFL for sample $\mathcal{A}_A$ subjected to 4.3 V_{RMS} and 70 °C for 5 days.

Table 4.21: Phase 3 ΔOFL tests.

$\mathcal{A}_j$	Setup	Duration	Phase	ΔOFL @ 400 Hz [dB]	ΔOFL @ 3000 Hz [dB]	Status
$\mathcal{A}_A$	APx	3720 Sweeps	Oven.	-0.35	-0.06	Pass
$\mathcal{A}_A$	APx	7440 Sweeps	Oven.	-0.41	-0.09	Pass
$\mathcal{A}_A$	ACT	7440 Sweeps	Immed.	+0.02	-0.58	Pass
			24h Recov.	+0.47	-0.83	Pass
$\mathcal{A}_B$	ACT	7440 Sweeps	Immed.	+0.08	+0.31	Pass
			24h Recov.	+0.23	+0.24	Pass

4.11.6 Phase 4: Stress Influence

During this test, actuator $\mathcal{A}_A$ was tested to see the impact of different voltage and temperature conditions has on ΔOFL, see Figure 4.25 and Table 4.22.

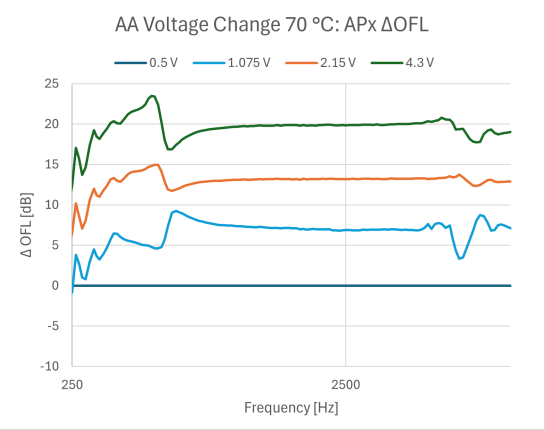

(a) Voltage change ΔOFL at 70 °C.

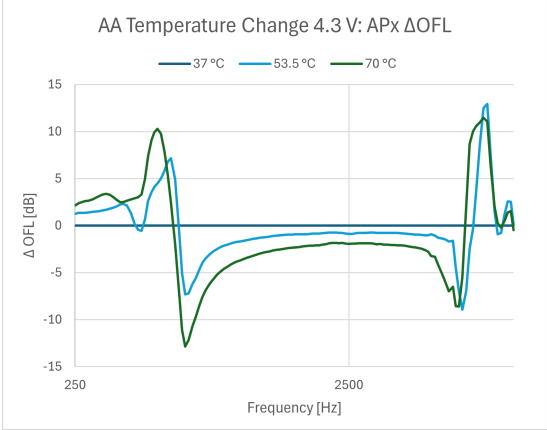

(b) Temperature change ΔOFL at 4.3 V_{RMS}.

Figure 4.25: ΔOFL change for sample $\mathcal{A}_A$ due to input parameters.

Table 4.22: Phase 4 ΔOFL tests.

Set	Condition	Phase	ΔOFL @ 400 Hz [dB]	ΔOFL @ 3000 Hz [dB]	ΔOFL @ Res Hz [dB]
$\mathcal{A}_A$	0.5 V_{RMS}	70 °C	0	0	0
$\mathcal{A}_A$	1.075 V_{RMS}	70 °C	+5.6	+6.9	+7.7
$\mathcal{A}_A$	2.15 V_{RMS}	70 °C	+13.8	+13.2	+12.8
$\mathcal{A}_A$	4.3 V_{RMS}	70 °C	+21.2	+19.8	+19.1
$\mathcal{A}_A$	37 °C	4.3 V_{RMS}	0	0	0
$\mathcal{A}_A$	53.5 °C	4.3 V_{RMS}	+1.3	-0.9	-3.4
$\mathcal{A}_A$	70 °C	4.3 V_{RMS}	+2.8	-2.1	-6.8

4.11.7 Requirement Specification Compliance

To ensure the finalised setup was fit for purpose, the setup was verified by checking if it fulfilled the requirement specification, see Appendix C. Table 4.23 provides the compliance matrix, detailing whether each mandatory Requirement (R) and Desire (D) was fulfilled, along with the results that verify the status.

Table 4.23: Requirements specification compliance matrix.

Cochlear/Chalmers		**Document type:**	**Requirement Specification Compliance Matrix**			
Development of Accelerated Life Testing Method for Bone Conduction Devices		***Created:*** ***Modified:***	**2026-05-07** **2026-05-13**			
Criteria		***Target Value***	***R/D***	***Weight***	***Status***	***Result / Explanation***
Function						
0	Accelerate Cochlear's Bone Conduction devices	3 Failure Modes (FM)	R		Yes	System setup successfully degraded the 3 failure modes
Simulated ALT duration.						
1.1	Maximum duration for 10 simulated years	< 1/2 year	R		Yes	3 distinct test configurations satisfy the < 26-week feasibility threshold.
1.2	Preferred duration for 10 simulated years	< 15 weeks	D	5	Yes	1 configurations meet the preferred 15-week timeline for rapid validation.
1.3	Maximum duration for 80 simulated years	< 1 year	D	1	No	Validation of extreme longevity is not achievable within 1 year
Input Data.						
2.1	Adhesive overstress limit (FM2)	TBD via testing	R		Yes	Thermal testing determined an adhesive limit of 75 °C
2.2	Nylon Thread-locker overstress limit (FM3)	TBD via testing	R		Yes	Thermal testing determined a thread-locker limit of 100 °C
2.3	Piezo overstress limit (FM3)	TBD via testing	R		Yes	Testing determined piezo overstress limits of 5 V and 100 °C
Setup.						
3.1	Stimulate actuator	2 V to limit of Req 2.3	R		Yes	Amplifier successfully supplied a continuous 4.3 V without exceeding the Req 2.3 limit
3.2	Heat actuator	37 °C to limit of Req 2.1/2.2	R		Yes	Chamber maintained 70 °C continuously, remaining safely below the physical limits
3.3	Measure actuator stimulation	Voltage	R		Yes	Multimeter successfully monitored the applied RMS voltage
3.4	Measure actuator temperature	Temperature	D	5	Yes	Thermocouples successfully tracked the actuator temperature continuously
3.5	Measure actuator performance after ALT	Output Force Level	R		Yes	Output Force Level was successfully measured post-ALT
3.6	Actuator mounting solution	±3% of 1.41 MPa	R		Yes	Rigid mounting solution has stress of 1.3699 MPa, matching the target within 3%
3.7	Signal equaliser	100 Hz-10 kHz	R		Yes	Signal generation setup maintained the defined frequency spectrum
3.8	Scalability	≥ 2 actuators	D	5	Yes	2 actuators was tested simultaneously
3.9	Compatibility	≥ 2 actuator variants	D	5	Yes	2 actuators variants was tested simultaneously
3.10	Continuous performance measurement	Automated digital transfer	D	4	Yes	Automated continuous exporting of raw data is uploaded onto the network drive
Maintenance						
4.1	Routine Inspection	Once a month	R		Yes	Routine visual and operational inspections were established
4.2	Automatic inspection	Once a day	D	3	Partial	Raw data sent to network drive, needs manual plotting
Budget						
5.1	Budget for procurement of material	≈0 SEK	D	5	Partial	System was constructed utilising existing CBAS HQ inventory, resulting in 200 SEK total expenditure

5
Discussion

Having conducted all experiments and gathered the corresponding results, this chapter presents a discussion of the chosen methodology, the performed experiments, and the accelerated lifetime test (ALT) approach itself. Furthermore, the chapter discusses limitations of the work, potential improvements to the developed methods.

5.1 Concept Evaluation

While the requirement specification was important for maintaining structure, defining requirements and desires too strictly at an early stage can limit innovation by reducing the number of possible design solutions. Relying too heavily on fixed categories may also cause a development team to overlook unconventional but better alternatives. In addition, the frequent reclassification of features during this project created extra administrative work that occasionally shifted focus away from the primary engineering goals.

The Pugh matrix proved to be a highly effective tool for highlighting design trade-offs and validating concept rankings. However, it is inherently sensitive to subjective scoring and the selection of the reference concept, particularly when evaluating abstract, early-stage ideas. The strategy of shifting the reference concept across iterations successfully mitigated some of this bias.

5.2 Repurposing Discarded Concepts

Importantly, the lower-scoring concepts eliminated during the Pugh and Kesselring matrices retained significant value. Rather than being discarded, they were used in the input testing. These methods were critical for establishing the overstress limits thresholds and evaluating physical properties that the ALT could not quantify, such as the pull-strength of the adhesive.

5.3 Data for Failure Modes Limitations

While the compiled data provided a basis for the ALT calculations, several parameters, such as activation energies and glass transition temperatures, should be regarded as approximations. Furthermore, the exact compositions of the adhesives

and piezoelectric elements used in the atBCD actuator were protected under non-disclosure agreements (NDAs), limiting the level of detailed material information that could be presented in this report.

To address these limitations without reducing the mathematical validity, conservative estimates were instead based on similar materials reported in academic literature and publicly available datasheets. As a result, the calculated acceleration factors should be viewed as well-informed engineering estimates rather than exact values.

5.4 Evaluation of Skull Simulator for Accelerated Life Testing

The simulation data comparing the TU-1000 skull simulator to the 6 kg human skull approximation served as the primary criterion for determining whether the current simulator provides a sufficiently representative environment for the ALT.

For primary axial loading, the simulator provided a relatively stable environment. The internal stress deviation of -0.45% remained within the predefined $\pm 3\%$ acceptance margin. However, the larger deviations in resonance frequency and surface stress suggest that the TU-1000 underestimates the mechanical damping and inertial resistance associated with a heavier skull approximation. The observed $+9.56\%$ increase in resonance frequency further indicates that the simulator possesses a lower effective mass than the human skull reference.

Because the surface stress deviation (-6.93%) exceeded the predefined acceptance margin, the current simulator baseline was considered non-conservative. Although the internal stress values remained acceptable, the underestimated surface stress indicates that the setup does not fully capture the maximum loading conditions experienced in the 6 kg skull approximation.

These findings suggest that the TU-1000 does not sufficiently replicate worst-case loading conditions for the ALT. Consequently, an alternative rigid mounting solution was investigated to better represent the mechanical boundary conditions of the human skull.

5.5 Validation of the 150 g Mounting Mass

The stress convergence observed during the rigid mounting study confirmed that a 150 g physical mount provids sufficient inertial resistance to accurately approximate a rigid boundary condition. Comparative analysis demonstrated that the simplified skull simulator baseline (1.31 MPa) underestimated the mechanical stresses experienced in situ. By contrast, the 150 g mount (1.37 MPa) more closely approximates the stress levels of the 6 kg human skull model (1.41 MPa).

The spring stiffness study further demonstrated that the geometry and mass of the mounting block were the primary contributors to the resulting internal stress levels. Variations in external spring stiffness produced only minor effects on the stress profile. Consequently, the physical dimensions and mass distribution of the mounting solution were therefore prioritised.

Hence, the 150 g mounting configuration was considered the optimal compromise for the ALT setup. It replicates representative the boundary conditions while avoiding the spatial limitations and handling difficulties associated with significantly larger mounting solutions, such as the 6 kg reference model.

Based on these findings, a 150 g brass mounting block was selected as the preferred ALT mounting solution. Brass is recommended due to its high density, which allows the mounting block to remain compact while still providing sufficient mass. In addition, brass is highly machinable, making it well suited for manufacturing and prototyping purposes.

5.6 Evaluation of the Manufactured Rigid Mounting Solution

The fabrication and subsequent validation of the 150 g brass mounting prototypes demonstrated that the design successfully translated the theoretical boundary conditions into a functional physical mounting solution.

Several design features incorporated into the prototype directly supports the testing requirements. The geometry ensures accurate alignment with the actuator connection point, while the central ϕ16 mm pedestal effectively isolates the mechanical coupling. Furthermore, the surface finish achieved during the turning process provides a flat and rigid interface, promoting efficient energy transfer between the actuator and the mounting mass.

The manufactured units achieved the target mass of more than 150 g and demonstrated mechanical compatibility with the actuator fasteners. These results confirmed that the custom mounting solution was functionally ready for integration into the ALT setup.

Following this integration, the measurement capabilities of the mounting solution were evaluated to verify its performance. Specifically, the mounting solution was compared to the TU-1000 skull simulator baseline. It was found that while the calculated standard gain was 13.8 dB, a modified gain of 17.1 dB was found to yield ΔOFL results most similar to the ACT baseline for this specific actuator. This adjustment highlights the importance of tuning the gain per actuator to compensate for minor variations.

5.7 Piezoelectric Element Element Overstress Limit Test (FM4)

The results indicate that testing the piezo at 100 °C is safe and does lead to significant degradation. While additional temperature points between 100 °C and 140 °C could be explored, it is recommended to remain below 140 °C. This recommendation is based on observations that, in at least one case, the capacitance measured after cooling to room temperature decreased relative to the baseline, suggesting the onset of degradation at higher temperatures.

The test conducted at 220 °C was performed to investigate at which temperature the heat no longer increases permittivity and polarity decreases due to heat, as discussed in Section 2.8.2. The observed loss in capacitance at 220 °C indicated that the piezoelectric material was approaching its Curie temperature. Although the material had not completely lost its polarity, the results suggest that depolarisation had begun due to the proximity to the Curie temperature. These findings are consistent with the theory presented in Section 2.8.2.

During testing, the K3 piezo experienced a wiring failure and was not repaired, resulting in missing data for several measurement points. Additionally, the data for the 100 1 V_{RMS} test of the K1 piezo was partially corrupted. Only the first 20 measurement points, corresponding to the low-frequency range, were recorded instead of the planned 250 points. Hence, this dataset is marked with an asterisk (*) in the table. Despite this limitation, the available data was used, as it still demonstrated a clear trend consistent with the expected behaviour. The test was not repeated due to lack of time.

The initial 100 °C test does not include a corresponding “RT After” value, as this measurement was conducted during the first iteration of the experiment. The data were recorded immediately after removal from the oven, without allowing the sample to cool to room temperature. To address this, the 100 °C test was repeated for one of the piezos using the same procedure as the other temperature tests. This measurement, labelled “100 (ii)”, included a proper in situ measurement as well as the proper cooling step. The second test resulted in slightly lower capacitance values compared to the initial method. Although this was not expected, it was attributed to unintentional differences in the applied excitation voltage, where a slightly lower voltage was used in the second test when measuring, resulting in a reduced measured capacitance. The results showed no significant difference between the original 100 °C measurement and the repeated test, indicating that the initial data is valid.

It was also noted that the "RT After" value for the 70 °C test for K1 and K4 had dropped compared to values around them, which did not follow the trend compared to the rest of the data. This drop was insignificant and hence the data was kept. Potential reasoning could be that K1 piezo’s "RT After" values were measured days after compared to the rest of the data points.

Additionally, during the combined thermal and 1 V_{RMS} excitation test, neither impedance nor capacitance showed significant deviation after cooling compared to their initial room temperature values. This suggested that low-level electrical excitation should not significantly influence the thermal degradation behaviour.

It should also be noted that each temperature condition was applied for only one hour. Longer exposure durations may lead to increased degradation, and therefore additional testing is recommended to evaluate time-dependent effects more comprehensively.

Moreover, as discussed in Section 2.8.2, an increase in capacitance leads to higher power requirements. This effect should be taken into account and further evaluated when designing the full ALT setup.

Furthermore, the observed behaviour of Q-factor and loss tangent was consistent with the theory. The focus was on the overall trend rather than the exact values. The results behaved as expected: when the quality factor (Q_ϕ) was high, the tangent loss was low, and when Q_ϕ was low, the tangent loss was high. The quality factor was calculated using Equation 2.12 presented in Section 2.8.1. The tangent loss was calculated using Equation 2.14 presented in the Section 2.8.2.

In conclusion, temperatures up to 100 °C can be considered safe for testing under the conditions studied, while temperatures approaching and above 140 °C may introduce a risk of excessive depolarisation and require further validation. A key improvement to the experimental methodology would be to extend the duration of thermal exposure beyond one hour to better capture long-term behaviour.

5.8 Nylon Thread-locker Element Overstress Limit Test (FM3)

The results across the evaluated temperatures reveal distinct changes in the degradation physics of the nylon thread-locker. The stable, passing residual torques at 37 °C validate the baseline ($\mu = 5.80$ Ncm, $\sigma = 0.31$ Ncm) as an accurate representation of normal operating conditions.

At 70 °C, the nylon thread-locker element demonstrated high structural stability, consistently maintaining average torques within the passing range (5.32–5.83 Ncm) even through the extended 60,000-minute testing period (5.70 Ncm). This profile aligns with predictable, long-term Arrhenius-rate thermal ageing, where minor internal stress relaxation occurs without compromising the polymer. Consequently, 70 °C is a valid acceleration temperature for the ALT that speeds up standard degradation without altering the material state.

In contrast, the behavioural patterns at 100 °C and 150 °C highlight the risks of excessive thermal acceleration. The high variance and functional failure (4.00 Ncm)

at 2.5 hours during the short-term 100 °C tests indicate that the polymer is approaching its softening regime. While the logarithmic 100 °C trials initially hovered at a marginal boundary (4.98–5.15 Ncm) showing viscoelastic relaxation, the 60,000-minute test revealed a critical breakdown. At this extended duration, the average torque spiked to 6.42 Ncm, rendering the result invalid. This resistance could be explained by a transition to thermal fusing due to the semi-crystalline structure of the polymer softening (Castagnet, 2009)

The boundaries of realistic acceleration physics were fundamentally breached at 150 °C. At 10,000 minutes, the average torque increased to 6.73 Ncm, crossing the upper statistical threshold ($> \mu + 2\sigma$) and registering as invalid due to potential thermal fusing, which is a non-representative failure mode.

Exposing the nylon to temperatures near its melting point or for extended durations at borderline temperatures like 100 °C caused the polymer to flow into the microscopic thread clearances and partially fuse the fastener assembly. The measured torque represents the destructive shearing of a fused polymer block rather than the representative friction of a functioning elastomeric thread-locker.

Because this localised fusing and subsequent seizing would not occur under normal operating conditions, both 150 °C and prolonged 100 °C exposures were considered overstress conditions that introduced non-representative structural behaviour. To ensure that the ALT continues to target the relevant failure mode, all subsequent thermal testing for the thread-locker should therefore remain below 100 °C, with 70 °C serving as the optimal baseline for reliable ALT extrapolation.

5.9 Adhesive Element Overstress Limit Test (FM2)

Two unexposed baseline control samples were tested to establish reference performance metrics. Baseline (1) recorded a maximum load of 229.45 N at a peak extension of 0.27 mm, while Baseline (2) recorded a significantly higher maximum load of 462.88 N at an extension of 0.28 mm. This large variation in maximum load could be due to difficulties in curing. During oven curing, the adhesive melted rapidly, and if the top component was even slightly tilted under the applied weight, the liquid adhesive tended to flow unevenly toward one side. Although adhesive was still visibly present around the entire joint, no clear differences in adhesive thickness could be observed. Another possible explanation for the variation is that the adhesive may have continued to gain strength after curing and thermal exposure (Poggi, 2026). As described in Chapter 3.9.3, the samples were intended to be tested after being rested for at least 24 hours after curing or thermal exposure. However, due to scheduling conflicts and limited availability of the test rig, this timing could not always be maintained consistently. Despite the high variance in ultimate load capacity, the extension prior to failure remained highly consistent across both controls, making the extension at break a much more reliable indicator of the material's true condition.

Looking at the extension results, the differences between the 70 °C and 100 °C samples show a major change in how the adhesive behaves. Following the 24-hour thermal exposure at 70 °C, the tested sample recorded a maximum load of 179.95 N at an extension of 0.27 mm. Although the load capacity was lower than the baseline values, the sample retained nearly all of its baseline extension capability, indicating consistent ductility. The behaviour at 70 °C matches normal ageing. Because this temperature is below the adhesive's glass transition temperature - T_g = 75–85 °C (Cochlear, 2026a) - its chemical structure stayed intact. This small change is simply normal thermal relaxation, where internal stresses from the curing process are released without making the material brittle (Odegard and Bandyopadhyay, 2011).

In contrast, the samples subjected to the 100 °C environment demonstrated the severe effects of testing above the material's T_g. The first sample, 100 °C (1), demonstrated an ultimate maximum load of 275.43 N, which falls within the wide variance of the established baselines. However, this thermal exposure resulted in a critical reduction in extension down to 0.17 mm. This corresponds to an approximate 40% decrease in ductility when compared to the baseline average. The elevated temperature promoted additional cross-linking within the polymer structure, increasing molecular rigidity and resulting in thermal embrittlement (Ishii et al., 2021), see Section 2.6.2 for more information regarding this transition. As a result, the adhesive transitioned from a ductile bonding material into a more brittle, glass-like state.

Furthermore, a second sample subjected to the same 100 °C environment, 100 °C (2), recorded a maximum load of 294.87 N but displayed drastically different ductile behaviour, reaching a peak extension of 0.31 mm before failure. The severe inconsistency in ductility and failure characteristics between the two 100 °C samples reinforces the conclusion that the adhesive suffers from critical thermal instability and unpredictable degradation at this elevated temperature.

Because this failure mechanism is associated with material overstressing rather than representative ageing, 100 °C was considered an invalid accelerated testing condition. To ensure that the ALT targets the relevant failure mode, testing should remain $\leq$ 70 °C.

5.10 atBCD Actuator Overstress Limit Test

An analysis of the combined test data from all four testing phases revealed several important insights regarding the baseline stability, behavioural limits, and failure mechanisms of the actuator piezos. By monitoring the response at both low (400 Hz) and mid-frequency (3000 Hz) operating points, the analysis was able to identify structural changes that may otherwise have been hidden when considering only the overall broadband response. The results highlighted several key observations.

5.10.1 OFL Measurement Variation and Baseline Stability (Phase 1)

The results from the phase 1 revealed a clear frequency-dependent behaviour in the reliability of the measurement setup. At low frequencies, such as 400 Hz, the measurement system was stable. Similarly, within the mid-frequency range, particularly between 2 and 4 kHz, the measurement system demonstrated high stability again, supporting the selection of 3000 Hz as the baseline. In this region, the maximum deviation remained within ±0.25 dB, indicating that the setup was sufficiently sensitive to detect the small performance changes relevant to this project.

At higher frequencies, above approximately 6 kHz, the observed deviations increased significantly. The distinct and opposing responses recorded from the two tested samples suggest that this variation was primarily caused by inherent manufacturing differences between individual actuators, which amplified resonant behaviour, rather than by measurement uncertainty originating from the measurement device.

5.10.2 Failure Threshold (Phase 2)

Phase 2's step-stress screening successfully identified the failure threshold of the actuator. Actuator $\mathcal{A}_1$ remained stable up to 7.5 V_{RMS}, with maximum deviations limited to +0.45 dB at 400 Hz and -0.64 dB at 3000 Hz, thereby satisfying the established pass criteria.

However, exposure to 11 V_{RMS} and 12 V_{RMS} resulted in immediate and irreversible degradation. At 12 V_{RMS}, the actuator exhibited permanent reductions of -8.57 dB at 400 Hz and -9.52 dB at 3000 Hz, even after the 24-hour recovery period. These results indicate permanent depolarisation or internal mechanical damage within the piezoelectric element.

5.10.3 Voltage Degradation Analysis (Phase 3)

Phase 3's endurance tests demonstrated a clear voltage-dependent reduction in actuator performance during sustained excitation. As the applied voltage increased from 4 V_{RMS} to 7 V_{RMS}, the immediate output decreased substantially, reaching as low as -14.78 dB at 3000 Hz during the 7 V_{RMS} test.

Despite these temporary reductions, the 24-hour recovery measurements from the 1-hour endurance tests were generally favourable. Except for one outlier, see Section 5.10.3.1 , all samples tested up to 7 V_{RMS} recovered substantially after the recovery period. The final deviations ranged between -1.43 dB and +0.45 dB, returning close to or within the predefined ±1.0 dB pass criterion. These findings suggest that the large performance losses observed during short-duration operation were primarily transient.

In contrast, supplementary 24-hour endurance tests performed using the rigid mounting solution revealed the limitations of this recovery behaviour during prolonged

exposure. While the 5 V_{RMS} test remained stable, recovering to +0.89 dB at 400 Hz and -0.55 dB at 3000 Hz, continuous operation at 7 V_{RMS} for 24 hours resulted in irreversible degradation, with permanent reductions of -11.81 dB at 400 Hz and -12.50 dB at 3000 Hz.

These results demonstrate that the actuator can tolerate short-duration operation at 7 V_{RMS}, but that sustained long-term operation must remain at lower voltage levels, such as 5 V_{RMS}, to avoid permanent piezoelectric degradation.

5.10.3.1 Abnormal Failure Mode ($\mathcal{A}_6$)

Sample $\mathcal{A}_6$ behaved as an outlier within the endurance dataset. Whereas prolonged voltage exposure generally resulted in a reduction in output force level (negative ΔOFL), $\mathcal{A}_6$ instead exhibited a permanent positive shift of +7.29 dB at 400 Hz and +6.98 dB at 3000 Hz during the 4 V_{RMS} test. Because the actuator failed to recover, the observed behaviour suggests a different mechanism compared to the degradation patterns seen in the other samples. Given the unusually large positive increase at a relatively low voltage, the most likely explanation is an operator-related installation error that affected the baseline measurement. However, the possibility of an internal mechanical defect altering the actuator preload or structural coupling cannot be excluded.

5.10.4 Thermal Stability (Phase 4)

Phase 4's thermal exposure tests isolated the influence of temperature on actuator performance. Rapid heating using the heat gun, which frequently exceeded the intended target temperature by approximately 20 °C due to limited temperature control, produced moderate to severe immediate response shifts. At the nominal 100 °C target, sample $\mathcal{A}_B$ exhibited a +1.69 dB deviation (Marginal), while sample $\mathcal{A}_C$ reached +2.38 dB (Fail) at 400 Hz. Similarly, the lower 70 °C target produced a marginal +1.84 dB shift in sample $\mathcal{A}_F$.

These results indicate a short-term sensitivity to rapid thermal gradients, most likely caused by temporary thermal expansion and material softening within the actuator structure (Nyström, 2026; Poggi, 2026).

However, under sustained thermal exposure in the oven for 24 hours at both 70 °C and 100 °C, followed by a 24-hour recovery period, all tested actuators returned to stable operating conditions. The final recovery measurements remained well within the predefined ±1.0 dB pass criterion. This demonstrates that the actuator components possess strong long-term thermal stability and can recover their normal functional behaviour once thermal equilibrium is re-established.

5.10.5 Testing Limitations

One limitation of the primary test phases was that they were predominantly performed using the standard TU-1000 skull simulator rather than the rigid mounting

solution. Although the skull simulator successfully replicated the acoustic impedance of the human skull, it did not fully reproduce the continuous mechanical stresses and boundary conditions experienced when the actuator was attached to the rigid mounting solution. To address this limitation, supplementary 24-hour endurance testing was performed in Phase 3 using the rigid mounting solution. These tests successfully identified the long-term failure threshold at 7 V_{RMS}, which was not detected during the shorter 1-hour skull simulator experiment. Nevertheless, the initial testing performed using the TU-1000 remained an important prerequisite, as it allowed the actuator's inherent transient and thermal behaviour to be evaluated independently before introducing the additional mechanical influences associated with the rigid mounting solution.

Another limitation was present during Phase 4's thermal exposure tests. Because the TU-1000 skull simulator and the measurement station could not be heated together with the actuator, the samples cooled rapidly while being transferred from the thermal exposure setup to the measurement setup. Consequently, the actuators were not measured exactly at the intended target temperature, which may have reduced the observed thermal influence during the measurements. Furthermore, the heat gun used for rapid thermal exposure lacked precise temperature control and frequently exceeded the intended target temperatures by approximately 20 °C, introducing additional uncertainty regarding the exact thermal loading applied to the actuators.

5.11 Accelerated Life Testing

The developed ALT method, which utilises both voltage excitation and elevated temperature to accelerate ageing of the actuator components, successfully fulfils all requirements and the majority of the desired criteria, as shown in Table 4.23.

5.11.1 Phase 1: Initial System Validation

The results from the 9-day ALT test showed a +0.97 dB immediate deviation in OFL at 400 Hz, increasing slightly to +1.03 dB after the 24-hour recovery period. At 3000 Hz, the deviations were +0.37 dB immediately after testing and +0.47 dB after recovery. The result indicates a minor performance increase at lower frequencies. While the negligible changes at 3000 Hz indicate that the actuator performance remains largely stable in the mid-frequency range. It is important to note that the interface cable connected to the actuator wiring detached during the test, see Figure 4.21 for visualisation of the setup. The exact time of the disconnection is unknown, meaning that the actuator may have been exposed only to thermal ageing without electrical excitation for up to five days. After the cable was reconnected, the test continued for an additional four days. Although component ageing validation was outside the scope of this test, the 9-day test corresponded to 15 years of adhesive element ageing, 7 months of nylon thread-locker element ageing, and 1 year and 3 months of piezoelectric element ageing, based on the acceleration factor calculations presented in Tables 4.18–4.20

5.11.2 Phase 2: System Scaling

The execution of Phase 2 successfully validated both the automated control architecture and the remote monitoring capabilities of the scaled system. The custom Python script managed the APx500 API without manual intervention, capturing the targeted 10 data exports over the course of 240 frequency sweeps. Furthermore, routing the exported CSV files directly to the shared Cochlear network drive proved to be an advantage. It confirmed that long-term ALTs can be securely and reliably monitored in real-time from the main CBAS network, eliminating the need for frequent physical inspections.

However, the results also clearly illustrate a time "penalty". While the targeted testing duration was 2 hours, the actual recorded run time extended to 2 hours and 17 minutes. This 17-minute discrepancy is a consequence of the sequential testing paradigm and software latency. Because the APx500 excites and measures the two actuators consecutively rather than simultaneously, and requires deliberate software pauses to safely process and write the exported data to the network drive, the total duration of a single measurement cycle increases.

Beyond the software constraints, the physical scalability of the setup remains bounded by hardware availability. Expanding the system to test larger batches of actuators simultaneously would require an increase in rigid mounting solutions, amplifier channels, and function generators, which must be carefully balanced against the resources available in the facility.

5.11.3 Phase 3: APx vs ACT ΔOFL Test

Phase 3 executed the validation between the automated APx setup and the established ACT baseline. While the APx system successfully tracked general ΔOFL over time, the observed changes were not directly proportional to the ACT results. This magnitude discrepancy is primarily attributed to the complex thermal and voltage effects acting on the materials during elevated testing in the oven, which differ from the ambient conditions of the ACT.

Additionally, the logged data revealed that the accelerometer's response becomes unstable at frequencies below 250 Hz. Consequently, the continuous in situ APx measurements should not be treated as performance characterisations. Instead, their primary purpose is to serve as a robust, real-time monitoring tool to verify that critical or catastrophic device failure has not occurred during prolonged stress testing.

5.11.4 Phase 4: Stress Influence

Phase 4 successfully isolated the individual contributions of electrical and thermal stresses on actuator performance, revealing distinctly different behavioural responses to each parameter.

The voltage variation profile (at a constant 70 °C) demonstrated a linear relationship between the applied voltage and the resulting ΔOFL. Rather than altering the shape of the frequency response, increasing the voltage effectively shifted the entire output curve upwards across the whole frequency range. For instance, stepping up to 4.3 V_{RMS} resulted in relatively uniform, large-scale output increases of +21.2 dB at 400 Hz and +19.8 dB at 3000 Hz. This indicates that the piezoelectric element's displacement scales predictably with electrical excitation under high thermal loads.

Conversely, the temperature variation profile (at a constant 4.3 V_{RMS}) produced a distinct, frequency-dependent tilt in the response curve. As the ambient temperature increased to 70 °C, the output became higher at lower frequencies (+2.8 dB at 400 Hz) while simultaneously dropping lower at higher frequencies (-2.1 dB at 3000 Hz). Furthermore, the primary resonance peak was visibly lower at these elevated temperatures. This behaviour points to the temperature-induced softening of the actuator's components, which alters the system's stiffness and dampens higher-frequencies.

Crucially, these findings contextualise the magnitude discrepancies observed during the APx versus ACT validation in Phase 3 due to the active stressors. The uniform upward shift driven by high voltages, combined with the frequency-dependent damping and peak attenuation caused by elevated temperatures, confirms that in situ measurements under accelerated environmental stress will inherently diverge from ambient, low-stress baseline characterisations.

5.11.5 Limitations

The first and most significant limitation, which consumed a substantial amount of time throughout the project, was the absence of prior internal input data and baseline ALT data at the start of the work. As a result, considerable time was required to establish the necessary input parameters and testing methodology. In addition, many of the developed methods required multiple iterations before reliable and repeatable results could be achieved. This was particularly true for the manufactured components, fixtures, and mounting solutions, where several redesigns and refinements were necessary throughout the development process. Had these methods and input datasets already existed or been further optimised beforehand, significantly more time could have been allocated to the actual ALT experiments and long-term testing. Nevertheless, future work would likely be able to complete the preparatory stages considerably faster, since the testing methods, fixtures, and sample designs developed during this thesis have now been established and validated.

Furthermore, the ALT requires continuous power throughout the duration of the test and periodic supervision to ensure stable operation, particularly in the event of loose connections or unexpected power losses.

Another limitation was the determination of activation energy (E_a) values. Relevant literature data was difficult to identify because activation energies are highly

dependent on the specific material composition and the failure mechanism being investigated. A similar challenge existed for the stress exponent n used in the inverse power law model. For the piezoelectric component, these parameters were partly supported by internal Cochlear sources (Cochlear, 2026a). However, for the remaining materials, the parameters were primarily estimated from available academic literature and public datasheets. Conservative parameter values were intentionally selected to avoid unrealistically high acceleration factors, particularly because the stress exponent has an exponential influence on the resulting calculations. Consequently, the calculated acceleration factors and equivalent ageing durations should be regarded as estimates rather than exact predictions.

One possible method for improving the validity of the ALT model would be to compare the accelerated ageing results with an already validated 10-year lifetime actuator. Another possible approach would be to operate such a reference actuator in parallel with the accelerated test samples and continuously compare their performance degradation throughout the test period. However, this approach also introduces limitations, since some components within an already validated actuator may not tolerate the elevated stress conditions required for accelerated testing.

Lastly, it is important to note that the investigated failure modes age at significantly different rates under the same accelerated test conditions. Consequently, a single ALT setup may overstress certain components long before the target lifetime of another component has been reached. For instance, an ALT conducted at 70 °C and 4 V_{RMS} would require 21.56 weeks to achieve a simulated 10-year lifetime for the nylon thread-locker. However, over the same duration, the piezoelectric element would correspond to approximately 21 simulated years of ageing, while the adhesive would reach an equivalent of approximately 254 years. This disparity demonstrates how the more robust components may become significantly overstressed in order to ensure that the weakest failure mode reaches the required reliability threshold. As a result, it may be more effective to primarily base the combined ALT duration on the piezoelectric element while performing separate dedicated ageing tests for the thread-locker and adhesive elements.

5.11.6 Answers to Research Questions

As the research questions (RQs) guided the direction of the thesis, answering them serves as the final validation of the developed ALT methodology.

RQ1: Which stressors most effectively accelerate these failure modes?
According to the calculated ALT durations for each failure mode, the most effective stressor depends heavily on the specific component. The adhesive element is most susceptible to temperature, whereas the piezoelectric element is primarily accelerated by elevated voltage. The nylon thread-locker element, on the other hand, exhibits a linear acceleration response but requires significantly higher stress levels to degrade at the same rate as the other components. While the results obtained in this thesis confirm that both elevated voltage and increased temperature suc-

cessfully contribute to accelerated degradation, their long-term combined influence remains uncertain. To fully understand these interactions and definitively determine which stressor drives the overall system ageing, separate long-term exposure tests for isolated stressors, alongside combined validation testing, should be conducted in future work.

RQ2: Can multiple stressors be combined in a single system without compromising validity?
The possibility of combining multiple stressors within a single ALT system was successfully demonstrated. Independent input testing identified suitable voltage and temperature limits, and short-duration ALT runs confirmed that simultaneous stressing is feasible. However, the long-term interaction between electrical and thermal overstressing remains insufficiently understood. Consequently, further long-term combined-stressor validation is required to determine whether additional unintended degradation mechanisms may emerge.

RQ3: How accurately does accelerated degradation correlate with the failure mode?
The accelerated degradation observed during the input testing correlated well with the investigated failure modes. The developed methodology is capable of identifying measurable changes in performance and material behaviour under accelerated conditions. Nevertheless, since most of the initial experiments were conducted with isolated stressors, the long-term correlation accuracy under combined stress conditions still requires further investigation.

RQ4: What inputs are required for the ALT?
The developed ALT methodology requires several critical input parameters, including baselines, acceleration model constants, activation energies, stress exponents, and experimentally determined overstress limits for each investigated failure mode. In addition, accelerometers, mounting solutions and OFL measurements are required for the ALT as well. Moreover, both Option A: Integrated Solution and Option B: Modular Solution utilise equipment already available at CBAS, only a cable was purchased during testing. As a result, the overall implementation cost was relatively low, making the system highly cost-efficient from a development perspective. However, the required instrumentation itself is expensive. For example, a professional audio analyser can cost approximately $10 000 (AP, 2008).

RQ5: How efficiently can the ALT methodology be scaled?
Both proposed ALT configurations are considered scalable. However, Option B provides significantly greater scalability due to its 12 amplifier channels, allowing multiple simultaneous tests to be conducted in parallel. In comparison, Option A is limited to two channels and therefore fewer simultaneous tests. However, Option A also provides integrated data acquisition and monitoring capabilities, which Option B lacks. Overall, the proposed ALT framework demonstrates good scalability, with the preferred configuration depending on Cochlear's future testing requirements and resource availability.

5.12 Ethical, Ecological and Societal Considerations

During the development of the ALT method, ethical, ecological, and societal considerations were taken into account. This chapter describes how these aspects were considered throughout the development of the proposed ALT methodology and testing approach, as well as the potential impact the developed ALT method may have from these perspectives.

5.12.1 Ethical Considerations

The implementation of ALT methods offers several ethical advantages. By reducing the time required to evaluate product lifetime, the time-to-market for medical implants can be shortened. This enables patients to benefit earlier from improved technologies. Furthermore, faster and more reliable lifetime predictions may reduce the need for revision surgeries, thereby decreasing patient risk, uncertainty, and psychological stress associated with implant longevity.

However, there are potential ethical limitations. Accelerated testing may not fully replicate all real-world conditions, which introduces uncertainty in the results. If not properly validated, this could lead to overestimation of product lifetime and, consequently, unrealistic expectations being communicated to patients. Ensuring robust validation of ALT models is therefore needed to avoid misleading claims.

5.12.2 Environmental Impact

From an environmental perspective, the proposed ALT methodology presents several benefits. Compared to conventional long-term testing methods, which can run continuously over several years, ALT significantly reduces the total testing duration. This leads to lower cumulative energy consumption per test cycle. Additionally, much of the required experimental setup either utilizes existing equipment available at Cochlear or components manufactured from a single material, which facilitates recycling.

Despite these advantages, there are also environmental drawbacks to consider. The reduced testing time enables a higher number of test iterations, which may result in equipment operating continuously (e.g., 24/7 usage), thereby offsetting some of the energy savings. Moreover, each new test iteration requires electrical energy and material resources, particularly when components or samples must be reproduced. The need for larger sample sizes to ensure statistical reliability can further increase material consumption. Additional custom equipment, such as specialized cables and fixtures, also contributes to resource use. Finally, destructive testing inherently leads to material waste, necessitating the production of replacement samples.

5.12.3 Societal Impact

The developed ALT approach also provides societal benefits. In particular, the use of a cost-effective skull simulator, manufactured from a single recyclable material, contributes to reducing overall testing costs. This makes advanced testing methodologies more accessible and scalable, potentially accelerating innovation within the field of biomedical implants.

Nevertheless, broader societal implications depend on the responsible implementation of the method, including transparent communication of its limitations and uncertainties.

6
Conclusion

This thesis successfully developed an accelerated life testing (ALT) methodology for Cochlear's active transcutaneous bone conduction device (atBCD). Through theoretical modelling, concept development, and practical experimentation, the work identified suitable acceleration stressors and experimentally determined safe accelerated operating ranges for the investigated failure modes.

Experimental methods were developed for adhesive degradation, nylon thread-lock loosening, and piezoelectric behavioural changes caused by ageing. The results demonstrated that thermal and electrical overstressing could be applied without causing immediate catastrophic failure, while still accelerating degradation mechanisms relevant to long-term device reliability.

In addition, a scalable ALT setup with automatic data logging and testing framework was successfully designed, and validated. The developed methodology enables simultaneous testing of multiple actuator systems and provides a foundation for future long-term reliability studies within Cochlear. To further validate the functionality and stability of the developed framework, an initial ALT run was started using an input voltage of 4.3 V_{RMS} and a temperature of 70 °C over a 9-day period to verify that the overall system operated as intended under combined stressing conditions.

Although complete lifetime correlation and full degradation validation were outside the scope of this thesis due to time limitations, the project established the necessary input data, experimental methods, and system architecture required for continued ALT implementation. The work therefore contributes both engineering and business value by supporting faster product development cycles, earlier verification of design changes, and reduced long-term testing durations.

7
Future Work

Future work should primarily focus on long-term validation of the developed accelerated life testing (ALT) methodology. Since this thesis mainly established the experimental methods, overstress limits, and system architecture, extended-duration testing is required to verify how accurately accelerated degradation correlates with real-world ageing and failure behaviour.

Additionally, further testing at different voltage and temperature combinations should be conducted and analysed using ALT distribution analysis methods, such as Weibull analysis, as recommended by Islam and Ahmad (1994). This would help establish statistically validated degradation trends and improve understanding of the system's true operational and overstress limits once larger numbers of iterations and samples have been tested, which could change the pass/fail criteria and acceleration models.

The developed input data experiments are currently specific to the investigated active transcutaneous bone conduction device (atBCD) actuator. Therefore, if other actuator generations or variants are to be evaluated, the input testing methodology and overstress characterization should be repeated and adapted accordingly. Future work could expand the methodology to additional actuator generations, alternative implant architectures, and other failure modes that were not included within the scope of this thesis due to time limitations.

Finally, the ALT infrastructure and wiring management could be further improved. One possible solution would be to construct small protective enclosures for each tested actuator. These enclosures should be compact while still providing sufficient space for both the actuator and its mounting solution. In addition, a foam-lined base could be incorporated to reduce vibrations transmitted during testing. The actuator wiring could then be connected to a reinforced cable harness protected by heat-shrink tubing and routed through organised cable channels between the climate chamber and the excitation system. Such a configuration would improve cable organisation and reduce the likelihood of critical connection points becoming loose during long-duration testing. This proposed solution would be compatible with both Option A and Option B. However, it may slightly reduce overall scalability and introduce additional soldered connection points, which themselves could become potential failure locations over extended operation. Furthermore, relocating the ALT setup may become more difficult if the cable management system is specifically designed around the layout of the current climate chamber.

Bibliography

Almefelt, L. (2024). Design methodology: The requirement specification. Lecture presented at PPU140 Design Methodology preparatory course, Chalmers University of Technology, November 12, 2024.

AP (2008). Audio precision introduces two-channel models of apx audio analyzer. `https://www.ap.com/news/audio-precision-introduces-two-channel-models-of-apx-audio-analyzer`. Accessed: 2026-05-17.

APC International (2026). Soft vs. hard piezo ceramic. `https://www.americanpiezo.com/knowledge-center/piezo-theory/ceramics/`. Accessed: 2026-03-16.

Azhirnian, A. (2026). Discussions with Cochlear's Senior Electroacoustic Development Armin Azhirnian. Meetings.

Bal-Ozturk, A., Cecen, B., Avci-Adali, M., Topkaya, S. N., Alarcin, E., Yasayan, G., Li, Y.-C. E., Bulkurcuoglu, B., Akpek, A., Avci, H., Shi, K., Shin, S. R., and Hassan, S. (2021). Tissue adhesives: From research to clinical translation. *Nano Today*, 36:101049. Accessed: 2026-04-09.

Bederna, F. (2026). Discussions Regarding Risks with Cochlear's Senior Acoustics Engineer Felicitas Bederna. Meetings.

Berger, K. W. (1976). Early Bone Conduction Hearing Aid Devices. *Archives of Otolaryngology*, 102(5):315–318.

Bhattacharya, A., Sen, A., and Das, S. (2010). An investigation on the anti-loosening characteristics of prevailing torque nuts under transverse vibration. *Mechanism and Machine Theory*, 45(8):1215–1225.

Bickford, J. H. (1995). *An Introduction to the Design and Behavior of Bolted Joints*. CRC Press, Boca Raton, FL, 3rd edition.

Castagnet, S. (2009). High-temperature mechanical behavior of semi-crystalline polymers and relationship to a rubber-like "relaxed" state. *Mechanics of Materials*, 41(2):75–86.

Cochlear (2026a). Cochlear's Internal Material.

Cochlear (2026b). Proven over time: Continuing professor clark's work. `https://www.cochlear.com/uk/en/about-us/proven-over-time`. Accessed: 2026-04-28.

Cochlear Limited (2026a). Cochlear® Osia® System. https://www.cochlear.com/us/en/home/products-and-accessories/cochlear-osia-system. Accessed: 2026-02-05.

Cochlear Limited (2026b). Cochlear™ Baha® System. https://www.cochlear.com/us/en/home/products-and-accessories/cochlear-baha-system. Accessed: 2026-02-05.

Electronics Tutorials (2026a). Capacitive reactance. Accessed: 2026-04-21.

Electronics Tutorials (2026b). Capacitor characteristics and quality factor. https://www.electronics-tutorials.ws/capacitor/cap_8.html. Accessed: 2026-04-22.

Electronics Tutorials (2026c). Impedance and complex impedance. https://www.electronics-tutorials.ws/accircuits/impedance.html. Accessed: 2026-04-22.

Electronics Tutorials (2026d). Power triangle and power factor. https://www.electronics-tutorials.ws/accircuits/power-triangle.html. Accessed: 2026-04-21.

Ellingson, S. W. (2018). *Electromagnetics, Vol. 1.* VT Publishing, Blacksburg, VA. Licensed under CC BY-SA 4.0.

Ferry, L., Sonnier, R., Lopez-Cuesta, J.-M., Petigny, S., and Bert, C. (2017). Thermal degradation and flammability of polyamide 11 filled with nanoboehmite. *Journal of Thermal Analysis and Calorimetry*, 129(2):1029–1037.

Frascio, M., Minuto, M., Musiari, F., Morchio, S., Usman, K. M., Dittamo, F., Zoppi, M., and Avalle, M. (2025). Thermal curing of adhesive joints enabled by precision heating multi-material additive manufacturing. *Journal of Manufacturing and Materials Processing*, 9(5).

Hong, C.-H., Kim, H.-P., Choi, B.-Y., Han, H.-S., Son, J. S., Ahn, C. W., and Jo, W. (2016). Lead-free piezoceramics – where to move on? *Journal of Materiomics*, 2(1):1–24.

Hooker, M. W. (1998). Properties of pzt-based piezoelectric ceramics between -150 and 250°c. Technical Report NASA/CR-1998-208708, National Aeronautics and Space Administration (NASA), Langley Research Center, Hampton, Virginia, USA. Accessed: 2026-03-16.

Hottinger Bruel & Kjaer (2025). Inverse power law relationship. https://help.reliasoft.com/reference/accelerated_life_testing_data_analysis/alt/inverse_power_law_relationship.html. Accessed: 2026-03-28.

Håkansson, B. and Carlsson, P. (1989). Skull simulator for direct bone conduction hearing devices. *Scandinavian Audiology*, 18(2):91–98. PMID: 2756338.

Håkansson, B., Reinfeldt, S., Persson, A.-C., Jansson, K.-J. F., Rigato, C., Hultcrantz, M., and Eeg-Olofsson, M. (2019). The bone conduction implant – a review and 1-year follow-up. *International Journal of Audiology*, 58(12):945–955. PMID: 31710259.

Håkansson, B. E. (2003). The Balanced Electromagnetic Separation Transducer: A New Bone Conduction Transducer. *The Journal of the Acoustical Society of America*, 113(2):818–825.

Håkansson, B. E., Tjellström, A., Rosenhall, U., and Carlsson, P. (1985). The Bone-Anchored Hearing Aid: Principal Design and a Psychoacoustical Evaluation. *Acta Oto-Laryngologica*, 100(3-4):229–239. PMID: 4061073.

InCure Lab (2026). Delamination problems in repeated heat cycle environments. `https://incurelab.com/wp/delamination-problems-in-repeated-heat-cycle-environments`. Accessed: 2026-04-13.

Ishii, H., Hirai, N., and Ohki, Y. (2021). Comparison of degradation behavior between soft and hard epoxy resins. *Journal of Nuclear Science and Technology*, 58(5):620–628. Accessed: 2026-04-20.

Islam, A. and Ahmad, N. (1994). Optimal design of accelerated life tests for the weibull distribution under periodic inspection and type i censoring. *Microelectronics Reliability*, 34(9):1459–1468.

Junker, G. H. (1969). New criteria for self-loosening of fasteners under vibration. *SAE transactions*, 78:314–335.

Kinloch, A. J. (1987). *Adhesion and Adhesives: Science and Technology*. Springer Dordrecht, Dordrecht, Netherlands, 1 edition.

Lakhloufi, H. (2026). Temperature-voltage acceleration models. `https://metricgate.com/docs/temperature-voltage-acceleration-models/`. Accessed: 2026-06-11.

Ling, Y. (2023). What is the curie temperature of piezoelectric ceramics? `https://products.meridianadhesives.com/storage/downloads/paqdrgvdmdzmcktljt9orprwnqch6u4g/360.pdf`. Accessed 2026-03-18.

Martinez, A. (2021). The evolution of the baha system 1977–2021. `https://hearandnow.cochlear.com/hearing-solutions/bone-conduction/evolution-of-baha/`. Accessed: 2026-04-28.

MatWeb, LLC (2026). Overview of materials for polyphthalamide (ppa). `https://www.matweb.com/search/DataSheet.aspx?MatGUID=5d10c9b3bb0c40398ea4f2b52da6ce64`. Accessed: 2026-03-26.

McKeen, L. W. (2012a). Chapter 2 - introduction to the properties of plastic and elastomer films. In McKeen, L. W., editor, *Film Properties of Plastics and Elastomers (Third Edition)*, Plastics Design Library, pages 19–55. William Andrew Publishing, Boston, third edition edition. Accessed: 2026-03-16.

McKeen, L. W. (2012b). Chapter 2 - introduction to the properties of plastic and elastomer films. In McKeen, L. W., editor, *Film Properties of Plastics and Elastomers (Third Edition)*, Plastics Design Library, pages 19–55. William Andrew Publishing, Boston, third edition edition. Accessed: 2026-03-16.

MED-EL (2026). Bonebridge. https://www.medel.com/en-gb/hearing-solutions/bonebridge. Accessed: 2026-02-23.

Moldoveanu, S. and David, V. (2021). Chapter 6 - solvent extraction. In Moldoveanu, S. and David, V., editors, *Modern Sample Preparation for Chromatography (Second Edition)*, pages 191–279. Elsevier, second edition edition. Accessed: 2026-03-16.

Mravljak, M. and Sernek, M. (2011). The influence of curing temperature on rheological properties of epoxy adhesives. *Drvna industrija*, pages 19–25.

Nelson, W. (1980). Accelerated Life Testing - Step-Stress Models and Data Analyses. *IEEE Transactions on Reliability*, R-29(2):103–108.

Nelson, W. (1990a). *Accelerated Testing: Statistical Models, Test Plans, and Data Analysis*. John Wiley & Sons, New York.

Nelson, W. (1990b). *Models for Life Tests with Constant Stress*. John Wiley Sons, Ltd.

NIST (2026a). Arrhenius model. https://www.itl.nist.gov/div898/handbook/apr/section1/apr151.htm. Accessed: 2026-03-10.

NIST (2026b). Molar gas constant. https://physics.nist.gov/cgi-bin/cuu/Value?r|search_for=gas. Accessed 2026-03-10.

Nyström, D. (2026). Discussions with Cochlear's Senior Project Engineer Dan Nyström. Meetings.

Odegard, G. M. and Bandyopadhyay, A. (2011). Physical aging of epoxy polymers and their composites. *Journal of Polymer Science Part B: Polymer Physics*, 49(24).

Oticon Medical (2026a). Ponto System. https://www.oticonmedical.com/solutions/bone-conduction/ponto-system. Accessed: 2026-02-23.

Oticon Medical (2026b). Sentio System. https://sentio.oticonmedical.com/. Accessed: 2026-02-23.

Park, P., Kim, G., and Barocio, E. (2025). Thermal fatigue of adhesive bonding in additively manufactured cf-pesu composites. Accessed: 2026-04-15.

Peñaranda, D., García, J. M., Aparicio, M. L., Montes, F., Barón, C., Jiménez, R. C., and Peñaranda, A. (2018). Retrospective analysis of skin complications related to bone-anchored hearing aid implant: association with surgical technique, quality of life, and audiological benefit. *Brazilian Journal of Otorhinolaryngology*, 84(3):324–331.

Pike, R. A. (2026). Adhesive. https://www.britannica.com/technology/adhesive. Accessed: 2026-04-08.

Poggi, L. (2026). Continuous Meetings and Discussion with Cochlear's Senior Mechanical Engineer and Supervisor Luke Poggi. Meetings.

Reinfeldt, S. (2009). *Bone Conduction Hearing in Human Communication : Sensitivity, Transmission, and Applications*.

Reinfeldt, S. (2026). Continous Meetings with Academic Supervisor Sabine Reinfeldt. Meetings.

Reinfeldt, S., Eeg-Olofsson, M., Fredén Jansson, K.-J., Persson, A.-C., and Håkansson, B. E. (2022). Long-term Follow-up and Review of the Bone Conduction Implant. *Hearing Research*, 421:108503. Acoustic Implant Technology.

Schenkelberg, F. (2026). Temperature & humidity accelerated life testing. `https://accendoreliability.com/temperature-humidity-accelerated-life-testing/`. Accessed: 2026-03-31.

Sittsamer, M. (2022). Understanding the 6ms of process control. `https://www.ease.io/blog/understanding-the-6ms-of-process-control/`. Accessed: 2026-05-21.

Stenfelt, S. and Goode, R. L. (2005). Bone-Conducted Sound: Physiological and Clinical Aspects. *Otology & Neurotology*, 26(6):1245–1261.

Stephen, J. T., Marshall, M. B., and Lewis, R. (2017). Relaxation of contact pressure and self-loosening in dynamic bolted joints. *Proceedings of the Institution of Mechanical Engineers, Part C: Journal of Mechanical Engineering Science*, 231(18):3462–3475.

Uchino, K. (2012). 3 - piezoelectric ceramics for transducers. In Nakamura, K., editor, *Ultrasonic Transducers*, Woodhead Publishing Series in Electronic and Optical Materials, pages 70–116. Woodhead Publishing. Accessed: 2026-03-17.

Ulrich, K. T. and Eppinger, S. D. (2015). *Product Design and Development*. McGraw-Hill Education, New York, 6 edition. Sixth edition.

Woo, C. (2019). Liquid thread locking solution for machinery assembly industry. In Rudawska, A., editor, *Adhesives and Adhesive Joints in Industry Applications*, chapter 7. IntechOpen, London.

Yujie (2025). Soft and hard pzt piezoelectric materials: Which one fits your application? `https://yujiepiezo.com/blog/understanding-pzt-material-types`. Accessed: 2026-03-16.

Zhao, L. (2024). A review of common acceleration models in accelerated life testing. *Academic Journal of Science and Technology*, 12(3):212–216.

A

Timetable

ID	Task Mod	Task Name	Duration	Start	Finish	Predece	Resource Names
1		**Pre-Study**	**4d**	**Tue 03/02/26**	**Fri 06/02/26**		
2		Current Product	3d	Tue 03/02/26	Thu 05/02/26		Viktor Larsson Rosén,Sam Azadi
3		Failure Modes of Current Product	3d	Wed 04/02/26	Fri 06/02/26		Viktor Larsson Rosén,Sam Azadi
4		Cochlear HQ Tour	0.5d	Tue 03/02/26	Tue 03/02/26		Sam Azadi,Viktor Larsson Rosén
5		**Customer Requirments**	**5d**	**Mon 09/02/26**	**Fri 13/02/26**		
6		Gather Customer Requirements and Needs	4d	Mon 09/02/26	Thu 12/02/26	2,3	Sam Azadi,Viktor Larsson Rosén
7		Assemble Requirement Spec.	1d	Fri 13/02/26	Fri 13/02/26	6	Sam Azadi
8		**Literature Study**	**9d**	**Mon 09/02/26**	**Thu 19/02/26**		
9		Competitors' Solutions	5d	Mon 09/02/26	Fri 13/02/26	2,3	Viktor Larsson Rosén
10		Scientific Papers	3d	Mon 16/02/26	Wed 18/02/26	7	Sam Azadi
11		Similar Failure Modes in Other Products Test Rigs	5d	Mon 09/02/26	Fri 13/02/26	2,3	Viktor Larsson Rosén
12		Compile the Information from Lit. Study	1d	Thu 19/02/26	Thu 19/02/26	10,11,9	Viktor Larsson Rosén,Sam Azadi
13		WP1 Literature Study	0d	Tue 17/02/26	Tue 17/02/26		
14		**Concept Generation**	**5d**	**Fri 20/02/26**	**Thu 26/02/26**		
15		Idea Generation	4d	Fri 20/02/26	Wed 25/02/26	12	Sam Azadi,Viktor Larsson Rosén
16		Compile List of Concepts	1d	Thu 26/02/26	Thu 26/02/26	15	Sam Azadi,Viktor Larsson Rosén
17		**Concept Screening**	**3d**	**Fri 27/02/26**	**Tue 03/03/26**		
18		Elimination Matrix	0.5d	Fri 27/02/26	Fri 27/02/26	16	Sam Azadi,Viktor Larsson Rosén
19		Pugh Matrix	1d	Fri 27/02/26	Mon 02/03/26	18	Sam Azadi,Viktor Larsson Rosén
20		Weighting Kesselring Matrix	1d	Mon 02/03/26	Mon 02/03/26	19	Sam Azadi
21		Propose and Choose Concept(s)	1d	Mon 02/03/26	Tue 03/03/26	20	Sam Azadi,Viktor Larsson Rosén
22		WP2 Product Concept	0d	Tue 03/03/26	Tue 03/03/26		
23		**Simulations**	**11.25d**	**Wed 04/03/26**	**Thu 19/03/26**		
24		**Simlified Actuator Modelling**	**8d**	**Wed 04/03/26**	**Fri 13/03/26**		
25		Initial CAD	1d	Wed 04/03/26	Wed 04/03/26	22	Sam Azadi
26		Refined CAD Model	3d	Thu 05/03/26	Mon 09/03/26	25	Viktor Larsson Rosén
27		Resonance Frequency	3d	Tue 10/03/26	Thu 12/03/26	26	Viktor Larsson Rosén
28		Analysis/Documentation	1d	Fri 13/03/26	Fri 13/03/26	27	Viktor Larsson Rosén
29		**Skull Simulator Modelling**	**3d**	**Thu 05/03/26**	**Mon 09/03/26**	**28**	
30		Point mass models	1d	Thu 05/03/26	Thu 05/03/26		Viktor Larsson Rosén
31		Fixed model	1d	Thu 05/03/26	Thu 05/03/26	30	Viktor Larsson Rosén
32		Spring-Mass-Damper Model	3d	Thu 05/03/26	Mon 09/03/26	31	Viktor Larsson Rosén
33		Analysis/Documentation	1d	Thu 05/03/26	Fri 06/03/26	32	Viktor Larsson Rosén

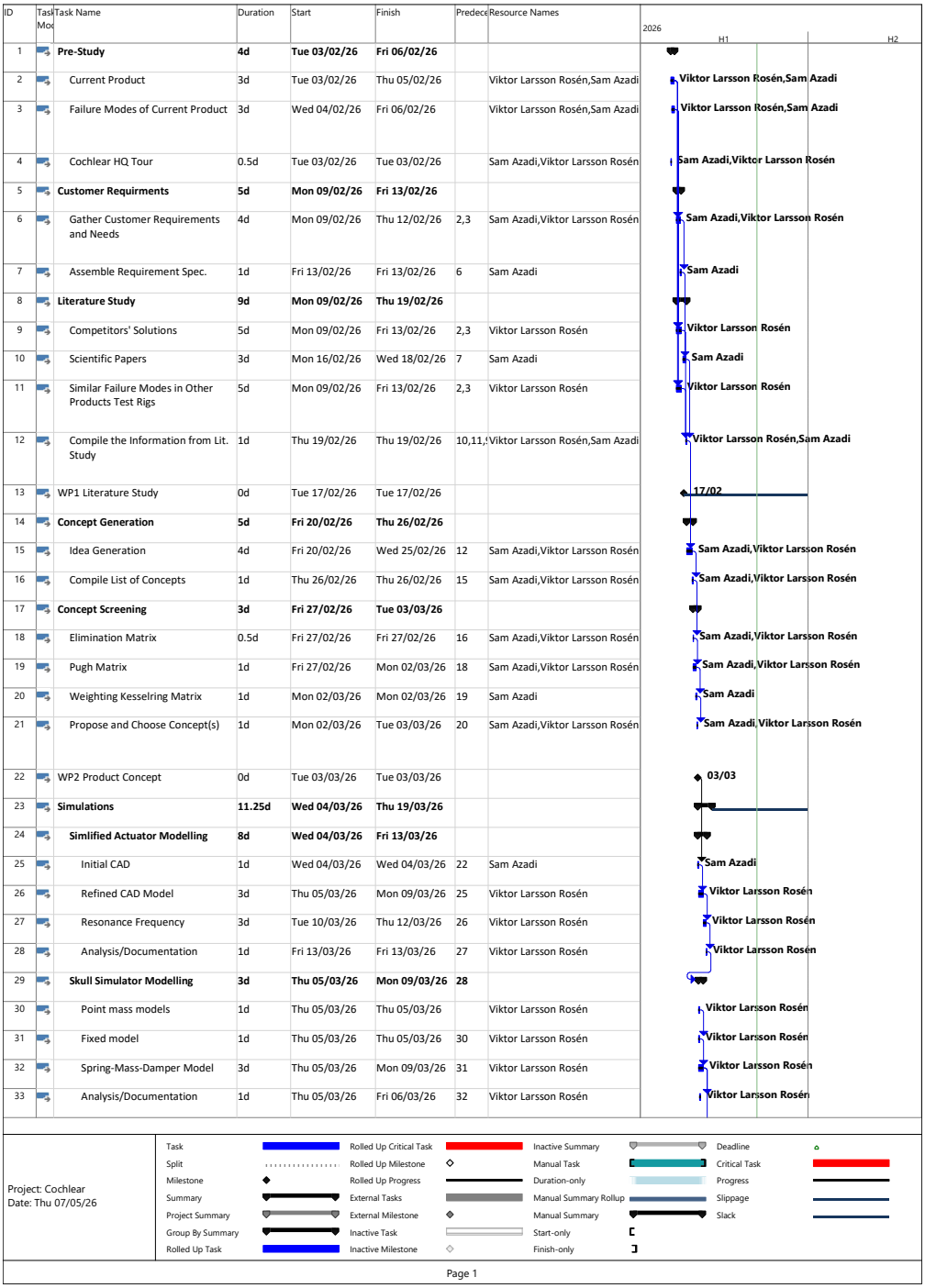

Figure A.1: Gantt chart.

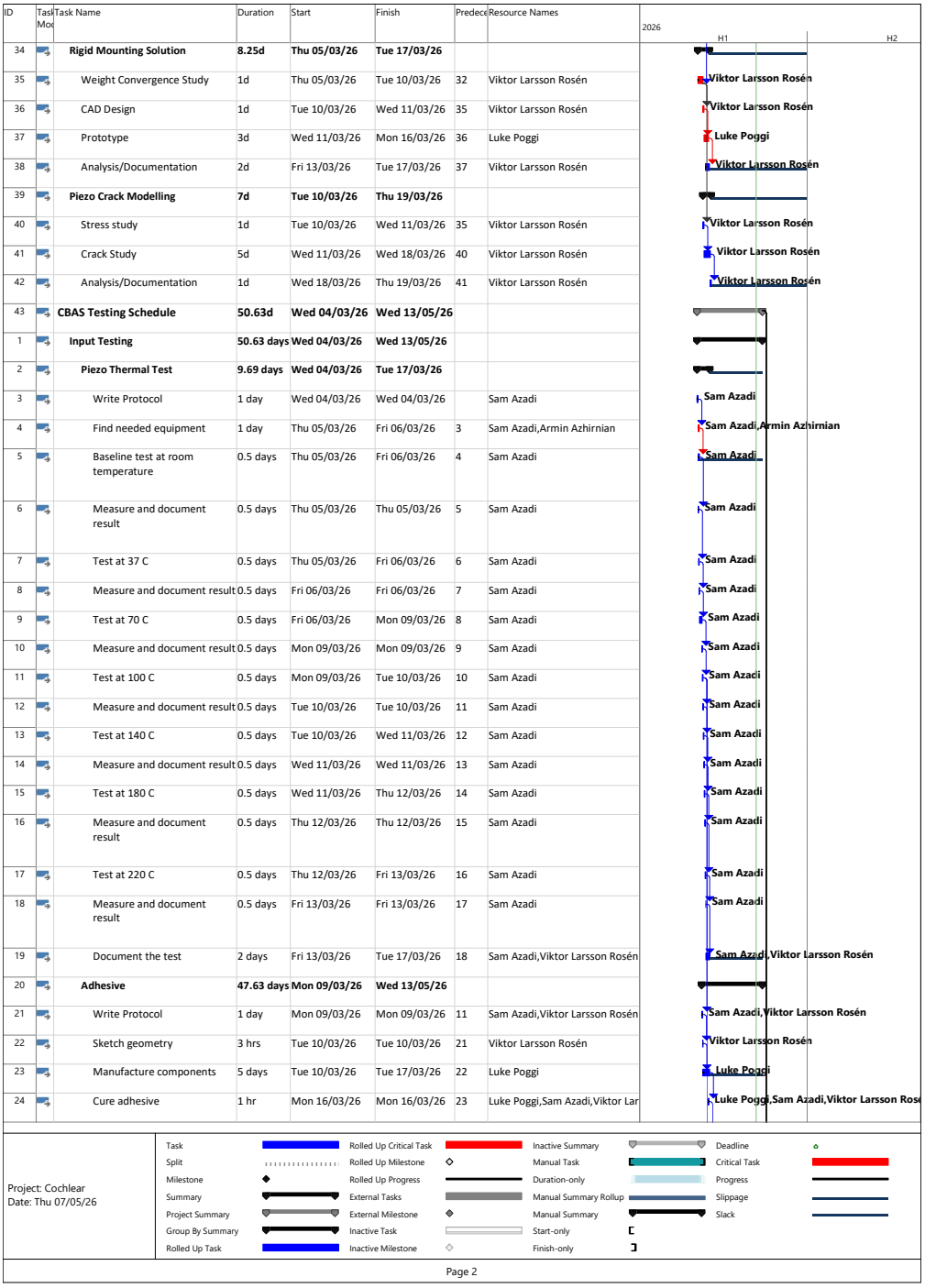

ID	Task Mod	Task Name	Duration	Start	Finish	Predece	Resource Names
34		**Rigid Mounting Solution**	**8.25d**	**Thu 05/03/26**	**Tue 17/03/26**		
35		Weight Convergence Study	1d	Thu 05/03/26	Tue 10/03/26	32	Viktor Larsson Rosén
36		CAD Design	1d	Tue 10/03/26	Wed 11/03/26	35	Viktor Larsson Rosén
37		Prototype	3d	Wed 11/03/26	Mon 16/03/26	36	Luke Poggi
38		Analysis/Documentation	2d	Fri 13/03/26	Tue 17/03/26	37	Viktor Larsson Rosén
39		**Piezo Crack Modelling**	**7d**	**Tue 10/03/26**	**Thu 19/03/26**		
40		Stress study	1d	Tue 10/03/26	Wed 11/03/26	35	Viktor Larsson Rosén
41		Crack Study	5d	Wed 11/03/26	Wed 18/03/26	40	Viktor Larsson Rosén
42		Analysis/Documentation	1d	Wed 18/03/26	Thu 19/03/26	41	Viktor Larsson Rosén
43		**CBAS Testing Schedule**	**50.63d**	**Wed 04/03/26**	**Wed 13/05/26**		
1		**Input Testing**	**50.63 days**	**Wed 04/03/26**	**Wed 13/05/26**		
2		**Piezo Thermal Test**	**9.69 days**	**Wed 04/03/26**	**Tue 17/03/26**		
3		Write Protocol	1 day	Wed 04/03/26	Wed 04/03/26		Sam Azadi
4		Find needed equipment	1 day	Thu 05/03/26	Fri 06/03/26	3	Sam Azadi,Armin Azhirnian
5		Baseline test at room temperature	0.5 days	Thu 05/03/26	Fri 06/03/26	4	Sam Azadi
6		Measure and document result	0.5 days	Thu 05/03/26	Thu 05/03/26	5	Sam Azadi
7		Test at 37 C	0.5 days	Thu 05/03/26	Fri 06/03/26	6	Sam Azadi
8		Measure and document result	0.5 days	Fri 06/03/26	Fri 06/03/26	7	Sam Azadi
9		Test at 70 C	0.5 days	Fri 06/03/26	Mon 09/03/26	8	Sam Azadi
10		Measure and document result	0.5 days	Mon 09/03/26	Mon 09/03/26	9	Sam Azadi
11		Test at 100 C	0.5 days	Mon 09/03/26	Tue 10/03/26	10	Sam Azadi
12		Measure and document result	0.5 days	Tue 10/03/26	Tue 10/03/26	11	Sam Azadi
13		Test at 140 C	0.5 days	Tue 10/03/26	Wed 11/03/26	12	Sam Azadi
14		Measure and document result	0.5 days	Wed 11/03/26	Wed 11/03/26	13	Sam Azadi
15		Test at 180 C	0.5 days	Wed 11/03/26	Thu 12/03/26	14	Sam Azadi
16		Measure and document result	0.5 days	Thu 12/03/26	Thu 12/03/26	15	Sam Azadi
17		Test at 220 C	0.5 days	Thu 12/03/26	Fri 13/03/26	16	Sam Azadi
18		Measure and document result	0.5 days	Fri 13/03/26	Fri 13/03/26	17	Sam Azadi
19		Document the test	2 days	Fri 13/03/26	Tue 17/03/26	18	Sam Azadi,Viktor Larsson Rosén
20		**Adhesive**	**47.63 days**	**Mon 09/03/26**	**Wed 13/05/26**		
21		Write Protocol	1 day	Mon 09/03/26	Mon 09/03/26	11	Sam Azadi,Viktor Larsson Rosén
22		Sketch geometry	3 hrs	Tue 10/03/26	Tue 10/03/26	21	Viktor Larsson Rosén
23		Manufacture components	5 days	Tue 10/03/26	Tue 17/03/26	22	Luke Poggi
24		Cure adhesive	1 hr	Mon 16/03/26	Mon 16/03/26	23	Luke Poggi,Sam Azadi,Viktor Lar

Figure A.2: Gantt chart (continued).

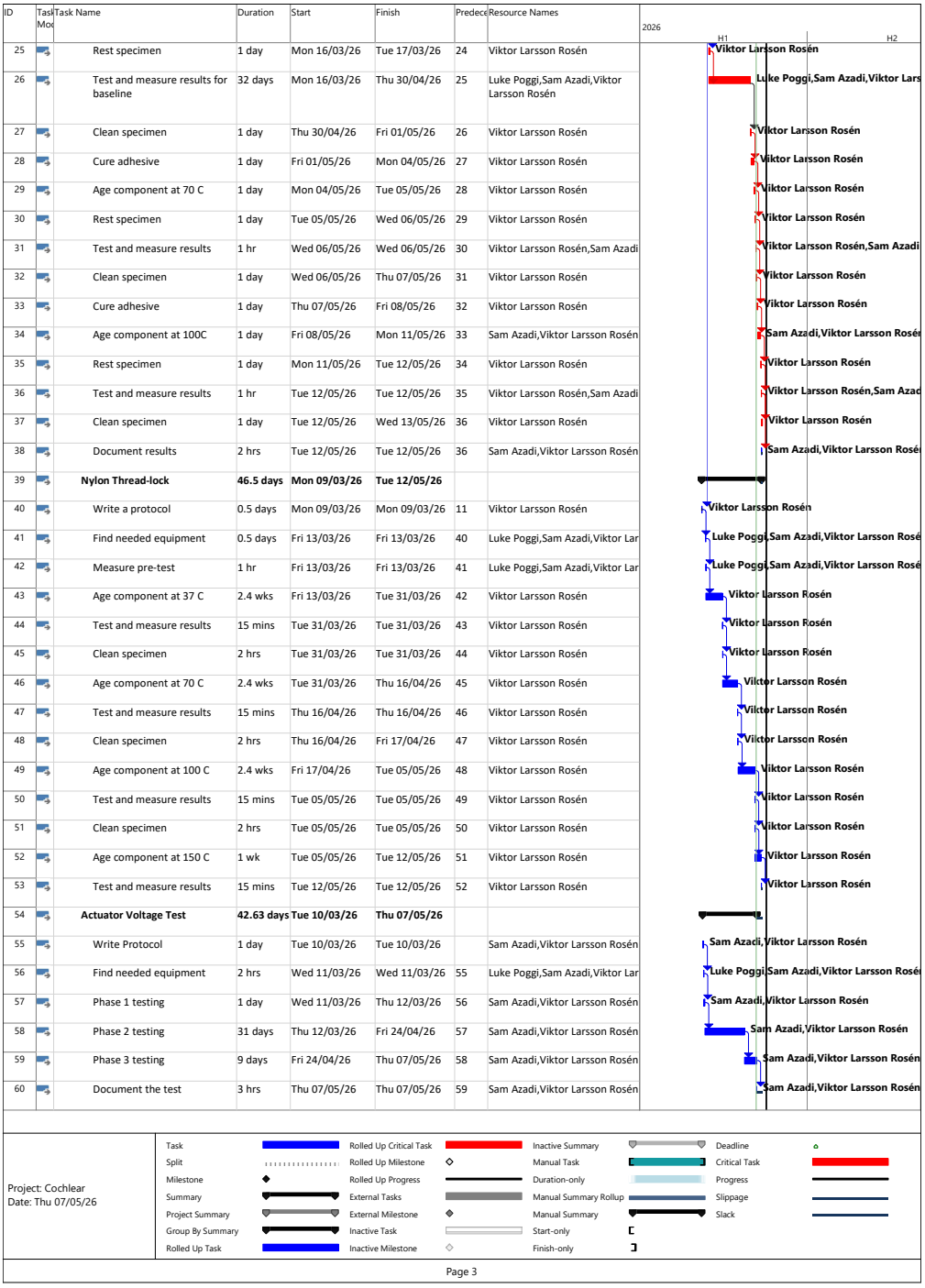

ID	Task Mode	Task Name	Duration	Start	Finish	Predecessors	Resource Names
25		Rest specimen	1 day	Mon 16/03/26	Tue 17/03/26	24	Viktor Larsson Rosén
26		Test and measure results for baseline	32 days	Mon 16/03/26	Thu 30/04/26	25	Luke Poggi,Sam Azadi,Viktor Larsson Rosén
27		Clean specimen	1 day	Thu 30/04/26	Fri 01/05/26	26	Viktor Larsson Rosén
28		Cure adhesive	1 day	Fri 01/05/26	Mon 04/05/26	27	Viktor Larsson Rosén
29		Age component at 70 C	1 day	Mon 04/05/26	Tue 05/05/26	28	Viktor Larsson Rosén
30		Rest specimen	1 day	Tue 05/05/26	Wed 06/05/26	29	Viktor Larsson Rosén
31		Test and measure results	1 hr	Wed 06/05/26	Wed 06/05/26	30	Viktor Larsson Rosén,Sam Azadi
32		Clean specimen	1 day	Wed 06/05/26	Thu 07/05/26	31	Viktor Larsson Rosén
33		Cure adhesive	1 day	Thu 07/05/26	Fri 08/05/26	32	Viktor Larsson Rosén
34		Age component at 100C	1 day	Fri 08/05/26	Mon 11/05/26	33	Sam Azadi,Viktor Larsson Rosén
35		Rest specimen	1 day	Mon 11/05/26	Tue 12/05/26	34	Viktor Larsson Rosén
36		Test and measure results	1 hr	Tue 12/05/26	Tue 12/05/26	35	Viktor Larsson Rosén,Sam Azadi
37		Clean specimen	1 day	Tue 12/05/26	Wed 13/05/26	36	Viktor Larsson Rosén
38		Document results	2 hrs	Tue 12/05/26	Tue 12/05/26	36	Sam Azadi,Viktor Larsson Rosén
39		**Nylon Thread-lock**	**46.5 days**	**Mon 09/03/26**	**Tue 12/05/26**		
40		Write a protocol	0.5 days	Mon 09/03/26	Mon 09/03/26	11	Viktor Larsson Rosén
41		Find needed equipment	0.5 days	Fri 13/03/26	Fri 13/03/26	40	Luke Poggi,Sam Azadi,Viktor Lar
42		Measure pre-test	1 hr	Fri 13/03/26	Fri 13/03/26	41	Luke Poggi,Sam Azadi,Viktor Lar
43		Age component at 37 C	2.4 wks	Fri 13/03/26	Tue 31/03/26	42	Viktor Larsson Rosén
44		Test and measure results	15 mins	Tue 31/03/26	Tue 31/03/26	43	Viktor Larsson Rosén
45		Clean specimen	2 hrs	Tue 31/03/26	Tue 31/03/26	44	Viktor Larsson Rosén
46		Age component at 70 C	2.4 wks	Tue 31/03/26	Thu 16/04/26	45	Viktor Larsson Rosén
47		Test and measure results	15 mins	Thu 16/04/26	Thu 16/04/26	46	Viktor Larsson Rosén
48		Clean specimen	2 hrs	Thu 16/04/26	Fri 17/04/26	47	Viktor Larsson Rosén
49		Age component at 100 C	2.4 wks	Fri 17/04/26	Tue 05/05/26	48	Viktor Larsson Rosén
50		Test and measure results	15 mins	Tue 05/05/26	Tue 05/05/26	49	Viktor Larsson Rosén
51		Clean specimen	2 hrs	Tue 05/05/26	Tue 05/05/26	50	Viktor Larsson Rosén
52		Age component at 150 C	1 wk	Tue 05/05/26	Tue 12/05/26	51	Viktor Larsson Rosén
53		Test and measure results	15 mins	Tue 12/05/26	Tue 12/05/26	52	Viktor Larsson Rosén
54		**Actuator Voltage Test**	**42.63 days**	**Tue 10/03/26**	**Thu 07/05/26**		
55		Write Protocol	1 day	Tue 10/03/26	Tue 10/03/26		Sam Azadi,Viktor Larsson Rosén
56		Find needed equipment	2 hrs	Wed 11/03/26	Wed 11/03/26	55	Luke Poggi,Sam Azadi,Viktor Lar
57		Phase 1 testing	1 day	Wed 11/03/26	Thu 12/03/26	56	Sam Azadi,Viktor Larsson Rosén
58		Phase 2 testing	31 days	Thu 12/03/26	Fri 24/04/26	57	Sam Azadi,Viktor Larsson Rosén
59		Phase 3 testing	9 days	Fri 24/04/26	Thu 07/05/26	58	Sam Azadi,Viktor Larsson Rosén
60		Document the test	3 hrs	Thu 07/05/26	Thu 07/05/26	59	Sam Azadi,Viktor Larsson Rosén

Figure A.3: Gantt chart (continued).

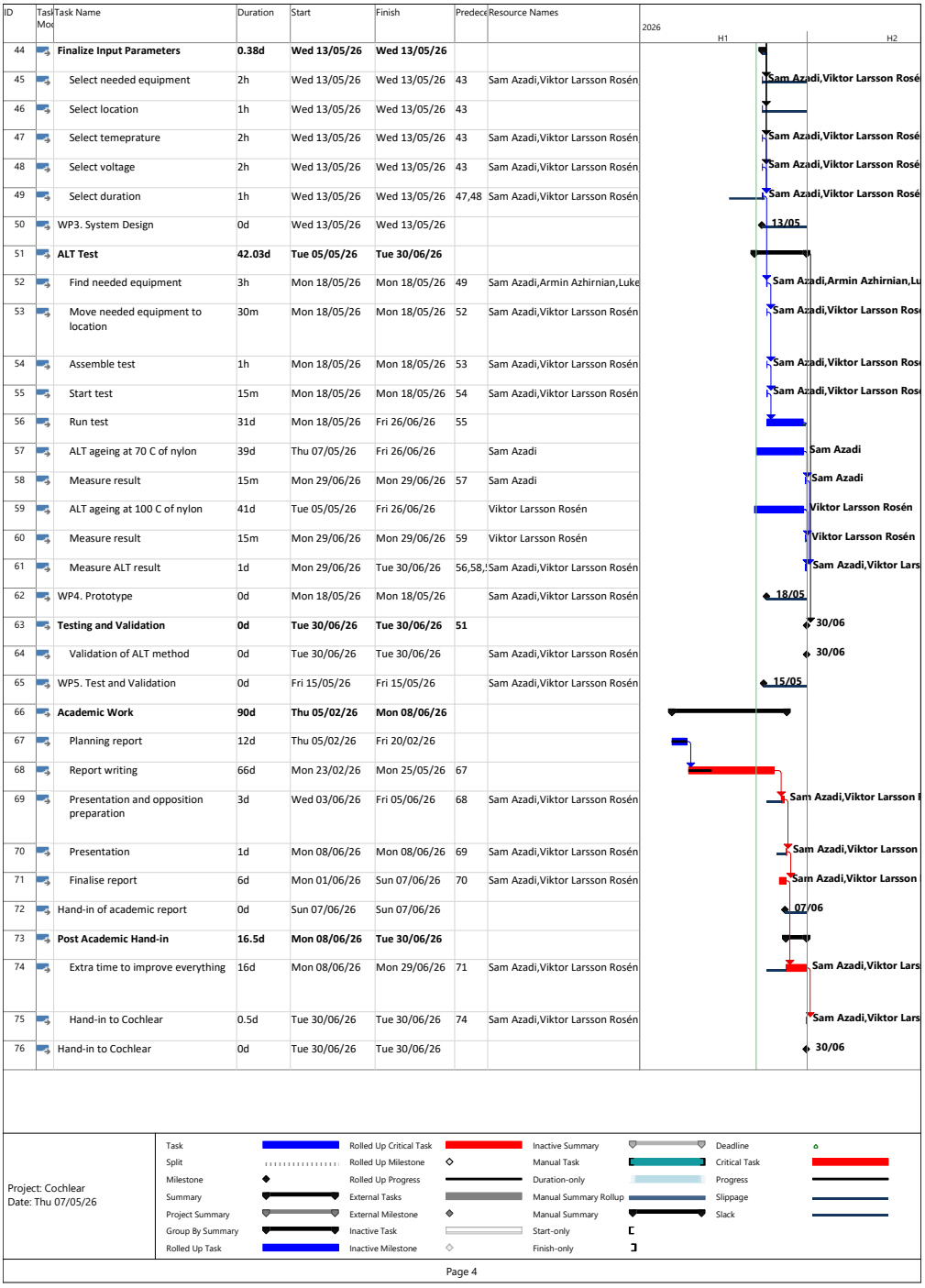

ID	Task Mod	Task Name	Duration	Start	Finish	Predece	Resource Names
44		**Finalize Input Parameters**	**0.38d**	**Wed 13/05/26**	**Wed 13/05/26**		
45		Select needed equipment	2h	Wed 13/05/26	Wed 13/05/26	43	Sam Azadi,Viktor Larsson Rosén
46		Select location	1h	Wed 13/05/26	Wed 13/05/26	43	
47		Select temeprature	2h	Wed 13/05/26	Wed 13/05/26	43	Sam Azadi,Viktor Larsson Rosén
48		Select voltage	2h	Wed 13/05/26	Wed 13/05/26	43	Sam Azadi,Viktor Larsson Rosén
49		Select duration	1h	Wed 13/05/26	Wed 13/05/26	47,48	Sam Azadi,Viktor Larsson Rosén
50		WP3. System Design	0d	Wed 13/05/26	Wed 13/05/26		
51		**ALT Test**	**42.03d**	**Tue 05/05/26**	**Tue 30/06/26**		
52		Find needed equipment	3h	Mon 18/05/26	Mon 18/05/26	49	Sam Azadi,Armin Azhirnian,Luke
53		Move needed equipment to location	30m	Mon 18/05/26	Mon 18/05/26	52	Sam Azadi,Viktor Larsson Rosén
54		Assemble test	1h	Mon 18/05/26	Mon 18/05/26	53	Sam Azadi,Viktor Larsson Rosén
55		Start test	15m	Mon 18/05/26	Mon 18/05/26	54	Sam Azadi,Viktor Larsson Rosén
56		Run test	31d	Mon 18/05/26	Fri 26/06/26	55	
57		ALT ageing at 70 C of nylon	39d	Thu 07/05/26	Fri 26/06/26		Sam Azadi
58		Measure result	15m	Mon 29/06/26	Mon 29/06/26	57	Sam Azadi
59		ALT ageing at 100 C of nylon	41d	Tue 05/05/26	Fri 26/06/26		Viktor Larsson Rosén
60		Measure result	15m	Mon 29/06/26	Mon 29/06/26	59	Viktor Larsson Rosén
61		Measure ALT result	1d	Mon 29/06/26	Tue 30/06/26	56,58,5	Sam Azadi,Viktor Larsson Rosén
62		WP4. Prototype	0d	Mon 18/05/26	Mon 18/05/26		Sam Azadi,Viktor Larsson Rosén
63		**Testing and Validation**	**0d**	**Tue 30/06/26**	**Tue 30/06/26**	**51**	
64		Validation of ALT method	0d	Tue 30/06/26	Tue 30/06/26		Sam Azadi,Viktor Larsson Rosén
65		WP5. Test and Validation	0d	Fri 15/05/26	Fri 15/05/26		Sam Azadi,Viktor Larsson Rosén
66		**Academic Work**	**90d**	**Thu 05/02/26**	**Mon 08/06/26**		
67		Planning report	12d	Thu 05/02/26	Fri 20/02/26		
68		Report writing	66d	Mon 23/02/26	Mon 25/05/26	67	
69		Presentation and opposition preparation	3d	Wed 03/06/26	Fri 05/06/26	68	Sam Azadi,Viktor Larsson Rosén
70		Presentation	1d	Mon 08/06/26	Mon 08/06/26	69	Sam Azadi,Viktor Larsson Rosén
71		Finalise report	6d	Mon 01/06/26	Sun 07/06/26	70	Sam Azadi,Viktor Larsson Rosén
72		Hand-in of academic report	0d	Sun 07/06/26	Sun 07/06/26		
73		**Post Academic Hand-in**	**16.5d**	**Mon 08/06/26**	**Tue 30/06/26**		
74		Extra time to improve everything	16d	Mon 08/06/26	Mon 29/06/26	71	Sam Azadi,Viktor Larsson Rosén
75		Hand-in to Cochlear	0.5d	Tue 30/06/26	Tue 30/06/26	74	Sam Azadi,Viktor Larsson Rosén
76		Hand-in to Cochlear	0d	Tue 30/06/26	Tue 30/06/26		

Figure A.4: Gantt chart (continued).

B

Risk Assessment

Table B.1: Full risk assessment. Completed with Poggi (2026); Bederna (2026).

Probability (P):	Consequence (C):	Risk assessment	ERICPD
4 Almost certain	4 Very serious	10 - 16 High risk	E = Eliminate
3 Likely	3 Serious	6 - 9 Medium risk	R = Reduce
2 Less likely	2 Minor	1 - 5 Low risk	I = Isolate
1 Unlikely	1 Insignificant		C = Control
			PPE = Personal protective equipment
			D = Discipline

Risk assessment performed/updated by:	
Sam Azadi, Felicitas Bederna, Viktor Larsson Rosén and Luke Poggi	
Assessed Master Thesis project:	
Development of Accelerated Life Testing Method for Bone Conducting Devices	
Date:	2026-02-23

No.	Risk (event)	Risk description (Cause)	Consequence	Comments, existing barriers, or if risk is identified at external collaborator	P	C	Assessed risk	Risk reduction action as per (ERICPD).	Responsible	Completion date	P	C	Remaining risk	Result / finishing conclusion, or description of future action. References (role, procedure, etc.).
E1	*Electrical shock or short circuit during testing*	*Prototype electronic systems may involve exposed conductors during early-stage development.*	*Electrical shock, burns, or fire.*	*Early testing prototype(s) have uninsulated wiring and workbench is cluttered, increasing chance of contact.*	2	3	6	*Reduce / Control: Insulate wiring, organise workbench, and use limited power.*	*All group members*	*Before prototype testing begins*	1	2	2	*Risk reduced to acceptable level once wiring is insulated and testing is performed with current limitation.*
M1	*Body parts caught in moving parts*	*Mechanical prototype includes exposed moving parts that are tested without guarding.*	*Pinch injury or bruising to body parts.*	*No guard is installed over the moving mechanism and control software lacks motion limits.*	3	4	12	*Control / PPE: Install guard, use PPEs and keep safe distance as well as introduce motion limits. Performing the initial tests at reduced speed could be helpful too.*	*All group members*	*Before full-speed mechanical testing*	1	2	2	*Guarding and frame stabilisation make the risk acceptable for supervised testing.*
C1	*Skin or eye contact with chemicals*	*During handling of chemicals used in prototype assembly and testing, accidental splashes or direct contact may occur.*	*Skin/eye irritation/injury, or chemical burns.*	*Chemicals are stored in the laboratory; safety data sheets (SDS) are available, but use of PPE and SDS is neglected by students.*	2	3	6	*Control / PPE: Do not neglect reviewing the safety data sheets before use and wearing appropriate PPE, use chemicals in ventilated areas and clean spills immediately.*	*All group members*	*Before use of chemicals*	1	2	2	*When ventilation is used and correct PPEs are used, risk is minimal and acceptable.*
C2	*Inhalation of adhesive fumes*	*Certain bonding agents used in prototype may expose user to dangerous chemicals in poorly ventilated spaces.*	*Headache, dizziness, respiratory irritation, or impaired concentration.*	*Ventilation present but not actively used, and no mandatory PPE.*	2	3	6	*Control / PPE: Use adhesives only in ventilated area or under fume extraction, wear gloves and mask or limit exposure time.*	*All group members*	*Before use of adhesives*	1	2	2	*When ventilation is used and correct PPEs are used, inhalation risk is minimal and acceptable.*
B/F1	*Burns from high temperature surfaces*	*Skin contact with high temperature surfaces - such as 3D-printing nozzles, soldering - during work.*	*Skin burns/injury.*	*Inadequate training and/or users ignoring safety instructions.*	2	3	6	*Reduce / PPE: Waiting for nozzle to cool down and by using gloves or a adequate tool(s).*	*All group members*	*Before use of equipment*	1	3	3	*Risk reduced once relevant safety equipments are used correctly.*
D1	*Unintentional sharing of confidential information*	*During reporting of technical details from Cochlear to the academic world, confidential information may be included unintentionally.*	*Breach of NDA, legal implications and loss of trust with Cochlear.*	*Project involves external collaboration with high amount of sensitive data.*	2	4	8	*Control / Discipline: Knowing of confidetially before starting the project and implementing mandatory document review by Cochlear before any submissions or public presentations. Possibilty to change scope if confidentiality constraints becomes too much of a hinderance.*	*All group members, Cochlear's supervisor*	*Before hand-ins*	1	4	4	*Probability of risk reduced due to review by Cochlear, consequence still equally high if breach occurs.*
H1	*Fabrication of user study or interview data*	*User study results, interview responses, or qualitative data may be deliberately fabricated due to time pressure, or lack of data.*	*Ethical violation, invalid research conclusions, academic misconduct, and loss of credibility*	*Limited traceability between reported results and original raw data.*	2	4	8	*Eliminate / Discipline: Maintain documented raw data records, review findings with supervisors and follow university research ethics guidelines.*	*All group members, supervisors*	*Throughout the project*	1	4	4	*With adequate documentation, transparency, and supervisory review, the likelihood of data fabrication is minimized. However, loss of academic integrity remains high.*
H2	*Excessive reliance on AI-generated content without critical evaluation*	*AI tools may be used extensively for analysis, and idea generation. If outputs are accepted without verification, incorrect information and fabricated references may be included in the thesis.*	*Inaccurate conclusions, academic integrity concerns and reduced originality.*	*Limited traceability and cross-checking against primary literature or supervisor review.*	2	4	8	*Control / Discipline: Critically evaluate all AI-generated content, verify technical claims, cross-check calculations independently, follow university AI-use guidelines, and review key sections with supervisor before submission.*	*All group members, supervisors*	*Throughout the project*	1	4	4	*When AI outputs are critically reviewed, verified, and aligned with university policies, the risk is reduced to an acceptable level.*
S1	*Unexpected mechanical movement due to software errors*	*Control software sends unintended commands to an actuator during integration testing.*	*Injury to personnel or damage to equipment.*	*Control software developed by students.*	2	3	6	*Reduce / Control: Implement software testing and validation before testing and conduct code review with expert(s).*	*All group members*	*Before operating motorized units*	1	3	3	*With validated control logic, the risk of uncontrolled motion is reduced to an acceptable level.*
W1	*Thesis scope could exceed available time and resources*	*The planned thesis work may include overly ambitious goals, and too many parallel tasks relative to the available timeframe and student experience.*	*Reduced quality, and increased likelihood of shortcuts.*	*Initial project scope is broad, no formal milestone review process defined by Cochlear and limited buffer time in schedule.*	1	3	3	*Reduce / Discipline: Prioritise RQs, add time buffers, agree on a regular supervision schedule and "gate" milestones. Reduce scope could be a possibilty*	*All group members, supervisors*	*At project start and reviewed continuously*	1	2	2	*With structured planning - and regular supervision - the project scope can be maintained within realistic limits.*
W2	*Ergonomic strain due to prolonged computer based work*	*The thesis involves extended periods of CAD modelling, programming, data analysis, and report writing. Sustained static posture, repetitive mouse/keyboard use may lead to body strain.*	*Body pain and wrist strain may lead to reduced concentration and productivity.*	*Cochlear provides height adjustable desks and chairs, no permanent workstations, and the possibilty to work from home, allowing variation in work posture and environment. However, individual workstation adjustment and break routines are not formally enforced.*	2	3	6	*Reduced / Control: Adjust desk and chair, alternate between sitting and standing, take breaks, and vary tasks throughout the day.*	*All group members*	*Throughout the project*	1	2	2	*Given the availability of ergonomic infrastructure, the risk of strain is low. Continuous awareness and posture variation remain necessary to maintain low risk.*
W3	*Insufficient guidance due to reluctance to ask questions*	*Student may avoid asking clarifying or safety related questions out of fear of appearing inexperienced.*	*Incorrect use of equipment or unsafe setup may lead to flawed experimental results and dangerous testing envorinment.*	*False fear culture by the students.*	3	4	12	*Reduce: Schedule regular supervision meetings and encourage open communication.*	*All group members, supervisors, Cochlear/Chalmers personnel*	*At project start*	1	4	4	*With supervision and open communication, probability risk of unsafe independent decision-making is considered low.*
X1	*Work at external collaborator without local safety introduction*	*Student starts working at an external collaborator site without receiving a formal safety briefing.*	*Exposure to unsafe equipment, processes, or emergency routines that the student is not familiar with.*	*External site has its own procedures, but the student has not yet been introduced to them.*	1	4	4	*Control / Discipline: Require a safety introduction at the external site, and document roles and responsibilities.*	*All group members, representative(s) from Cochlear*	*Before using dangerous stuff*	1	2	2	*Risk acceptable once local safety training is completed and responsibilities are established.*

C

Requirements Specification

Table C.1: Requirements specification.

Cochlear/Chalmers		**Document type:**	**Requirement Specification**			
Development of Accelerated Life Testing Method for Bone Conduction Devices		***Created:*** ***Modified:***	**2026-02-16** **2026-05-07**			
Criteria		***Target Value***	***R/D***	***Weight***	***Verification Method***	***Justification***
Function						
0	Accelerate Cochlear's Bone Conduction devices	3 Failure Modes (FM)	R		Test and Analysis	Thesis scope
Simulated ALT duration.						
1.1	Maximum duration for 10 simulated years	< 1/2 year	R		Analysis	To test new BCD iterations
1.2	Preferred duration for 10 simulated years	< 15 weeks	D	5	Analysis	> ×5 better than current
1.3	Maximum duration for 80 simulated years	< 1 year	D	1	Analysis	Patient lifetime guaranteed
Input Data.						
2.1	Adhesive overstress limit (FM2)	TBD via testing	R		Test	Prevents invalid failure modes
2.2	Nylon Thread-locker overstress limit (FM3)	TBD via testing	R		Test	Prevents invalid failure modes
2.3	Piezo overstress limit (FM3)	TBD via testing	R		Test	Prevents invalid failure modes
Setup.						
3.1	Stimulate actuator	2 V to limit of Req 2.3	R		Test	Provides the vibrational stress for ALT
3.2	Heat actuator	37 °C to limit of Req 2.1/2.2	R		Test	Provides the thermal stress for ALT
3.3	Measure actuator stimulation	Voltage	R		Demonstration	Verification of ALT voltage
3.4	Measure actuator temperature	Temperature	D	5	Demonstration	Verification of ALT temperature
3.5	Measure actuator performance after ALT	Output Force Level	R		Demonstration	Analysis of ALT results
3.6	Actuator mounting solution	±3% of 1.41 MPa	R		Analysis	Simulate realistic stress levels
3.7	Signal equaliser	100 Hz-10 kHz	R		Test	Ensures a realistic frequency spectrum
3.8	Scalability	≥ 2 actuators	D	5	Demonstration	Reduces statistical uncertainty
3.9	Compatibility	≥ 2 actuator variants	D	5	Demonstration	Forward compatibility with future designs
3.10	Continuous performance measurement	Automated digital transfer	D	4	Demonstration	Tracks actuator performance degradation
Maintenance						
4.1	Routine Inspection	Once a month	R		Inspection	To ensure the test is running
4.2	Automatic inspection	Once a day	D	3	Demonstration	Provides continuous monitoring
Budget						
5.1	Budget for procurement of material	≈0 SEK	D	5	Analysis	Utilization of existing internal resources

D

Data for Failure Modes

Table D.1: ALT model parameters and constants.

Parameters/Constants	Value	Unit	Source
T_{use}	37	°C	(Cochlear, 2026a)
V_{use}	< 2	V	(Cochlear, 2026a)
h_{use}	16	hours/day	(Cochlear, 2026a)
R	8.314	J/(mol·K)	(NIST, 2026b)

Table D.2: FM2: Adhesive failure parameters and sources.

Parameter	Value	Unit	Source
E_a	$\approx$ 124 000	J/mol	(Cochlear, 2026a)
T_g	$\approx$ 75–85	°C	(Cochlear, 2026a)
n_M	2	-	Estimated

Table D.3: FM3: Nylon thread lock loosening parameters.

Parameter	Value	Unit	Source
E_a	$\approx$ 37 300	J/mol	(Ferry et al., 2017)
T_g	$\approx$ 98.3	°C	(MatWeb, LLC, 2026)
n_M	2	-	Estimated

Table D.4: FM4: Piezo behaviour change parameters.

Parameter	Value	Unit	Source
E_a	$\approx$ 38 600	J/mol	(Cochlear, 2026a)
T_C	$\approx$ 300–400	°C	(Cochlear, 2026a)
n_V	3	-	(Cochlear, 2026a)

E

Concept Screening

E.1 Elimination Matrix

Table E.1: Elimination matrix.

Chalmers Created: 2026-02-24 Modified: 2026-02-24	**Elimination Matrix**	Does this concept provide conditions representative of those that cause the failure mode?	Can the concept actually stress the relevant failure mode?	Can the test conditions be controlled and adjusted?	Can failure onset or progrssion be detected and measured?	Can this be built and run without excessive setup risk or resource demands?	**Elimination requirements:** (+) Yes (-) No (?) More information needed (!) Check the product spec	
Cochlear	**Development of Accelerated Life Testing Method for Bone Conducting Devices**						**Decision:** (+) Proceed with concept (-) Eliminate the concept (?) More information needed (=) Got combined/Too similar	
Nr	**Name**	**Description**	**Plausibility**	**Failure Mode**	**Controllability**	**Observability**	**Feasability**	**Comments**	**Decision**
1	FM0.1	Set the entire acuator at high temperature.	+	+	+	+	+	Missing the affect of Piezo vibration.	+
2	FM0.2	Set the entire acuator at high temperature (Pre-ageing) and after perform a piezo vibration test at a elevated voltage over use frequencies (200-8000Hz).	+	+	+	+	+	Pre-ageing might have different affects than simultaneous temperature and vibration.	+
3	FM0.3	Set the entire acuator at high temperature during a piezo vibration test at a elevated voltage over use frequencies (200-8000Hz).	+	+	+	+	+		+
4	FM0.4	Set the entire acuator at high temperature during a piezo vibration test at a elevated voltage over resonant frequencies (900-1100Hz) for harsher conditions.	+	+	+	+	+		+
5	FM1.1	[redacted]							+
6	FM1.2								-
7	FM1.3								-
8	FM1.4								-
9	FM1.5								-
10	FM1.6								-
11	FM1.7								+
12	FM1.8								+
13	FM1.8								=
14	FM1.9								=
15	FM2.1	Glue togheter two plates or acuator whilst submerged in Simulated Body Fluid (SBF) at high temperature.	-					Simulated Body Fluid (SBF) not representative of cause of failure mode.	-
16	FM2.2	Ultrasonic Aging by subjecting the glue bond between two plates or acuator to continuous high-frequency vibration while immersed in SBF.	-					Simulated Body Fluid (SBF) not representative of cause of failure mode.	-
17	FM2.3	Thermal ageing of glue inbetween piezo and backplate at high temperature.	+	+	+	+	+	Missing the affect of Piezo vibration.	+
18	FM2.4	Thermal ageing of glue inbetween two plates at high temperature.	+	+	+	+	+	Missing the affect of Piezo vibration. Plates might lead to false conclusions.	+

Table E.1: Elimination matrix (continued).

Chalmers Created: 2026-02-24 Modified: 2026-02-24	Elimination Matrix	Does this concept provide conditions representative of those that cause the failure mode?	Can the concept actually stress the relevant failure mode?	Can the test conditions be controlled and adjusted?	Can failure onset or progression be detected and measured?	Can this be built and run without excessive setup risk or resource demands?	**Elimination requirements:** (+) Yes (-) No (?) More information needed (!) Check the product spec	
Cochlear	**Development of Accelerated Life Testing Method for Bone Conducting Devices**						**Decision:** (+) Proceed with concept (-) Eliminate the concept (?) More information needed (=) Got combined/Too similar	
Nr	**Name**	**Description**	**Plausibility**	**Failure Mode**	**Controllability**	**Observability**	**Feasability**	**Comments**	**Decision**
19	FM3.1	Tighten the screw to a specific torque in situe and store the device at an high temperature.	+	+	+	+	+	Missing the affect of Piezo vibration.	+
20	FM3.2	Tighten the screw to a specific torque in situe and store the device at high temperature (Pre-ageing) and after perform a Junker vibration test.	+	+	+	+	-	Junker vibration testing machine has very high reasource demands	-
21	FM3.3	Tighten the screw to a specific torque in situe and store the device at high temperature during a Junker vibration test.	+	+	+	+	-	Junker vibration testing machine has very high reasource demands	-
22	FM3.4	Tighten the screw to a specific torque in situe and store the device at high temperature during a fluxuating Junker vibration test.	+	+	+	+	-	Junker vibration testing machine has very high reasource demands	-
23	FM3.5	Tighten the screw to a specific torque in situe and store the device at high temperature (Pre-ageing) and after perform a mechanical vibration test.	+	+	+	+	+	Pre-ageing might have different affects than simultaneous temperature and vibration.	+
24	FM3.6	Tighten the screw to a specific torque in situe and store the device at high temperature during a mechanical vibration test.	+	+	+	+	+		+
25	FM3.7	Tighten the screw to a specific torque in situe whilst submerged in Simulated Body Fluid (SBF) at high temperature.	-					Simulated Body Fluid (SBF) not representative of cause of failure mode.	-
26	FM3.8	Screw Loosening Junker test (DIN 65151)	+	+	+	+	-	Junker vibration testing machine has very high reasource demands	-

E.2 Pugh Matrices

Table E.2: First Pugh matrix.

	Current test (7 year)	FM0.1	FM0.2	FM0.3	FM0.4	FM1.1	FM2.3	FM2.4	FM3.1	FM1.7	FM1.8	FM3.5	FM3.6
Criteria	**Score**	**Score**	**Score**	**Score**	**Score**	**Score**	**Score**	**Score**	**Score**	**Score**	**Score**	**Score**	**Score**
Acceleration Factor	0	1	1	1	1	1	1	1	1	1	1	1	1
Multi-mode Capability	0	0	0	0	0	-1	-1	-1	-1	-1	-1	-1	-1
Isolate Failure Mode	0	0	0	0	0	1	1	1	1	1	1	1	1
Distortion Risk	0	0	0	0	0	1	1	1	1	1	1	1	1
Scalability of test	0	0	0	0	0	0	0	0	0	0	0	0	0
Operational Complexity	0	1	1	1	1	1	1	1	1	-1	-1	-1	-1
Repeatability	0	1	1	1	1	1	1	1	1	1	1	1	1
Safety risk	0	1	0	0	0	1	1	1	1	-1	-1	-1	-1
Enviroment	0	-1	0	0	0	-1	-1	-1	-1	-1	-1	-1	-1
Cost	0	1	1	1	1	1	1	1	1	1	1	1	1
Total scores	0	4	4	4	4	5	5	5	5	1	1	1	1
Rank		2	2	2	2	1	1	1	1	3	3	3	3

Table E.3: Second Pugh matrix.

	FM1.1	FM0.1	FM0.2	FM0.3	FM0.4	FM2.3	FM2.4	FM3.1
Criteria	**Score**	**Score**	**Score**	**Score**	**Score**	**Score**	**Score**	**Score**
Acceleration Factor	0	0	1	1	1	0	1	0
Multi-mode Capability	0	1	1	1	1	0	0	0
Isolate Failure Mode	0	-1	-1	-1	-1	0	0	0
Distortion Risk	0	0	1	1	1	0	-1	-1
Scalability of test	0	0	0	0	0	0	0	0
Operational Complexity	0	-1	-1	-1	-1	-1	-1	-1
Repeatability	0	0	0	0	0	0	0	0
Safety risk	0	0	0	0	0	0	0	0
Enviroment	0	0	1	1	1	0	0	0
Cost	0	-1	-1	-1	-1	-1	-1	-1
Total scores	0	-2	1	1	1	-2	-2	-3
Rank		2	1	1	1	2	2	3

Table E.4: Third Pugh matrix.

	FM0.3	FM0.2	FM0.4	FM1.1
Criteria	**Score**	**Score**	**Score**	**Score**
Acceleration Factor	0	-1	1	-1
Multi-mode Capability	0	0	0	-1
Isolate Failure Mode	0	0	0	1
Distortion Risk	0	0	-1	-1
Scalability of test	0	0	0	1
Operational Complexity	0	0	0	1
Repeatability	0	0	0	0
Safety risk	0	0	0	0
Enviroment	0	-1	0	-1
Cost	0	0	0	1
Total scores	0	-2	0	0
Rank		2	1	1

E.3 Kesselring Matrix

Table E.5: Kesselring matrix.

Chalmers		**Kesselring Matrix**									
Created: 2026-02-24		**Cochlear**									
Modified: 2026-03-02		***Development of Accelerated Life Testing Methodfor Bone Conducting Devices***									
		Solution alternative									
		Ideal		**#3 FM0.3**		**#4 FM0.4**		**#5 FM1.1**		**Subpar**	
Criteria											
Name	w	v	t	v	t	v	t	v	t	v	t
Multi-modes efficiency	0,05	5	0,25	5	0,25	5	0,25	1	0,05	1	0,05
Performance (FM1)	0,19	5	0,95	3	0,57	3	0,57	5	0,95	1	0,19
Performance (FM2)	0,14	5	0,7	5	0,7	4	0,56	1	0,14	1	0,14
Performance (FM3)	0,14	5	0,7	5	0,7	4	0,56	1	0,14	1	0,14
Performance (FM4)	0,22	5	1,1	5	1,1	4	0,88	1	0,22	1	0,22
Fidelity & Validity	0,17	5	0,85	5	0,85	3	0,51	3	0,51	1	0,17
Variance	0,08	5	0,4	4	0,32	2	0,16	5	0,4	1	0,08
Cost & Efficiency	0,02	5	0,1	3	0,06	3	0,06	5	0,1	1	0,02
	Total:	40	**5,05**	35	**4,55**	28	**3,55**	22	**2,51**	8	**1,01**
	Rank:			**1**		**2**		**3**			
	Decision:	***Propose alternative #3: FM0.3***									

Table E.6: Kesselring weight pairwise comparison.

	Multi-modes efficiency	Performance (FM1)	Performance (FM2)	Performance (FM3)	Performance (FM4)	Fidelity & Validity	Variance	Cost & Efficiency	Score	Weight
Multi-modes efficiency	0,5	0	0	0	0	0	0	1	**1,5**	**0,05**
Performance (FM1)	1	0,5	1	1	0	0,5	1	1	**6**	**0,19**
Performance (FM2)	1	0	0,5	0,5	0	0,5	1	1	**4,5**	**0,14**
Performance (FM3)	1	0	0,5	0,5	0	0,5	1	1	**4,5**	**0,14**
Performance (FM4)	1	1	1	1	0,5	0,5	1	1	**7**	**0,22**
Fidelity & Validity	1	0,5	0,5	0,5	0,5	0,5	1	1	**5,5**	**0,17**
Variance	1	0	0	0	0	0	0,5	1	**2,5**	**0,08**
Cost & Efficiency	0	0	0	0	0	0	0	0,5	**0,5**	**0,02**
									32	

Multi-modes efficiency Accelerates multiple failure modes without interference

1	2	3	4	5
Accelerates only 1 failure mode; no interaction	Partially accelerates a second mode but with negligible impact	Clearly accelerates 2 failure modes without mutual interference	Accelerates 3 failure modes simultaneously with controlled interaction	Accelerates all 4 failure modes simultaneously with no distortion or cross-interference

Performance (FM1)

1	2	3	4	5

Performance (FM2) Accuracy of adhesive failure mechanism and progression

1	2	3	4	5
Failure mechanism incorrect or not reproducible	Failure occurs but driven by non-representative conditions	Correct failure mode observed but with simplified or biased propagation	Realistic initiation and propagation of failure	Highly accurate failure behavior with correct interface physics and progression

Performance (FM3) Accuracy of thread loosening behavior and mechanics

1	2	3	4	5
Loosening mechanism not representative or not observable	Loosening occurs but driven by unrealistic load paths	General loosening trend captured but lacks mechanical fidelity	Realistic loosening behavior with correct load transfer and dynamics	Highly accurate representation of loosening including preload loss mechanisms and interaction effects

Performance (FM4) Accuracy of piezo fatigue degradation and failure behavior

1	2	3	4	5
Fatigue behavior not representative; failure mode incorrect	Fatigue observed but dominated by artificial or non-relevant effects	General fatigue trend captured but lacks accuracy in degradation path	Realistic fatigue progression with correct electromechanical coupling	Highly accurate fatigue behavior with correct failure mechanisms and measurable degradation evolution

Fidelity & Validity Matches real-world physics and interactions

1	2	3	4	5
Significant deviation from real failure mechanisms; artificial effects dominate	Partial realism; some mechanisms correct but key distortions present	Mostly realistic; minor non-critical deviations	Highly realistic behavior with correct interactions between components	Fully representative of real-world physics and multi-mode interactions Repeatability

Variance Variance between runs, setup sensitivity

1	2	3	4	5
High variability; results strongly dependent on setup/operator	Noticeable variability; limited statistical confidence	Acceptable repeatability with moderate variance	High repeatability; low sensitivity to setup variationst	Very high repeatability; consistent results across runs and conditions

Cost & Efficiency Cycle time, resource consumption, setup, automation

1	2	3	4	5
High cost, long setup and test time, low efficiency	Moderate cost with some inefficiencies	Balanced cost and efficiency; acceptable resource use	Efficient setup and execution; good automation potential	Highly efficient, low cost per test, fast cycles, highly automated Risk

Figure E.1: Kesselring criteria.

F

Technical Drawings

F.1 Rigid Mounting Solution

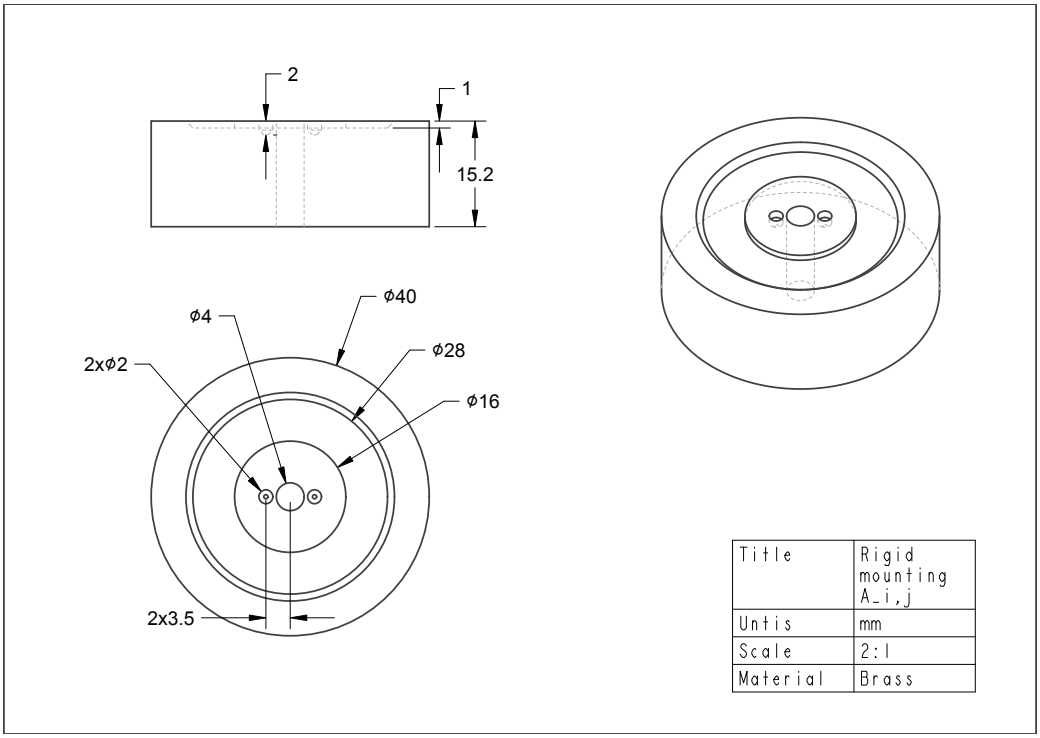

Figure F.1: Technical drawing of Rigid Mounting Solution for $\mathcal{A}_{i,j}$.

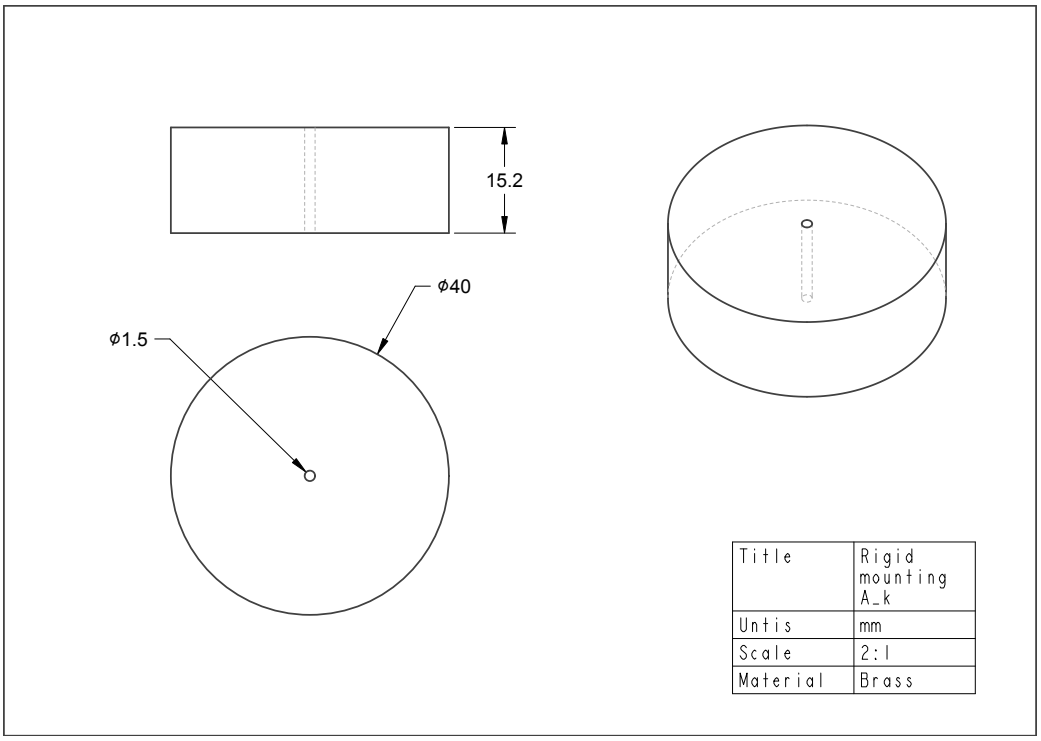

Figure F.2: Technical drawing of Rigid Mounting Solution for $\mathcal{A}_k$.

F.2 Rigid Mounting Solution with Accelerometer

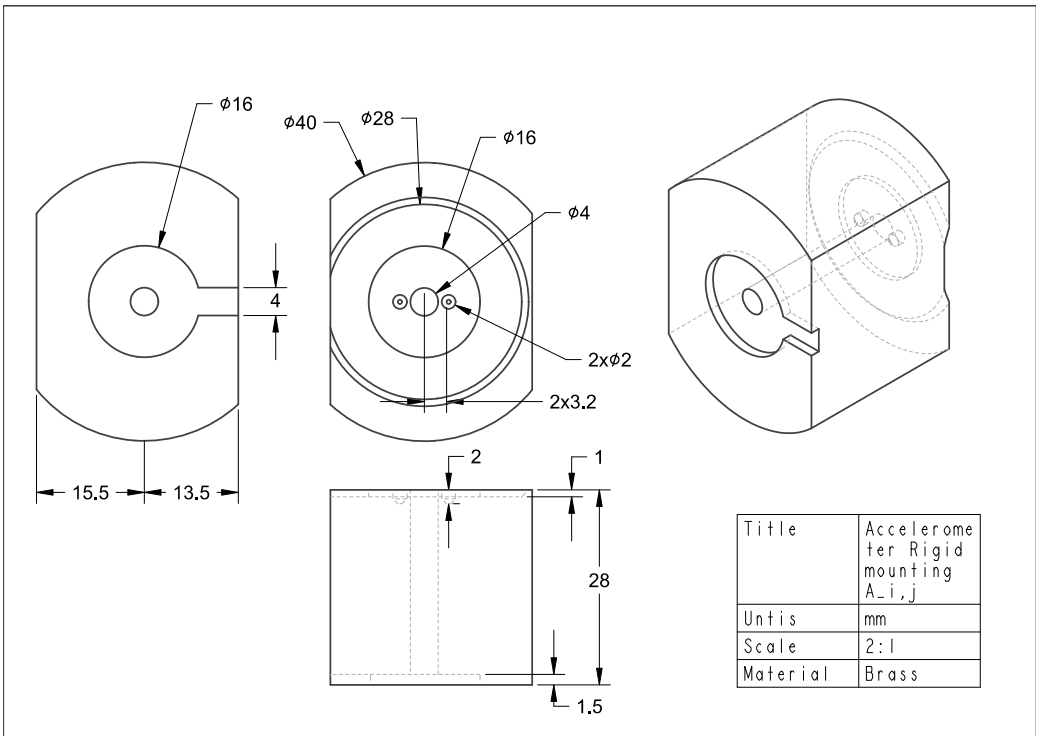

Figure F.3: Technical drawing of Rigid Mounting Solution for $\mathcal{A}_{i,j}$ with accelerometer.

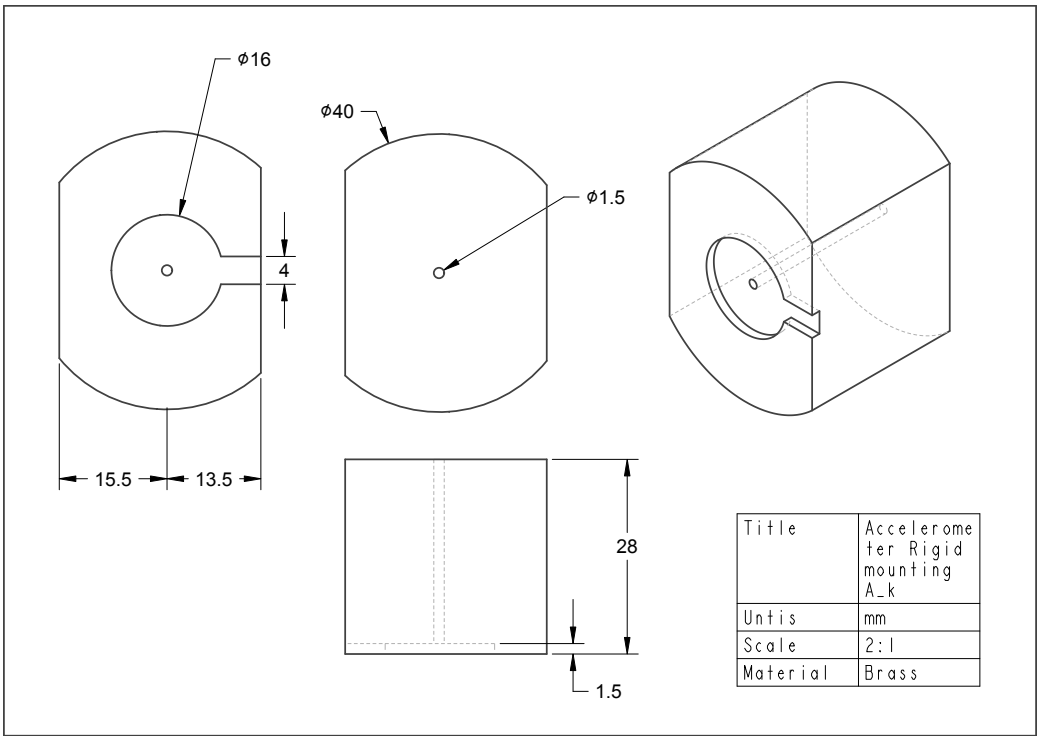

Figure F.4: Technical drawing of Rigid Mounting Solution for $\mathcal{A}_k$ with accelerometer.

F.3 Adhesive Specimen

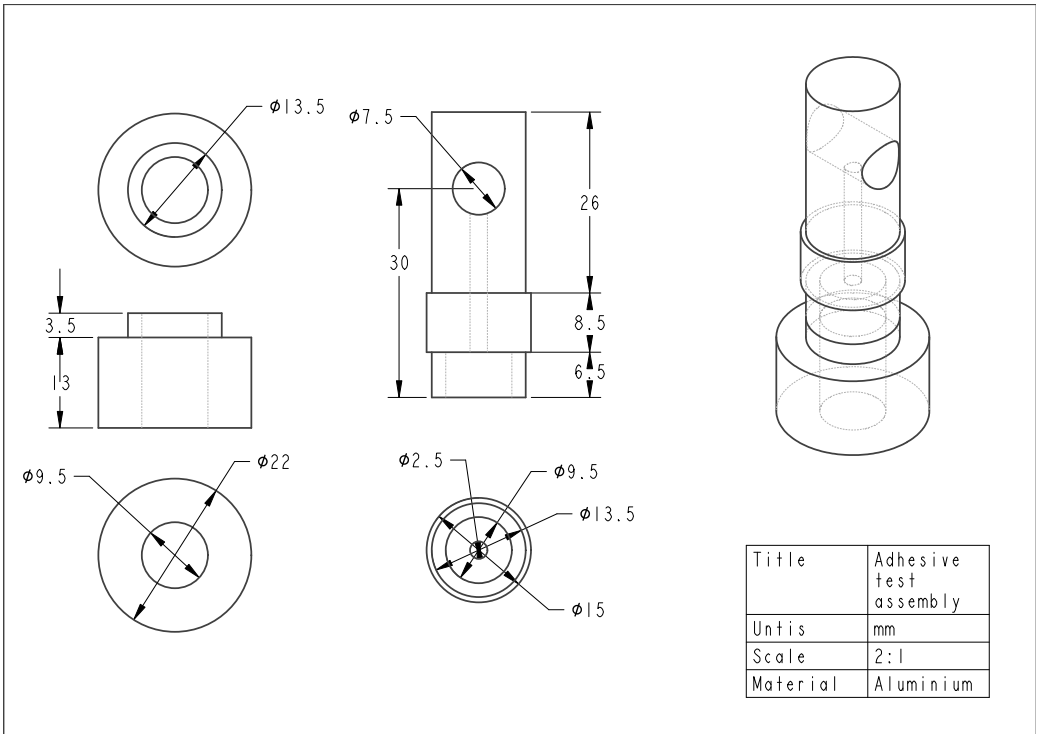

Figure F.5: Technical drawing of the adhesive specimen.

G

APx500 Script

```
import clr
import sys
import os
import datetime
import time
import shutil

# ========================================
# SYSTEM CONFIGURATION
# ========================================
APX_VERSION = "9.0"

api_path_1 = fr"C:\Program Files\Audio Precision\APx500 {APX_VERSION}\API\
    AudioPrecision.API.dll"
api_path_2 = fr"C:\Program Files\Audio Precision\APx500 {APX_VERSION}\API\
    AudioPrecision.API2.dll"

try:
    clr.AddReference(api_path_1)
    clr.AddReference(api_path_2)
    from AudioPrecision.API import *
    import System
except Exception as e:
    print(f"Could not load APx API. Ensure APx500 v{APX_VERSION} is installed.")
    sys.exit(1)

def main():
    print("Initializing APx500 Software...")
    try:
        APx = APx500_Application()
    except:
        print("Failed to connect to APx500. Ensure the software is installed.")
        sys.exit(1)

    APx.Visible = True

    # ========================================
    # USER CONFIGURATION
    # ========================================
    active_outputs = "Both"           # SET TO "A" OR "Both"

    total_test_hours = 24
    save_interval_hours = 0.5
    time_per_sweep_seconds = 30  # A: ca 10 s, Both: 30 s

    base_save_dir = r"G:\Public\luke\SamViktor_ALT\APx_Test_Results"

    template_A = r"G:\Public\luke\SamViktor_ALT\APx500 Templates\ALT_A_Sweep.
    approjx"
    template_Both = r"G:\Public\luke\SamViktor_ALT\APx500 Templates\ALT_Both_Sweep.
    approjx"

    # ----------------------------------------
    # THE STATIC FILES SET IN YOUR APX GUI STEPS
```

```
    # ----------------------------------------
    static_csv_A = os.path.join(base_save_dir, "temp_export_A.csv")
    static_csv_B = os.path.join(base_save_dir, "temp_export_B.csv")
    # ========================================

    # Load the correct template based on user config
    run_mode = active_outputs.strip().upper()
    if run_mode == "A":
        project_path = template_A
    else:
        project_path = template_Both

    print(f"\nOpening project template for mode: {run_mode}...")
    if not os.path.exists(project_path):
        print(f"FATAL ERROR: Could not find template file at:\n{project_path}")
        sys.exit(1)

    APx.OpenProject(project_path)

    # --- MANUAL PAUSE (MAKE TWEAKS IN APx NOW) ---
    print("\n" + "="*55)
    print("[!] ACTION REQUIRED IN APx GUI [!]")
    print(f"Template '{os.path.basename(project_path)}' loaded successfully.")
    print("\nTake your time to configure APx before continuing:")
    print("  - Ensure hardware connection is green.")
    print("  - Update Generator Voltage or Sweep Frequencies if needed.")

    if run_mode == "A":
        print("  - Ensure EXACTLY 2 Signal Paths exist in this order:")
        print("    1. Sweep Output A (Normal)")
        print(f"    2. Export Output A (Sweep + Export) -> temp_export_A.csv")
    else:
        print("  - Ensure EXACTLY 4 Signal Paths exist in this order:")
        print("    1. Sweep Output A (Normal)")
        print("    2. Sweep Output B (Normal)")
        print(f"    3. Export Output A (Sweep + Export) -> temp_export_A.csv")
        print(f"    4. Export Output B (Sweep + Export) -> temp_export_B.csv")

    print("="*55)
    input("\nPress ENTER here in the console when you are ready to begin the test
    loop...")

    # --- CONNECT TO THE SIGNAL PATHS (Done AFTER you press enter) ---
    all_paths = []
    try:
        if run_mode == "A":
            sp_sweep_A = APx.Sequence.GetSignalPath(0)  # Path 1
            sp_export_A = APx.Sequence.GetSignalPath(1) # Path 2
            all_paths = [sp_sweep_A, sp_export_A]
        else:
            sp_sweep_A = APx.Sequence.GetSignalPath(0)  # Path 1
            sp_sweep_B = APx.Sequence.GetSignalPath(1)  # Path 2
            sp_export_A = APx.Sequence.GetSignalPath(2) # Path 3
            sp_export_B = APx.Sequence.GetSignalPath(3) # Path 4
            all_paths = [sp_sweep_A, sp_sweep_B, sp_export_A, sp_export_B]
    except Exception as e:
        print(f"FATAL ERROR: Could not map signal paths. Ensure you have the
    correct number of paths. ({e})")
        sys.exit(1)

    # Helper function to easily switch paths
    def run_single_path(target_path):
        for sp in all_paths:
            sp.Checked = (sp == target_path)
        APx.Sequence.Run()

    # --- DIRECTORY SETUP ---
    timestamp = datetime.datetime.now().strftime("%Y-%m-%d_%H-%M-%S")
    target_dir = os.path.join(base_save_dir, f"TestRun_{run_mode}_{timestamp}")
    if not os.path.exists(target_dir):
```

```
        os.makedirs(target_dir)

    # --- CALCULATIONS ---
    total_loops = int(round((total_test_hours * 3600) / time_per_sweep_seconds))
    loops_per_save = int(round((save_interval_hours * 3600) /
    time_per_sweep_seconds))
    if loops_per_save < 1: loops_per_save = 1

    print(f"\nTarget Time: {total_test_hours} hours | Save Interval: {
    save_interval_hours} hours")
    print(f"Calculated Total Loops: {total_loops}. Saving every {loops_per_save}
    loops.")
    print(f"Final files will be saved to: {target_dir}\n")

    # --- MAIN LOOP ---
    for i in range(1, total_loops + 1):
        is_save_loop = (i % loops_per_save == 0) or (i == total_loops)

        if not is_save_loop:
            # ========================================
            # NORMAL LOOP (NO EXPORTING)
            # ========================================
            print(f"Loop {i}/{total_loops} running normal sweeps...")

            if run_mode in ["A", "BOTH"]:
                run_single_path(sp_sweep_A) # Runs Path 1

            if run_mode == "BOTH":
                run_single_path(sp_sweep_B) # Runs Path 2

        else:
            # ========================================
            # SAVE LOOP (EXPORTS ONLY)
            # ========================================
            print(f"Loop {i}/{total_loops} running EXPORT sweeps...")

            # --- RUN & SAVE OUTPUT A ---
            if run_mode in ["A", "BOTH"]:
                run_single_path(sp_export_A) # Runs Export A
                time.sleep(2) # Brief wait for hard drive to write CSV

                base_A = f"Loop_{i}_Output_A_{timestamp}"

                if os.path.exists(static_csv_A):
                    shutil.move(static_csv_A, os.path.join(target_dir, f"{base_A}.
    csv"))
                    print(f"    [SUCCESS] Saved Output A CSV")
                else:
                    print(f"    [!] Warning: Missing {static_csv_A}")

            # --- RUN & SAVE OUTPUT B ---
            if run_mode == "BOTH":
                run_single_path(sp_export_B) # Runs Export B
                time.sleep(2) # Brief wait for hard drive to write CSV

                base_B = f"Loop_{i}_Output_B_{timestamp}"

                if os.path.exists(static_csv_B):
                    shutil.move(static_csv_B, os.path.join(target_dir, f"{base_B}.
    csv"))
                    print(f"    [SUCCESS] Saved Output B CSV")
                else:
                    print(f"    [!] Warning: Missing {static_csv_B}")

    print("\nTesting Complete.")

if __name__ == "__main__":
    main()
```

Listing G.1: Python script for APx500 ALT test automation.

DEPARTMENT OF ELECTRICAL ENGINEERING
CHALMERS UNIVERSITY OF TECHNOLOGY
Gothenburg, Sweden
www.chalmers.se

CHALMERS
UNIVERSITY OF TECHNOLOGY